

REPORT DOCUMENTATION PAGE

Form Approved OMB No. 0704-0188

Public reporting burden for this collection of information is estimated to average 1 hour per response, including the time for reviewing instructions, searching existing data sources, gathering and maintaining the data needed, and completing and reviewing the collection of information. Send comments regarding this burden estimate or any other aspect of this collection of information, including suggestions for reducing the burden, to Department of Defense, Washington Headquarters Services, Directorate for Information Operations and Reports (0704-0188), 1215 Jefferson Davis Highway, Suite 1204, Arlington, VA 22202-4302. Respondents should be aware that notwithstanding any other provision of law, no person shall be subject to any penalty for failing to comply with a collection of information if it does not display a currently valid OMB control number.

PLEASE DO NOT RETURN YOUR FORM TO THE ABOVE ADDRESS.

1. REPORT DATE (DD-MM-YYYY) 05-05-2003		2. REPORT TYPE Final Report		3. DATES COVERED (From - To) 20 April 2001 - 21-Oct-03	
4. TITLE AND SUBTITLE Analysis of curved micro strip antennas				5a. CONTRACT NUMBER F61775-01-WE024	
				5b. GRANT NUMBER	
				5c. PROGRAM ELEMENT NUMBER	
6. AUTHOR(S) Professor Zvonimir Sipus				5d. PROJECT NUMBER	
				5d. TASK NUMBER	
				5e. WORK UNIT NUMBER	
7. PERFORMING ORGANIZATION NAME(S) AND ADDRESS(ES) University of Zagreb Unska 3 Zagreb HR-10000 Croatia				8. PERFORMING ORGANIZATION REPORT NUMBER N/A	
9. SPONSORING/MONITORING AGENCY NAME(S) AND ADDRESS(ES) EOARD PSC 802 BOX 14 FPO 09499-0014				10. SPONSOR/MONITOR'S ACRONYM(S)	
				11. SPONSOR/MONITOR'S REPORT NUMBER(S) SPC 01-4024	

12. DISTRIBUTION/AVAILABILITY STATEMENT

Approved for public release; distribution is unlimited.

13. SUPPLEMENTARY NOTES

20040210 114

14. ABSTRACT

This report results from a contract tasking University of Zagreb as follows: The contractor will investigate simulation tools for analyzing single-curved and double-curved microstrip patch antennas. These tools will overcome a key limitation in existing laboratory computer simulations, which are unable to approximate the electromagnetic characteristics of dual curvature conformal arrays.

15. SUBJECT TERMS

EOARD, Antennas, Microwave Technology, Conformal Array Antennas

16. SECURITY CLASSIFICATION OF:**a. REPORT**
UNCLAS**b. ABSTRACT**
UNCLAS**c. THIS PAGE**
UNCLAS**17. LIMITATION OF ABSTRACT**
UL**18. NUMBER OF PAGES**
105**19a. NAME OF RESPONSIBLE PERSON**
MICHAEL KJ MILLIGAN, Lt Col, USAF**19b. TELEPHONE NUMBER (Include area code)**
+44 (0)20 7514 4955

REPORT FOR CONTRACT F61775-01-WE024

Analysis of Curved Microstrip Antennas

by

**Zvonimir Sipus
Niksa Burum
Radovan Zentner**

SUBMITTED BY: Dr. Zvonimir Sipus
Faculty of Electrical Engineering and Computing
University of Zagreb
Unska 3
Zagreb, HR-10000, Croatia

18 April 2003

DISTRIBUTION STATEMENT A
Approved for Public Release
Distribution Unlimited

TABLE OF CONTENTS

1 INTRODUCTION.....	3
2 PROBLEM IDENTIFICATION AND ITS SIGNIFICANCE.....	6
3 PROJECT OBJECTIVE AND REALIZED OUTCOMES.....	9
4 PROJECT OUTCOMES.....	12
4.1 ANALYSIS OF MICROSTRIP PATCH ANTENNAS ON SPHERICAL STRUCTURES.....	13
4.1.1 Introduction.....	13
4.1.2 Method of Analysis.....	13
4.1.3 Calculation of Green's Function.....	15
4.1.4 Numerical Considerations.....	17
4.1.5 Mutual Coupling.....	19
4.1.6 Far-Field Calculations.....	23
4.1.7 Effects of the Sphere Curvature.....	25
4.1.8 Laboratory Model.....	32
APPENDIX I: Selection of Basis Function.....	35
APPENDIX II: Electromagnetic Field Radiated by an Current Shell.....	36
4.2 ANALYSIS OF APERTURE COUPLED PATCH ANTENNAS ON CIRCULAR-CYLINDRICAL AND SPHERICAL STRUCTURES.....	38
4.2.1 Introduction.....	38
4.2.2 Method of Analysis.....	38
5 USER'S MANUAL.....	45
5.1 INTRODUCTION TO SMIPA.....	46
5.1.1 Introduction.....	46
5.1.2 Problem Domain Description.....	47
5.1.3 Text File Interface.....	48
5.2 UPGRADE OF THE PROGRAM CYMPA.....	56
5.2.1 Introduction.....	56
5.2.2 Differences between Cylindrical and Spherical Program.....	57
6 BENCHMARKS.....	59
6.1 SPHERICAL 16 ELEMENT ARRAY FOLLOWING THE ICOSAHEDRON GRID –RADIATION BY SIMPLE MODEL.....	60
6.1.1 Introduction.....	61
6.1.2 Summary technical description.....	62
6.1.3 Numerical results.....	63
6.2 SPHERICAL 16 ELEMENT ARRAY FOLLOWING THE ICOSAHEDRON GRID –RADIATION BY RIGOROUS MODEL.....	65
6.2.1 Introduction.....	66
6.2.2 Summary technical description.....	68
6.2.3 Numerical results.....	69
6.3 RECTANGULAR PATCH ANTENNA ON SPHERICAL STRUCTURE.....	71
6.3.1 Introduction.....	72

6.3.2 Summary technical description	73
6.3.3 Numerical and experimental results	74
6.4 CIRCULAR PATCH ANTENNA ON SPHERICAL STRUCTURE	76
6.4.1 Introduction	77
6.4.2 Summary technical description	78
6.4.3 Numerical and experimental results	79
6.5 MUTUAL COUPLING OF TWO RECTANGULAR PATCHES PRINTED ON SPHERICAL STRUCTURE	81
6.5.1 Introduction	82
6.5.2 Summary technical description	83
6.5.3 Numerical results	84
6.6 APERTURE-COUPLED CYLINDRICAL PATCH ANTENNA	86
6.6.1 Introduction	87
6.6.2 Summary technical description	88
6.6.3 Numerical results	89
7 SMIPAWIN AND CYMPAWIN USER'S MANUAL	92
Introduction	93
The Installation of the Software	94
Using SMiPAWin (CympaWin)	94
Input and output files	95
The user interface properties	95
Some SMiPAWin (CympaWin) windows	97
Troubleshooting	100
8 CONCLUSIONS	101
9 BIBLIOGRAPHY	104

1 INTRODUCTION

Introduction

The constant development in wireless system technologies enables innovative new applications that introduce new challenges and demands on antenna engineers. These trendlines show need for advanced smart antenna systems in communications and surveillance with a variety of beamforming and beamsteering capabilities. Additionally, electromagnetic performances of antenna have often to comply with physical system requirements such as customized shape and/or lightweight. Curved conformal microstrip arrays have a potential to meet all these requirements.

The antenna arrays that conform to cylindrical structure can enable radiation pattern with directed beams in arbitrary directions, or omnidirectional pattern in plane perpendicular to the cylinder. With their cylindrically shaped structure they can be easily mounted on various airborne objects (fighter jets, smart missiles, rockets) without disturbing their aerodynamical properties. On the other hand, spherical arrays can steer single or multiple beams throughout the complete hemisphere without loss of gain in any direction. Therefore, spherical array is good candidate for satellite terminals, telemetry and command applications.

As long as the radius of the curved structure is large compared to the wavelength, the antenna can be approximated with the planar structure of infinite extent. However, this is not the case for the most of the practical conformal antennas. Therefore, computational tools are required which enable fast and accurate analysis of modern conformal air interfaces. Additionally, in case of array applications, it is critical to be able to take into account the mutual coupling between the array elements. In more detail, the mutual coupling can cause significant change in element pattern of array elements, and therefore must be included in the design.

In course of this project a computer program is developed that performs a rigorous analysis of spherical and cylindrical arrays of microstrip patch elements. The dielectric structure of the antenna or the antenna array is rigorously taken into account by using proper Green's functions in spectral domain. The Method of moments (MoM) is applied to analyze array by means of element-by-element approach, thus taking the mutual coupling into account as well. All important information about the antenna array can be calculated by the software: the input port impedance, radiation pattern as well as the mutual coupling between the elements can be obtained.

The capabilities and accuracy of the computer program are tested on different practical designs. One of them, the spherical test model, is developed for this purpose. The comparison of some spherical and cylindrical designs with their planar counterparts is given in order to show impact of curvature on input impedance and radiation properties. All of these results will be presented in this report.

2 PROBLEM IDENTIFICATION AND ITS SIGNIFICANCE

Problem Identification and its Significance

Conformal antennas are defined as antennas that conform to the structure for other reason than electromagnetic. This reason can be aerodynamic, hydrodynamic, aesthetic or coverage reason. Because of these potential advantages over planar antennas conformal microstrip patch antennas have been proposed for a wide range of applications. For example, future military airborne and space-based sensors will require active electronically scanned array antennas. Planar arrays are possible solution. However, planar arrays have inherent disadvantage because they can be electronically scanned to only about 60 degrees from boresight, and the gain falls with scanning angle. The conformal arrays can scan the beam without drop of the gain, and the size of the conformal antenna needed for obtaining the same gain as its planar counterpart is approximately the same. Spherical arrays have possibility of directing single or multiple beams through complete hemisphere and, therefore, spherical arrays are an attractive solution for satellite tracking, telemetry and command applications. Other example is cylindrical microstrip arrays mounted on smart missiles and rockets without disturbing aerodynamic properties.

Conventional phased array antennas are thick, heavy and expensive, and require large amounts of power. Future military airborne and space-based phased arrays will use conformal, low-weight and low-power elements in order to meet extremely stringent system requirements. Therefore, new solutions are proposed for such applications. One of the most promising is to use Micro Electro Mechanical Switches (MEMS) as an essential part of the low-loss phase shifters. The proposed architecture for the building block of phased arrays is a sandwich structure where microstrip antenna, RF-distribution layer, T/R-switch, low noise amplifiers, power amplifiers and phase shifters are built in a microstrip multilayer structure. The radiating element in this geometry is an aperture-coupled microstrip patch antenna.

The traditional approach of analyzing conformal microstrip antennas is to approximate the conformal structure with locally planar one, and then to use some method for planar antennas. This is a reasonable approximation if the radius of the structure curvature is large. However, for small radiuses the properties of the antenna begin to differ significantly from their planar counterpart.

Some differences between planar and cylindrical patch antennas are as follows. For axially polarized patch antennas the input impedance will significantly drop with decrease of the structure radius. For patches polarized in circumferential direction the change of input impedance is opposite, i.e. input impedance will grow with decrease of the structure radius. The amplitude of surface waves, and therefore mutual coupling, is enlarged in axial direction and

reduced in circumferential direction in comparison to the planar case. The radiation pattern can be significantly changed in circumferential direction. For example, we can get omnidirectional radiation pattern if the patch is almost wrapped-around, where in the planar case the backward radiation is always weak. The resonant frequency is almost the same for axially polarized patches, and it is significantly changed for patches polarized in circumferential direction.

Spherical antennas have different properties. The resonant frequency is changed a lot with decrease of the structure radius, while the resonant resistance stays almost constant. The mutual coupling effects are reduced in comparison to the planar case. Like in the cylindrical case, the radiation pattern can be significantly modified. As expected, the back-radiation is smaller for spheres with larger radius.

The significant differences in properties of conformal antennas show that programs for analyzing planar microstrip antennas are not sufficiently accurate for design of conformal antennas, and thus there is a need for programs for analyzing conformal microstrip antennas. Such programs will rigorously take into account the effects of the curvature, and therefore will help the engineers in designing the conformal antennas.

Uniqueness: It was planned to develop two programs as outcomes of the project: (a) program for analyzing patch arrays printed on spherical structures, and (b) program for analyzing aperture-coupled patch arrays on cylindrical structures (the upgrade of the existing program "CyMPA"). Spherical patch antennas are rarely considered in scientific literature. Till now only a single patch of circular or ring shape, fed by a coax-line, on single-layer spherical structure is analyzed (state of art about this subject can be found e.g. in recently published book: K.L.Wong, "Design of Nonplanar Microstrip Antennas and Transmission Lines", Wiley 1999.). Therefore, the development of the program for analyzing arrays of rectangular or circular patches, where mutual coupling between elements are rigorously taken into account, is scientifically new. The chosen analysis method for aperture-coupled conformal patches is extension of the method which is used for planar geometries, and which in planar case shows good agreement between calculated and experimental results.

3 PROJECT OBJECTIVE AND REALIZED OUTCOMES

Project objective and realized outcomes

We proposed a two-phase, 24-month effort to develop a model for analyzing single-curved and double-curved conformal microstrip antennas. It was planned to develop two computer programs as outcomes. First proposed program is for analyzing patch arrays printed on spherical structures, where the patches are of rectangular or circular shape and the feeding structure is microstrip transmission line, coaxial transmission line, or aperture-coupled feeding. The interest for such a program is due to the fact that conformal arrays in some applications cannot be approximated as cylindrical ones, i.e. as structures with one curvature direction, and thus another curvature direction should be taken into account. Second proposed program is an upgrade of the program "CyMPA" that analyzes patch arrays on cylindrical structures (i.e. on single-curved structures). The upgrade will include the analysis of aperture-coupled patch arrays on cylindrical structures.

It was planned that both programs calculate the following antenna characteristics:

- current distribution at each patch in the array
- input impedance at each input port in the array
- mutual coupling between each two patches in the array
- radiation pattern of the array when all mutual couplings are taken into account
- radiation pattern of the array without taking mutual coupling into account (fast calculations of the radiation pattern needed for making first design of the array).

During first 12 months phase we have developed:

(a) Program "SMiPA" that analyzes patch arrays printed on spherical structures. The patches are of rectangular or circular shape, and they can be fed by microstrip or coaxial transmission line. The program calculates:

- current distribution at each patch in the array
- input impedance at each input port in the array
- radiation pattern of the array without taking mutual coupling into account.

- (b) The upgrade of the program "CyMPA" that calculates aperture-coupled patch antennas on cylindrical structures. Therefore, with the upgraded program it is possible to fully analyze aperture-coupled cylindrical patch arrays (input impedance, mutual coupling, radiation pattern with/without considering mutual coupling).

The results of the second 12 months phase are:

- (a) We have finished the program for analyzing spherical patch arrays. The newly developed part of the program calculates:
- mutual coupling between each two patches in the array
 - radiation pattern of the array when all mutual couplings are taken into account
 - aperture coupling as a feeding possibility.
- (b) We have developed an experimental model for testing the program for analyzing spherical arrays since there are only a few experimental results in literature in connection with spherical patch antennas.

The developed programs are written in FORTRAN program language since there is no faster program language for computational physics (computational electromagnetics). Program is independent on the machine, and it can be compiled and run on every machine that has FORTRAN 90 compiler. Furthermore, for MS Windows PC environment, a graphical user interface is developed to make setting of input parameters easier, and to obtain graphical presentation of the results. On other machines or operating systems communication with the program is made via input/output ASCII files. In more details, the input file should be filled before running the program, and the results are written into the output file that can be graphically presented by any graphical program.

4 PROJECT OUTCOMES

4.1 Analysis of microstrip patch antennas on spherical structures

4.1.1 Introduction

The purpose of this chapter is to describe a program that analyzes microstrip patch arrays on spherical structures. The patches can be of rectangular or circular shape, and the spherical dielectric structure can be multilayered. The program calculates radiation pattern of the array, input impedance of each patch element and mutual coupling coefficients between each two patch elements. The patches can be fed by coaxial or microstrip transmission line, or they can be aperture-coupled (the model for analyzing aperture-coupled patches is described in next chapter). The structure is rigorously taken into account by using proper Green's functions, and the electric field integral equation is numerically solved by applying moment method.

4.1.2 Method of Analysis

The geometry of the problem is shown in Figure 4.1. The rectangular or circular patches are placed on or embedded in a multilayer spherical structure. The radius of the grounded sphere and of the patches are r_{GND} and r_{patch} , respectively. The dimensions of each quasi-rectangular patch are W_θ and W_ϕ ($W_\theta = 2\theta_p r_{patch}$, $W_\phi = 2\phi_p r_{patch}$) and the dimension of each circular patch is W_θ ($W_\theta = 2\theta_p r_{patch}$). The distances of the feeding point from the center of the patch in the θ and ϕ directions are θ_{feed} and ϕ_{feed} , respectively. Two types of feeding structures are analyzed in this chapter: coax line feeding and microstrip line feeding.

To determine the current on the patches, we consider the integral equation for electric field components tangential to the patches [1]:

$$(\mathbf{E}_{inc}(\mathbf{J}_{feed}) + \mathbf{E}_{scat}(\mathbf{J}_{patch}))_{tan} = 0 \quad (1)$$

Here \mathbf{J}_{feed} and \mathbf{J}_{patch} denote the current on the patch and the feeding structure, respectively. The unknown patch current is expanded into sum of the basis functions:

$$\mathbf{J}_{patch} = \sum_{i=1}^N \alpha_i \mathbf{J}_i \quad (2)$$

The unknown coefficients α_i are determined by applying the moment method (MoM). We have used the same test functions as basis functions (Galerkin's method).

$$-\sum_{i=1}^N \alpha_i (\mathbf{J}_j, \mathbf{E}_{scat}(\mathbf{J}_i)) = (\mathbf{J}_j, \mathbf{E}_{inc}(\mathbf{J}_{feed})) . \quad (3)$$

The elements of the impedance matrix $[Z_{ji}]$ and voltage vector $[V_i]$ inside the moment method ($[Z_{ji}] \cdot [\alpha_i] = [V_i]$) are calculated in the spectral domain. Since the problem is defined in the spherical coordinate system we apply the vector-Legendre transformation to the patch current [2] - [4]. This technique transforms the three-dimensional problem into spectrum of one-dimensional problems.

$$\mathbf{J}(r, \theta, \phi) = \begin{bmatrix} J_r \\ J_\theta \\ J_\phi \end{bmatrix} = \sum_{m=-\infty}^{\infty} \sum_{n=|m|}^{\infty} \bar{\mathbf{L}}(n, m, \theta) \tilde{\mathbf{J}}(r, n, m) e^{jm\phi} \quad (4a)$$

$$\tilde{\mathbf{J}}(r, n, m) = \frac{1}{2\pi S(n, m)} \int_{-\pi}^{\pi} \int_0^{\pi} \bar{\mathbf{L}}(n, m, \theta) \mathbf{J}(r, \theta, \phi) \sin\theta e^{-jm\phi} d\theta d\phi \quad (4b)$$

$$\bar{\mathbf{L}}(n, m, \theta) = \begin{bmatrix} P_n^{|m|}(\cos\theta) \sqrt{n(n+1)} & 0 & 0 \\ 0 & \frac{\partial P_n^{|m|}(\cos\theta)}{\partial \theta} & \frac{-jm P_n^{|m|}(\cos\theta)}{\sin\theta} \\ 0 & \frac{jm P_n^{|m|}(\cos\theta)}{\sin\theta} & \frac{\partial P_n^{|m|}(\cos\theta)}{\partial \theta} \end{bmatrix} \quad (4c)$$

$$S(n, m) = \frac{2n(n+1)(n+|m|)!}{(2n+1)(n-|m|)!} \quad (4d)$$

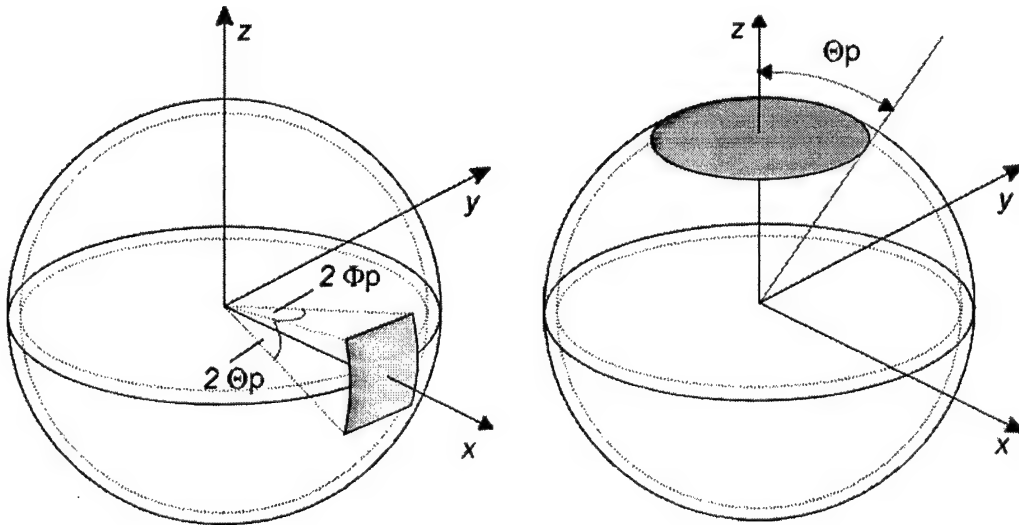


Figure 4.1. Patch antennas on spherical structure. (a) rectangular patch, (b) circular patch.

Here $P_n^{(m)}(\cos\theta)$ are the associated Legendre functions of the first kind. The elements of the moment method matrix Z_{ji} can be expressed as:

$$Z_{ji} = - \int_{patch} \mathbf{J}_j^T(r_{patch}, \theta, \phi) \left(\sum_m \sum_{n>|m|} \bar{\mathbf{L}}(m, n, \theta) \bar{\bar{\mathbf{G}}}(m, n) \tilde{\mathbf{J}}_i(m, n) e^{jm\phi} \right) \cdot r_{patch}^2 \sin\theta \, d\theta \, d\phi \quad (5)$$

where \mathbf{J}_j^T is transposed test function, and $\bar{\bar{\mathbf{G}}}(m, n)$ and $\tilde{\mathbf{J}}_i(m, n)$ are the Green's function and the basis function in spectral domain. After changing the order of summation and integration we get

$$Z_{ji} = - \sum_m \sum_{n>|m|} 2\pi S(n, m) r_{patch}^2 \tilde{\mathbf{J}}_j^T(-m, n) \bar{\bar{\mathbf{G}}}(m, n) \tilde{\mathbf{J}}_i(m, n) \quad (6)$$

In the case of the coax feeding, the radius of the probe is usually a very small fraction of the wavelength and the quantity $r_{patch} - r_{GND}$ is usually small in comparison to the wavelength. Therefore, the probe is modeled as a filament with a constant current

$$\mathbf{J}_{feed}(r, \theta, \phi) = \hat{r} \frac{1}{r^2 \sin\theta} \delta(\theta - \theta_{feed}) \delta(\phi - \phi_{feed}) \quad r_{GND} \leq r \leq r_{patch}, \quad (7)$$

where θ_{feed} and ϕ_{feed} are the θ and ϕ coordinates of the coax probe. The microstrip line can be also simply modeled by a filament with a constant current placed close to the edge of the patch since microstrip line and coax line have similar field distribution around the feeding point. Furthermore, if the feeding point of the coax line is close to the patch edge, the input impedances of the patch antennas fed by a microstrip line and fed by a coax line are very similar [5] - [7].

Using the reaction theorem we can calculate the elements of the excitation vector for coaxially-fed patch antennas as

$$V_j = (\mathbf{J}_{feed}, \mathbf{E}_{scat}(\mathbf{J}_j)) \quad (8a)$$

$$V_j = \sum_m \sum_{n>|m|} \bar{\mathbf{L}}(m, n, \theta_{feed}) e^{jm\phi_{feed}} \int_{probe} \bar{\bar{\mathbf{G}}}(r, m, n) \tilde{\mathbf{J}}_i(m, n) dr \quad (8b)$$

4.1.3 Calculation of Green's Function

The Green's functions are determined in spectral domain, which was one of the reasons for using spectral approach. The G1DMULT subroutine calculates spectral domain Green's functions of planar, circular cylindrical and spherical multilayer structures. For each input value of the spectral variables the subroutine calculates the value of the electric and magnetic field at user-specified locations inside or outside the multilayer structure. The structure parameters are given as inputs to the subroutine. The material layers can have arbitrary complex permittivities and permeabilities.

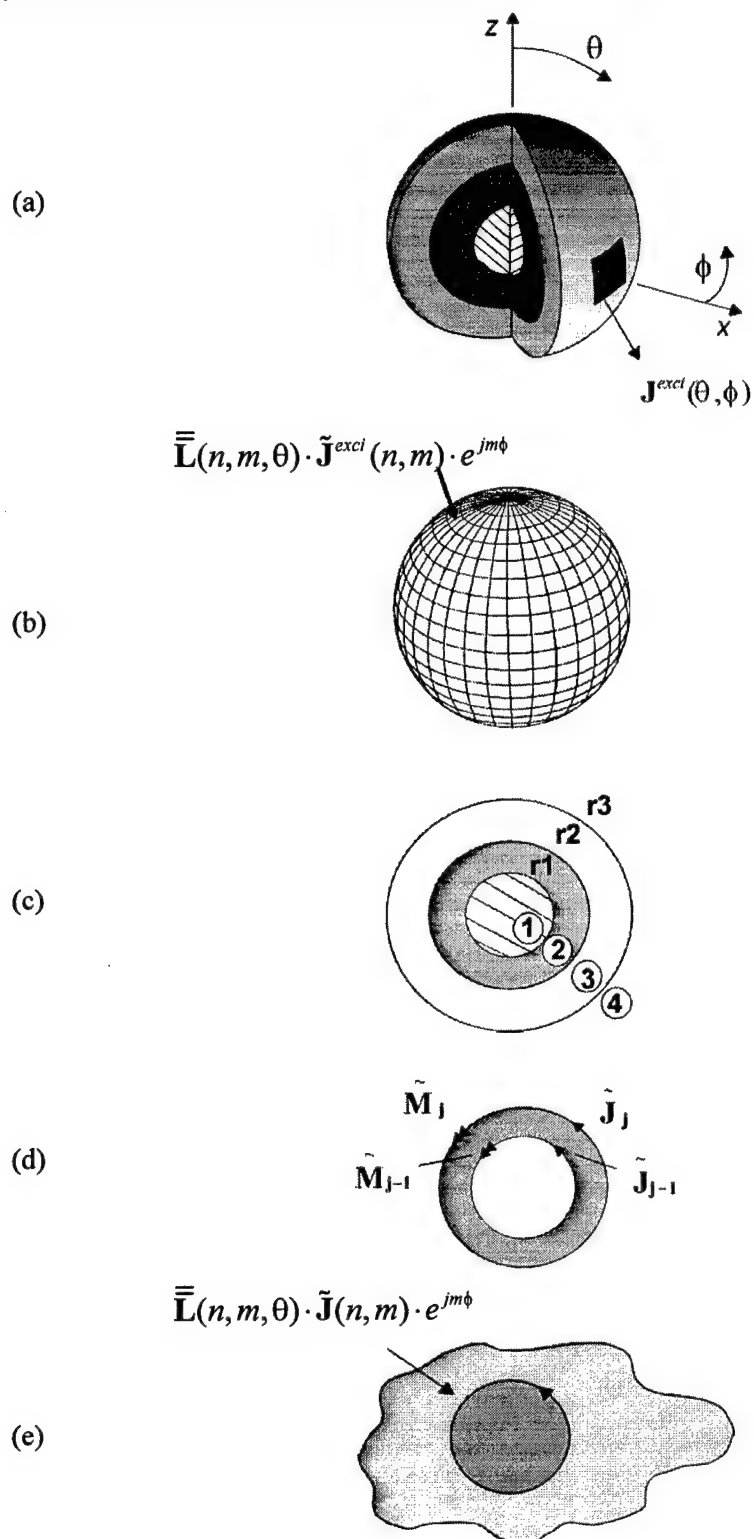


Figure 4.2. Structuring of a 3D field problem with a spherical layered structure into subproblems.

The solution procedure makes use of the Fourier transformation technique. The 3D elements (Fig 4.2.a) are replaced by equivalent or physical current excitations of electric and magnetic type, which are then Fourier transformed. By the vector Legendre transformation, the 3D excitations are transformed into harmonic current shells (see Fig. 4.2.b). If the source is infinitely thin in r direction, we get one discrete current shell per source, otherwise we get a continuous distribution of current shells in r -direction. The E- and H-fields induced by the harmonic current sources have the same harmonic variations in θ and ϕ as the source. Therefore, only the field variation in the direction perpendicular to the boundaries is unknown, so we have a harmonic one-dimensional (1D) field problem. In this way the spectral domain problem is interpreted as a 1D spatial domain problem consisting of the 1D multilayer structure and harmonic 1D sources in the form of current shells.

The harmonic 1D problem is solved by making use of equivalent problems, one for each layer (Figs. 4.2.c and 4.2.d). The unknowns are the tangential E- and H- fields at the layer boundaries. Since the variation of the E- and H-fields in the direction tangential to the boundaries is harmonic with known periodicity, we only need to determine the complex field amplitudes at the interfaces, i.e., we have four unknowns per boundary. The algorithm connects all equivalent subproblems into a system of $4(N_{\text{layer}}-1)$ linear equations with the same number of unknowns (N_{layer} denotes the number of layers). Once the amplitudes of the tangential fields have been determined, it is easy to determine the field amplitudes anywhere in the multilayer structure by applying the homogeneous region equivalent of the layer inside which we want to determine the field value. The core problem in the formulation is to calculate the E- and H- fields due to a harmonic current shell in a homogeneous region (Fig. 4.2.e). More details about the G1DMULT algorithm can be found in [8].

4.1.4 Numerical Considerations

4.1.4.1 New definition of vector-Legendre transformation and normalized Legendre polynomials

We notice numerical problems in calculating Legendre polynomials and $S(n,m)$ for large n , specially if $m \approx n$ when both Legendre polynomials and $S(n,m)$ become very large, and the solution is unstable (both terms are needed for performing the vector-Legendre transformation; notice that the number of used modes depends on the structure radius). To find a numerically stable solution first we have introduced an alternative definition of the vector-Legendre transformation:

$$\mathbf{J}(r, \theta, \phi) = \sum_{m=-\infty}^{\infty} \sum_{n=|m|}^{\infty} \frac{1}{\sqrt{2\pi S(n,m)}} \bar{\bar{\mathbf{L}}}(n, m, \theta) \tilde{\mathbf{J}}(r, n, m) e^{jm\phi}, \quad (9a)$$

$$\tilde{\mathbf{J}}(r, n, m) = \int_{-\pi}^{\pi} \int_0^{\pi} \frac{1}{\sqrt{2\pi S(n,m)}} \bar{\bar{\mathbf{L}}}(n, m, \theta) \mathbf{J}(r, \theta, \phi) \sin\theta e^{-jm\phi} d\theta d\phi. \quad (9b)$$

The expressions for $\bar{\bar{\mathbf{L}}}(n, m, \theta)$ and $S(n, m)$ are the same as before (see equations (4.c) and (4.d)). The new definition of the vector-Legendre transformation and the inverse vector-Legendre transformation is symmetric, i.e. in both cases Legendre polynomials and their derivatives, appearing in matrix $\bar{\bar{\mathbf{L}}}(n, m, \theta)$, are divided with $\sqrt{S(n, m)}$.

Second step in finding numerically stable solution has been in defining normalized Legendre polynomials $\bar{P}_n^{|m|}$ and their derivatives as

$$\bar{P}_n^{|m|} = P_n^{|m|} \sqrt{\frac{(n-|m|)!}{(n+|m|)!}}, \quad \frac{\partial \bar{P}_n^{|m|}(\cos\theta)}{\partial \theta} = \frac{\partial P_n^{|m|}(\cos\theta)}{\partial \theta} \sqrt{\frac{(n-|m|)!}{(n+|m|)!}}. \quad (10)$$

Notice that for normalization factor we have chosen the rapidly growing term inside $\sqrt{S(n,m)}$ (see eq. (4.d)). By using the following asymptotic formulas [9]

$$P_n^{|m|}(\cos\theta) \cong \frac{\Gamma(n+|m|+1)}{\Gamma(n+3/2)} \sqrt{\frac{2}{\pi \sin\theta}} \cos \left[\left(n + \frac{1}{2} \right) \theta - \frac{\pi}{4} + \frac{|m|\pi}{2} \right], \quad (11)$$

$$\lim_{n \rightarrow \infty} \frac{\Gamma(n+a)}{\Gamma(n+b)} = n^{a-b}, \quad (12)$$

the normalized Legendre functions converge for large n to the expression

$$\lim_{n \rightarrow \infty} \bar{P}_n^{|m|}(\cos\theta) = \lim_{n \rightarrow \infty} P_n^{|m|}(\cos\theta) \sqrt{\frac{(n-|m|)!}{(n+|m|)!}} = \sqrt{\frac{2}{\pi n \sin\theta}} \cos \left[\left(n + \frac{1}{2} \right) \theta - \frac{\pi}{4} + \frac{|m|\pi}{2} \right]. \quad (13)$$

Notice that it is numerically stable to calculate the upper expression. The term $\bar{L}/\sqrt{S(n,m)}$ in equations (9a) and (9b) enables us to calculate normalized Legendre polynomials instead of Legendre polynomials, and $2n(n+1)/(2n+1)$ instead of $S(n,m)$, both of them are numerically stable. Thus, divisions of very large numbers are avoided.

The recursive equations for the normalized Legendre polynomials and their derivatives are:

$$\bar{P}_{n+1}^{|m|}(z) \sqrt{(n+1+|m|)(n+|m|)} = \frac{1}{n-|m|+1} \cdot \left((2n+1) z \bar{P}_n^{|m|}(z) \sqrt{(n+|m|)(n-|m|+1)} - (n+|m|) \bar{P}_{n-1}^{|m|}(z) \sqrt{(n-|m|)(n-|m|+1)} \right), \quad (14)$$

$$(z^2-1) \frac{\partial \bar{P}_n^{|m|}(z)}{\partial z} \sqrt{n+|m|} = n z \bar{P}_n^{|m|}(z) \sqrt{n+|m|} - (n+|m|) \bar{P}_{n-1}^{|m|}(z) \sqrt{n-|m|}. \quad (15)$$

With the new definition of vector-Legendre transformation the elements needed for moment method procedure are calculated as:

$$Z_{ji} = - \sum_m \sum_{n>|m|} r_{patch}^2 \tilde{\mathbf{J}}_j^T(-m,n) \tilde{\tilde{\mathbf{G}}}(m,n) \tilde{\mathbf{J}}_i(m,n) \quad (16)$$

$$V_j = \sum_m \sum_{n=|m|} \frac{1}{\sqrt{2\pi S(n,m)}} \tilde{\tilde{\mathbf{L}}}(m,n,\theta_{feed}) e^{jmb_{feed}} \int_{probe} \tilde{\tilde{\mathbf{G}}}(r,m,n) \tilde{\mathbf{J}}_i(m,n) dr \quad (17)$$

4.1.4.2 Asymptotic formulas for spherical Bessel and Hankel functions

The Green's functions for spherical structures contain the Schelkunoff type of spherical Bessel and Hankel functions, see Appendix II. We notice numerical problems in calculating Bessel/Hankel functions of large order (e.g. of order larger than 200; this happens when the radius of the structure is large). Therefore, special techniques are needed to handle cylinders with large radii. We have implemented Debye's asymptotic formulas for Bessel and Hankel functions of large orders [9], [10]

$$\hat{J}_m(x) \cong \frac{e^{(m+1/2)(\tanh \alpha - \alpha)} \sqrt{x}}{\sqrt{4(m+1/2) \tanh \alpha}} \left[1 + \frac{3t - 5t^3}{24(m+1/2)} \right] \quad (18a)$$

$$\hat{H}_m^{(2)}(x) \cong j \frac{e^{(m+1/2)(\alpha - \tanh \alpha)} \sqrt{x}}{\sqrt{(m+1/2) \cdot \tanh \alpha}} \left[1 - \frac{3t - 5t^3}{24(m+1/2)} \right]. \quad (18b)$$

where α and t are defined as $\cosh \alpha = (m+1/2)/x$ and $t = \coth \alpha$. Notice that the exponential parts of Bessel and Hankel approximate formulas have opposite behavior, i.e. the arguments of the exponential functions have the same absolute values and opposite signs. On the other hand Green's functions for spherical multilayer structures can be written in terms of products $\hat{J}_m(\cdot) \hat{H}_m^{(2)}(\cdot)$ (see Appendix II for exact expressions). Therefore, Debye's asymptotic formulas are applied to products $\hat{J}_m(\cdot) \hat{H}_m^{(2)}(\cdot)$ with extracted exponential parts, and thereby, we avoid numerical problems. The condition for order m of Bessel/Hankel functions at which asymptotic formulas start to be used take care that $|m-x| \geq |x|^{1/3}$ for all used arguments x [10].

4.1.5 Mutual Coupling

First step in determining S -parameters is to determine the currents on all patches, i.e. the integral equation for tangential components of the electric field is solved by applying the moment method. For N patches in the array, we need to solve the linear system $[Z][\alpha^k] = [V^k]$ N times ($k = 1, \dots, N$), once for each excitation port. In more details, $[V^k]$ vectors correspond to a physical situation in which a unit current is entering the k th port while the remaining $N-1$ ports are open-circuited. Fortunately, the matrix $[Z]$ is unchanged in all cases.

After determining the amplitudes of basis functions $[\alpha^k]$ we calculate the voltage at port l by summation $-\sum_i V_i^l \alpha_i^k$, i.e., the lk element of the impedance port matrix is

$$Z_{lk}^{port} = -\sum_i V_i^l \alpha_i^k. \quad (19)$$

Scattering matrix elements are calculated from the impedance port matrix:

$$[S] = ([Z^{port}] - [Z^0])([Z^{port}] + [Z^0])^{-1} \quad (20)$$

where $[Z^0]$ is a diagonal matrix with elements Z^0 - the characteristic impedance of the feeding transmission lines.

The elements of the moment method matrix Z_{ji} are excitation vector V_j are calculated in the spectral domain. The expression for element of the moment method matrix Z_{ji} is:

$$Z_{ji} = - \sum_m \sum_{n > |m|} r_{patch}^2 \tilde{\mathbf{J}}_j^T(-m, n) \tilde{\mathbf{G}}(m, n) \tilde{\mathbf{J}}_i(m, n) \quad (21)$$

In matrix notation equation (21) can be written as:

$$[Z]_{ji} = - \sum_m \sum_{n > |m|} [\tilde{\mathbf{Z}}]_{ji}, \quad \tilde{\mathbf{Z}}_{ji}(n, m) = r_{patch}^2 \tilde{\mathbf{J}}_j^T(-m, n) \tilde{\mathbf{G}}(m, n) \tilde{\mathbf{J}}_i(m, n) \quad (22)$$

In the array case basis and test function can be located on different patches. In that case calculation of elements $\tilde{\mathbf{Z}}_{ji}$ is numerically complex.

Let us first consider mutual coupling between two patches displaced in the ϕ direction (see Fig. 4.3). If we assume that the test function is placed on the first patch and the basis function is placed on the second patch, then the element of moment method matrix is given as :

$$\begin{aligned} \tilde{\mathbf{Z}}_{ji}^{12}(n, m) &= r_{patch}^2 \left(\tilde{\mathbf{J}}_j^1(-m, n) \right)^T \tilde{\mathbf{G}}(m, n) \tilde{\mathbf{J}}_i^2(m, n) \\ &= r_{patch}^2 \left(\tilde{\mathbf{J}}_j^c(-m, n) \right)^T \tilde{\mathbf{G}}(m, n) \tilde{\mathbf{J}}_i^c(m, n) e^{jm(\beta_1 - \beta_2)} \end{aligned} \quad (23)$$

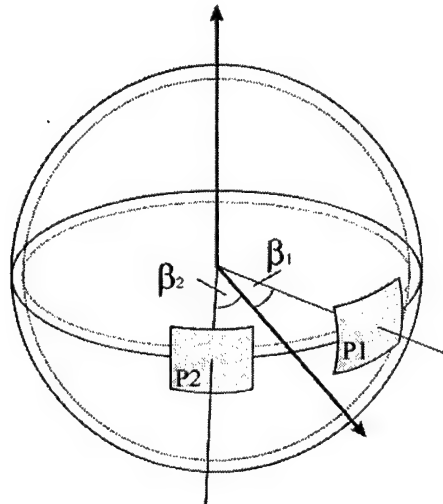


Figure 4.3. Patch array of two patches displaced in the ϕ direction.

Here the upper indexes 1,2 denote the patch number where the basis/test function is located, and the index c denotes the centered basis or test function (i.e. the center has coordinates $\theta = \pi/2$ and $\phi = 0$). In matrix notation the moment method matrix has a shape

$$[\tilde{Z}] = \begin{bmatrix} \begin{bmatrix} \tilde{Z}_{11}^{cc} & \tilde{Z}_{12}^{cc} & \dots & \tilde{Z}_{1B}^{cc} \\ \tilde{Z}_{21}^{cc} & \tilde{Z}_{22}^{cc} & \dots & \tilde{Z}_{2B}^{cc} \\ \dots & \dots & \dots & \dots \\ \tilde{Z}_{B1}^{cc} & \tilde{Z}_{B2}^{cc} & \dots & \tilde{Z}_{BB}^{cc} \end{bmatrix} & \begin{bmatrix} \tilde{Z}_{11}^{cc} & \tilde{Z}_{12}^{cc} & \dots & \tilde{Z}_{1B}^{cc} \\ \tilde{Z}_{21}^{cc} & \tilde{Z}_{22}^{cc} & \dots & \tilde{Z}_{2B}^{cc} \\ \dots & \dots & \dots & \dots \\ \tilde{Z}_{B1}^{cc} & \tilde{Z}_{B2}^{cc} & \dots & \tilde{Z}_{BB}^{cc} \end{bmatrix} e^{jm(\beta_1 - \beta_2)} \\ e^{jm(\beta_2 - \beta_1)} \begin{bmatrix} \tilde{Z}_{11}^{cc} & \tilde{Z}_{12}^{cc} & \dots & \tilde{Z}_{1B}^{cc} \\ \tilde{Z}_{21}^{cc} & \tilde{Z}_{22}^{cc} & \dots & \tilde{Z}_{2B}^{cc} \\ \dots & \dots & \dots & \dots \\ \tilde{Z}_{B1}^{cc} & \tilde{Z}_{B2}^{cc} & \dots & \tilde{Z}_{BB}^{cc} \end{bmatrix} & \begin{bmatrix} \tilde{Z}_{11}^{cc} & \tilde{Z}_{12}^{cc} & \dots & \tilde{Z}_{1B}^{cc} \\ \tilde{Z}_{21}^{cc} & \tilde{Z}_{22}^{cc} & \dots & \tilde{Z}_{2B}^{cc} \\ \dots & \dots & \dots & \dots \\ \tilde{Z}_{B1}^{cc} & \tilde{Z}_{B2}^{cc} & \dots & \tilde{Z}_{BB}^{cc} \end{bmatrix} \end{bmatrix} \quad (24)$$

where B denotes the number of basis/test functions defined at each patch. Notice that numerically there is no difference in analyzing a single patch and an array of patches with centers located at the line $\theta = 90^\circ$.

For calculating mutual coupling between two patches spaced in θ direction (see Fig. 4.4) it has been found convenient to introduce local coordinate systems with origins located at the center of each patch antenna. The vector-Legendre transformation of the basis/test function located at the displaced patch is calculated using transformation of coordinates from global to local coordinate system. In this way the basis function in the spectral domain is:

$$\tilde{J}(r, n, m) = \frac{1}{\sqrt{2\pi S(n, m)}} \int_{\text{patch}} \bar{L}(m, n, \theta) \sin\theta e^{-jm\phi} J(r, \theta', \phi') \left| \frac{\partial(\theta, \phi)}{\partial(\theta', \phi')} \right| d\theta' d\phi' \quad (25)$$

where θ' and ϕ' are coordinates in local coordinate system and $|\partial(\theta, \phi)/\partial(\theta', \phi')|$ is the Jacobian determinant

$$\left| \frac{\partial(\theta, \phi)}{\partial(\theta', \phi')} \right| = \begin{vmatrix} \frac{\partial\theta}{\partial\theta'} & \frac{\partial\theta}{\partial\phi'} \\ \frac{\partial\phi}{\partial\theta'} & \frac{\partial\phi}{\partial\phi'} \end{vmatrix} \quad (26)$$

The transformation from global to local coordinate system is given by [11]

$$\cos\theta' = \sin(\alpha - \pi/2) \sin\theta \cos(\phi - \beta) + \cos(\alpha - \pi/2) \cos\theta \quad (27a)$$

$$\cot\phi' = \frac{\cos(\alpha - \pi/2) \sin\theta \cos(\phi - \beta) - \sin(\alpha - \pi/2) \cos\theta}{\sin\theta \sin(\phi - \beta)} \quad (27b)$$

Here α and β are the θ - and ϕ -coordinates of the patch center. To make calculations faster we have “forced” separation of θ and ϕ variables (which is strictly not possible) and approximated the double integral with calculating numerically only θ integration. In ϕ -direction we have supposed that the patch has constant width (i.e that the patch edges follow the constant ϕ -lines), and consequently we have performed the ϕ -integration analytically. Therefore, for each patch with different θ coordinate we need to numerically calculate the following integral

$$\int \bar{L}(m, n, \theta) \sin \theta J(\theta) \frac{d\theta}{d\theta} d\theta$$

The moment method matrix for two patches displaced in θ -direction using B basis function is given as:

$$[\tilde{Z}] = \begin{bmatrix} \tilde{Z}_{11}^{cc} \tilde{Z}_{12}^{cc} \dots \tilde{Z}_{1B}^{cc} \\ \tilde{Z}_{21}^{cc} \tilde{Z}_{22}^{cc} \dots \tilde{Z}_{2B}^{cc} \\ \dots \dots \dots \\ \tilde{Z}_{B1}^{cc} \tilde{Z}_{B2}^{cc} \dots \tilde{Z}_{BB}^{cc} \\ \tilde{Z}_{11}^{21} \tilde{Z}_{12}^{21} \dots \tilde{Z}_{1B}^{21} \\ \tilde{Z}_{21}^{21} \tilde{Z}_{22}^{21} \dots \tilde{Z}_{2B}^{21} \\ \dots \dots \dots \\ \tilde{Z}_{B1}^{21} \tilde{Z}_{B2}^{21} \dots \tilde{Z}_{BB}^{21} \end{bmatrix} \begin{bmatrix} \tilde{Z}_{11}^{12} \tilde{Z}_{12}^{12} \dots \tilde{Z}_{1B}^{12} \\ \tilde{Z}_{21}^{12} \tilde{Z}_{22}^{12} \dots \tilde{Z}_{2B}^{12} \\ \dots \dots \dots \\ \tilde{Z}_{B1}^{12} \tilde{Z}_{B2}^{12} \dots \tilde{Z}_{BB}^{12} \\ \tilde{Z}_{11}^{cc} \tilde{Z}_{12}^{cc} \dots \tilde{Z}_{1B}^{cc} \\ \tilde{Z}_{21}^{cc} \tilde{Z}_{22}^{cc} \dots \tilde{Z}_{2B}^{cc} \\ \dots \dots \dots \\ \tilde{Z}_{B1}^{cc} \tilde{Z}_{B2}^{cc} \dots \tilde{Z}_{BB}^{cc} \end{bmatrix} \quad (28)$$

Notice that boldfaced elements of the moment method matrix have to be calculated using basis function in the local coordinate system. If the patches are displaced both in θ and ϕ directions, then we need to combine both described methods.

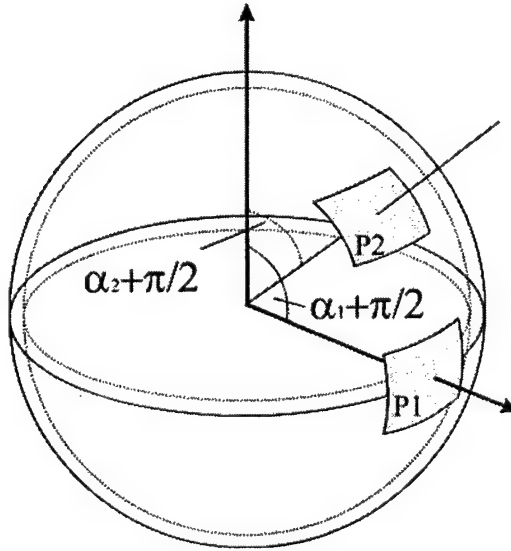


Figure 4.4. Patch array of two patches displaced in the θ -direction.

The accuracy of calculation of basis function in spectral domain is shown in Fig. 4.5. The S_{21} coefficient, calculated both in a rigorous and in an approximate way, is compared for patches displaced in E- and H-plane. One of the patches was placed at center position ($\theta = \pi/2, \phi = 0$), and the other patch was moved in the θ -direction. The dimensions of the patches are $5.1 \text{ cm} \times 5.1 \text{ cm}$, and the considered spherical structure has the following parameters: $R_{\text{GND}} = 18.7 \text{ cm}$, $\epsilon_r = 1.0$; $h = 0.52 \text{ cm}$. It can be seen that we can apply the approximate way of calculating spectral-domain basis functions except for rectangular patches placed in small regions around the poles.

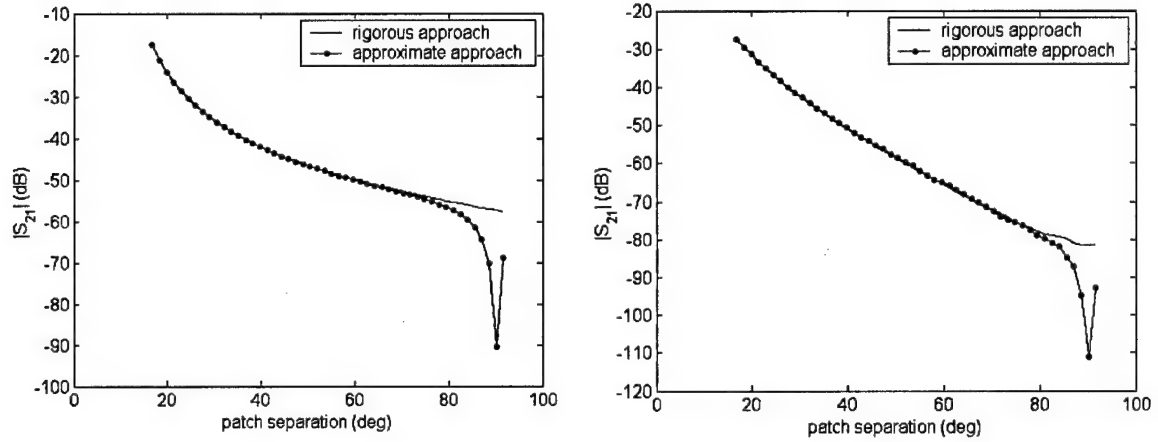


Figure 4.5. Comparison of rigorous and approximate way of calculating vector-Legendre transformation of basis and test functions. (a) coupling in E-plane, (b) coupling in H-plane.

4.1.6 Far-Field Calculations

The far field radiation pattern is obtained as follows. If we consider for example the ϕ -component of the electric field in the outermost region with the r -coordinate larger than the r -coordinate of the patch, we have only outward-traveling waves described by $a_{nm}^i \hat{H}_n^{(2)}(k_0 r)$. Therefore, in the outermost region we can connect the ϕ -component of the electric field with different r -coordinates r_1 and r_2 as

$$\tilde{E}_\phi(r_1, n, m) = \tilde{E}_\phi(r_2, n, m) \frac{\hat{H}_n^{(2)}(k_0 r_1)}{\hat{H}_n^{(2)}(k_0 r_2)} \approx \tilde{E}_\phi(r_2, n, m) \frac{j^{n+1} e^{-jk_0 r_1}}{\hat{H}_n^{(2)}(k_0 r_2)} \quad (29)$$

Here r_1 represents the r -component of the far field pattern. The final solution is obtained by superposing the spectral solutions, see eq. (4). When calculating far field of spherical array it has been found convenient to introduce a local coordinate system with the origin located at the position of each antenna element. For circular patches the z' -axis of local system is oriented along the direction of the pattern maximum of the individual element and the x' -axis is taken in the z - z' plane. If the center of the patch element is at the point $P(r, \alpha_n, \beta_{nm})$ the coordinates in the local coordinate system are determined using the following transformation relations (see [11] for details):

$$\cos\theta' = \sin\alpha_n \sin\theta \cos(\phi - \beta_{nm}) + \cos\alpha_n \cos\theta \quad (30a)$$

$$\cot\phi' = \frac{\cos\alpha_n \sin\theta \cos(\phi - \beta_{nm}) - \sin\alpha_n \cos\theta}{\sin\theta \sin(\phi - \beta_{nm})} \quad (30b)$$

$$\hat{e}_{\theta'} = -\frac{\cos\theta \sin\alpha_n \cos(\phi - \beta_{nm}) - \sin\theta \cos\alpha_n}{\sin\theta'} \hat{e}_{\theta} + \frac{\sin\alpha_n \sin(\phi - \beta_{nm})}{\sin\theta'} \hat{e}_{\phi} \quad (30c)$$

$$\hat{e}_{\phi'} = -\frac{\sin\alpha_n \sin(\phi - \beta_{nm})}{\sin\theta'} \hat{e}_{\theta} - \frac{\cos\theta \sin\alpha_n \cos(\phi - \beta_{nm}) - \sin\theta \cos\alpha_n}{\sin\theta'} \hat{e}_{\phi} \quad (30d)$$

θ and ϕ field components produced by antenna element placed at the point $P(r, \alpha_n, \beta_{nm})$ are:

$$E_{\theta, \alpha_n \beta_{nm}} = -\left[\frac{\cos\theta \sin\alpha_n \cos(\phi - \beta_{nm}) - \sin\theta \cos\alpha_n}{\sin\theta'} f_{\theta}(\theta', \phi') + \frac{\sin\alpha_n \sin(\phi - \beta_{nm})}{\sin\theta'} f_{\phi}(\theta', \phi') \right] \quad (31a)$$

$$E_{\phi, \alpha_n \beta_{nm}} = \left[\frac{\sin\alpha_n \sin(\phi - \beta_{nm})}{\sin\theta'} f_{\theta}(\theta', \phi') - \frac{\cos\theta \sin\alpha_n \cos(\phi - \beta_{nm}) - \sin\theta \cos\alpha_n}{\sin\theta'} f_{\phi}(\theta', \phi') \right] \quad (31b)$$

For rectangular patches the x' axis of local system is oriented normal to the patch, i.e. for center element axes x and x' are in the same direction (see Fig. 4.1). If α_n and β_{nm} are the θ and ϕ coordinate of the patch center, the coordinates in the local coordinate system are determined using the following equations

$$\cos\theta' = \sin(\alpha_n - \pi/2) \sin\theta \cos(\phi - \beta_{nm}) + \cos(\alpha_n - \pi/2) \cos\theta \quad (32a)$$

$$\cot\phi' = \frac{\cos(\alpha_n - \pi/2) \sin\theta \cos(\phi - \beta_{nm}) - \sin(\alpha_n - \pi/2) \cos\theta}{\sin\theta \sin(\phi - \beta_{nm})} \quad (32b)$$

$$\hat{e}_{\theta'} = -\frac{\cos\theta \sin(\alpha_n - \pi/2) \cos(\phi - \beta_{nm}) - \sin\theta \cos(\alpha_n - \pi/2)}{\sin\theta'} \hat{e}_{\theta} + \frac{\sin(\alpha_n - \pi/2) \sin(\phi - \beta_{nm})}{\sin\theta'} \hat{e}_{\phi} \quad (32c)$$

$$\hat{e}_{\phi'} = -\frac{\sin(\alpha_n - \pi/2) \sin(\phi - \beta_{nm})}{\sin\theta'} \hat{e}_{\theta} - \frac{\cos\theta \sin(\alpha_n - \pi/2) \cos(\phi - \beta_{nm}) - \sin\theta \cos(\alpha_n - \pi/2)}{\sin\theta'} \hat{e}_{\phi} \quad (32d)$$

Far field produced by spherical antenna array is:

$$\mathbf{E}(\theta, \phi) = \sum_{n,m} \mathbf{E}_{\alpha_n \beta_{nm}}(\theta', \phi') \quad (33)$$

In order to steer the beam throughout the whole hemisphere the arrays should have a grid suitable for spherical structure, such as icosahedron structure depicted in figure 4.6. In this example the basic grid triangle element corresponds to $1/16$ of the triangle that builds up the icosahedron structure, i. e. side of the basic grid triangle equals to $1/4$ of the side of the icosahedron triangle.

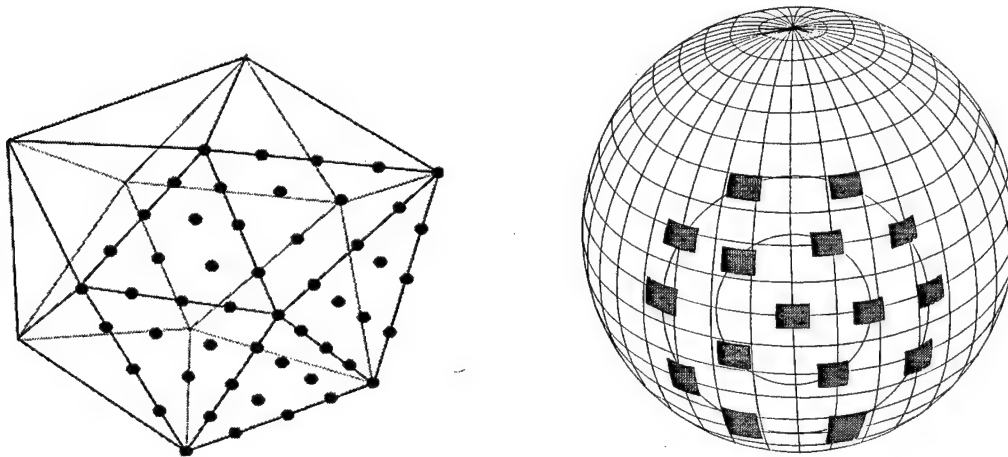


Figure 4.6. Spherical array following the icosahedron grid

4.1.7 Effects of the Sphere Curvature

The effects of the sphere size on the input impedance and radiation pattern will be illustrated in the following examples. The quasi-rectangular patch of dimension $2.5 \text{ cm} \times 4.0 \text{ cm}$ is printed on the single-layer dielectric substrate with dielectric constant $\epsilon_r = 2.52$ and thickness $h = 1.58 \text{ mm}$. Both θ - and ϕ -polarized patches are considered, and the patch length in resonance direction is 2.5 cm in both cases. The difference between two cases is in the patch shape, i.e. the patch edges follow the constant θ and ϕ lines (see Fig. 4.7). Therefore, the θ -polarized patch has constant length in resonance direction (2.5 cm), while the resonant length of the ϕ -polarized patches varies from 2.5 cm in the center of the patch up to 1.74 cm at the patch edge (for 2.5 cm sphere radius). The feed point is placed 1.1 cm from the patch center.

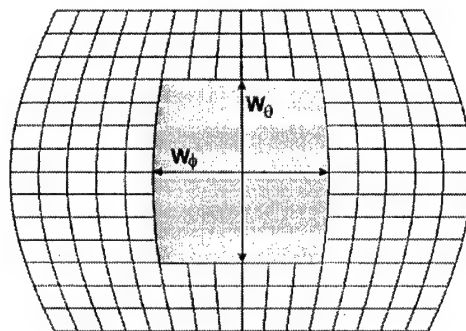


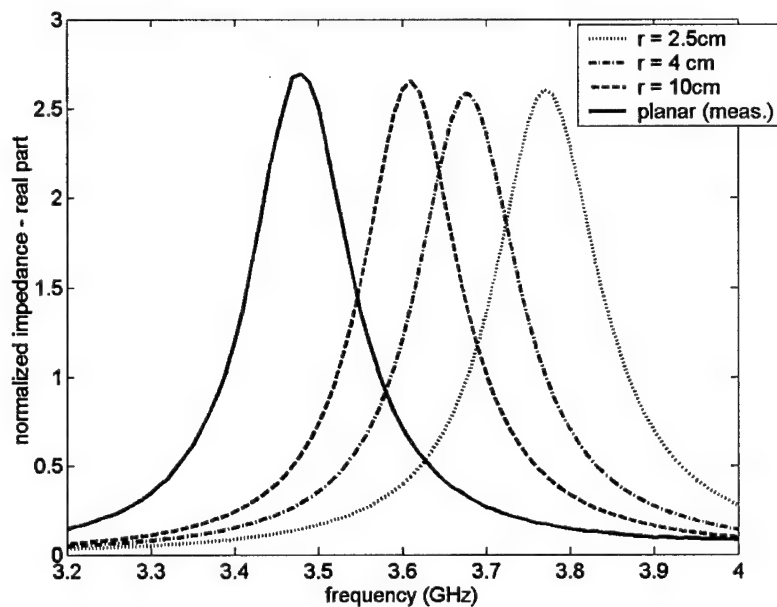
Figure 4.7. Geometry of the problem - azimuthal equatorial projection.

The influence of the sphere radius on input impedance of the spherical patch is shown in Figures 4.8 and 4.9. For comparison, the measured input impedance of the planar patch antenna with same dimensions is also given. It can be seen that the sphere radius mostly influences the resonant frequency, and the change of resonant frequency is stronger for the ϕ -polarized patch (since the average patch length is shorter for the ϕ -polarized patch). The resonant resistance is almost constant for the θ -polarized patch and it is slowly changing for the ϕ -polarized patch.

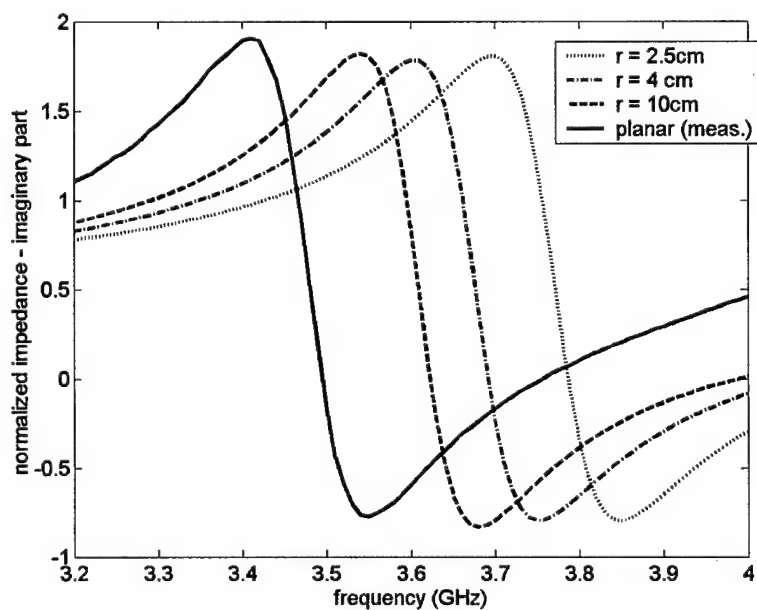
The effect of the radius of the ground plane (grounded shell) on radiation pattern is given in Fig. 4.10. For comparison, the calculated radiation pattern of the planar patch antenna with same dimensions is also given. The operating frequency is 3.6 GHz. It can be seen that with enlarging the radius of the sphere the main lobe of the spherical patch antenna approaches the main lobe of the planar counterpart. As expected, the back-radiation is smaller for spheres with larger radius.

For building up a spherical array grid, the icosahedron structure is very suitable basis. Beside the beam steering throughout the whole hemisphere, this grid enables beam width variation by changing the number of excited elements. To illustrate this, radiation pattern calculation of a spherical array with a grid as depicted in figure 4.6 (where basic triangle side is 1/4 of the icosahedron triangle) is performed. Activated area, i. e. amount of excited elements was varied from angle $\alpha = 15, 30$ and 45 degrees. This corresponds to 6, 16 and 31 activated elements, respectively. The example in Fig. 4.6b corresponds to $\alpha = 30$ degrees. The array grounded shell radius is 20 cm, size of the patches is $2.5 \text{ cm} \times 2.5 \text{ cm}$, and substrate and frequency of analysis are the same as in Figs. 4.8 - 4.10. The patches are phase corrected in order to compensate the propagation path difference. The radiation pattern for all three different activated areas is given in figure 4.11. As expected, with enlarging the number of activated elements the main beam is narrower. However, the back radiation increases with increase of number of activated elements.

The influence of the sphere radius on mutual coupling level is shown in Fig. 4.12. Two rectangular patches of dimension $10.57 \text{ cm} \times 6.55 \text{ cm}$ are printed on the single-layer dielectric substrate with dielectric constant $\epsilon_r = 2.5$ and thickness $h = 1.575 \text{ mm}$. The position of the probe is 1.5 cm from the center of the patch. The working frequency for planar patch is 1.41 GHz. For spherical case the working frequency is changed a bit in order to obtain good matching (the needed shift of resonant frequency depends on the sphere radius). The magnitude of the S_{21} parameter, both in E- and H-plane, is shown as a function of spacing between patch edges. For comparison, the measured results of planar case are also given [12]. It can be seen that the coupling is weaker for spherical case in comparison to the planar one, especially in H-plane. However, for smaller structure radii mutual coupling starts to be oscillatory.



(a)



(b)

Figure 4.8. Input impedance of a θ -polarized quasi-rectangular patch printed on a spherical structure for different sphere radii; (a) real part, (b) imaginary part.

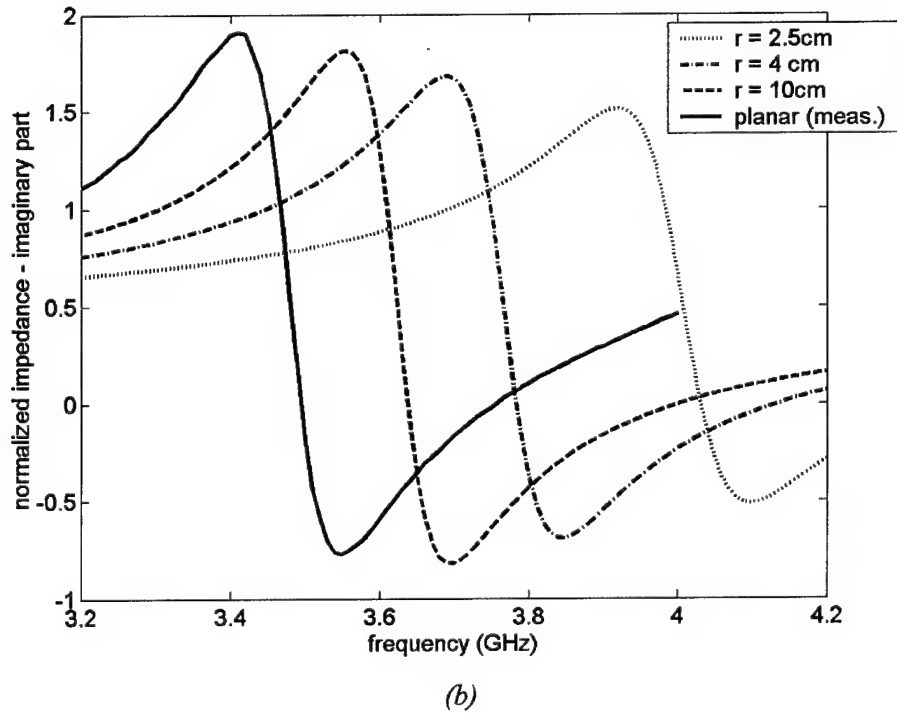
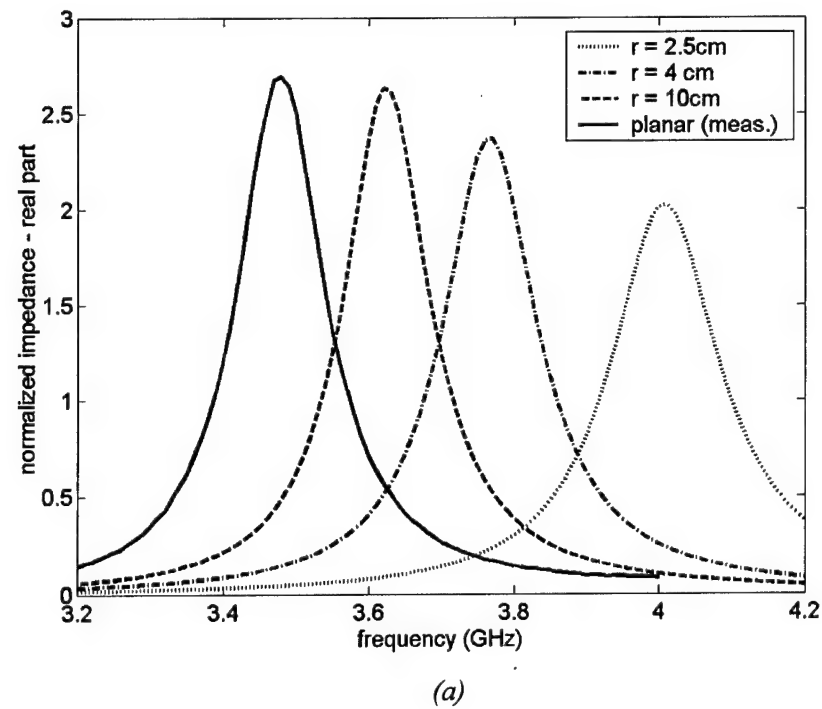
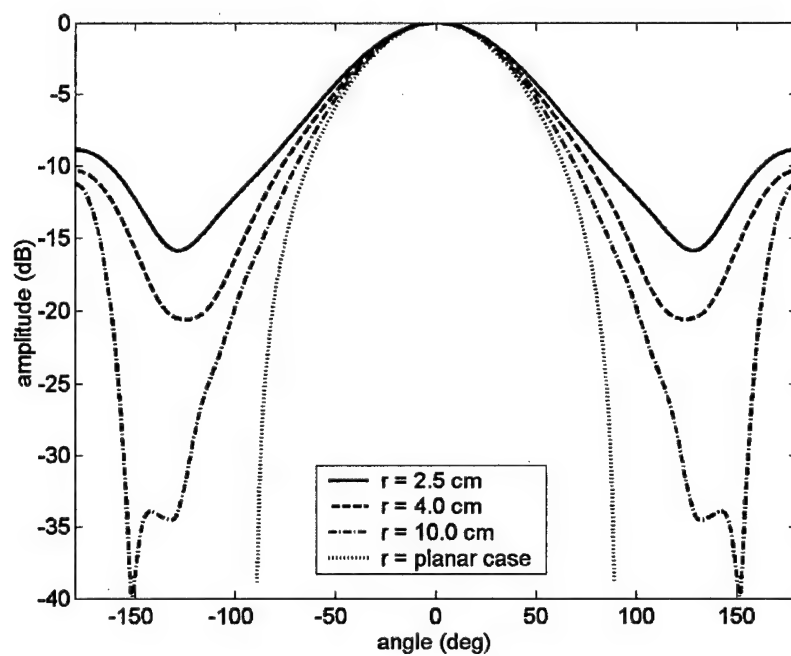
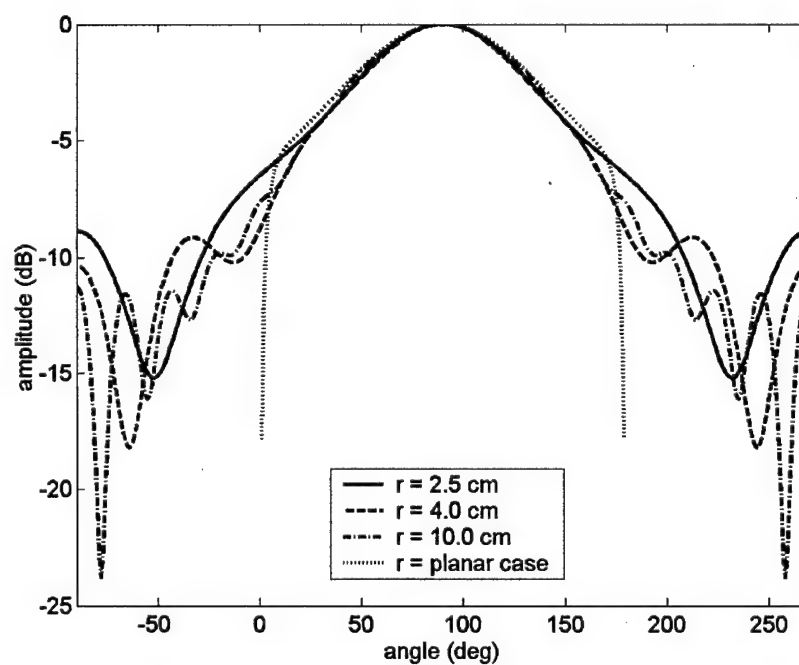


Figure 4.9. Input impedance of a ϕ -polarized quasi-rectangular patch printed on a spherical structure for different sphere radii; (a) real part, (b) imaginary part.

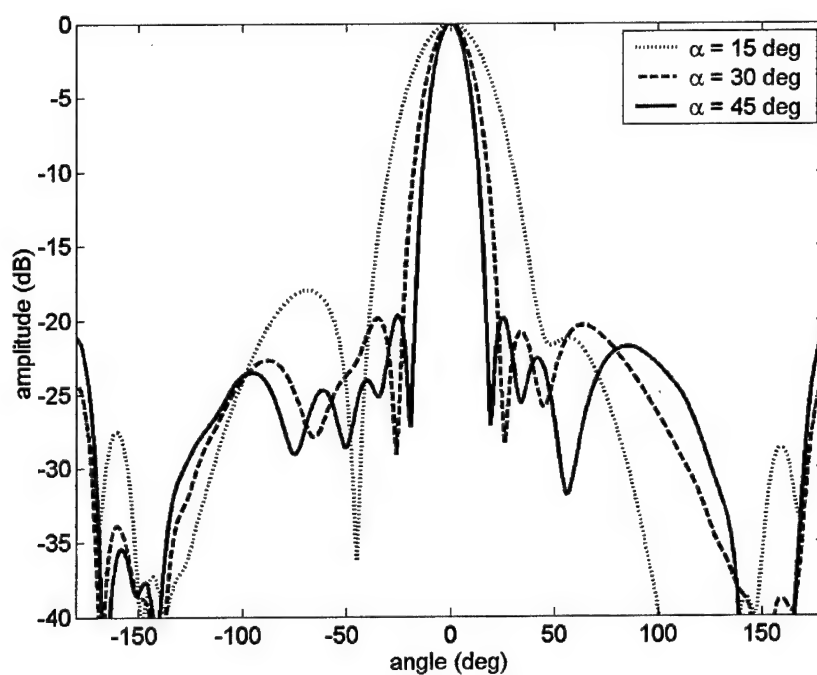


(a)

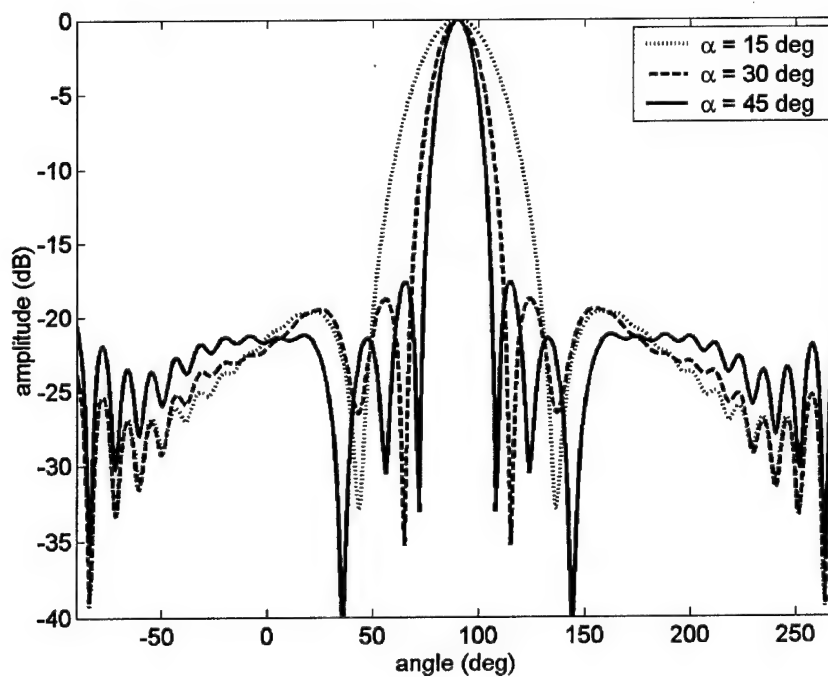


(b)

Figure 4.10. Radiation pattern of a spherical rectangular patch antenna for different sphere radii; (a) H-plane, (b) E-plane.



(a)



(b)

Figure 4.11. Radiation pattern of a spherical patch array with elements placed uniformly by utilizing the symmetry properties of the icosahedron. (a) H-plane, (b) E-plane.

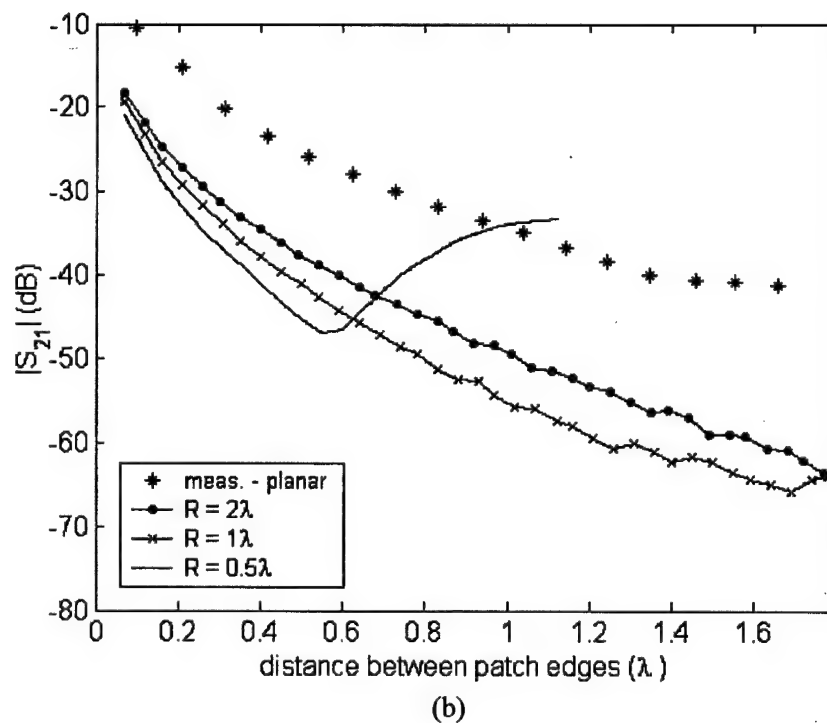
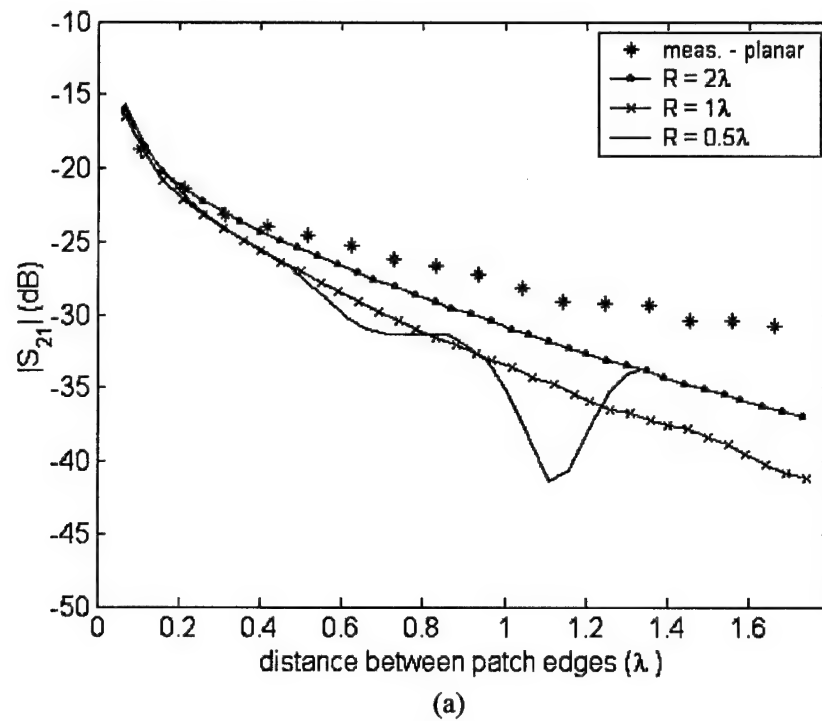


Figure 4.12. Magnitude of S_{21} parameter of a two-patch array as a function of spacing between patch edges. (a) E-plane, (b) H-plane.

4.1.8 Laboratory Model

In order to validate the calculation results a laboratory model shown in figure 4.13 was developed, which enabled simple measurements of different array configurations. The laboratory model was built from a copper half-sphere of radius $a = 18.7$ cm at which patches can be mounted at arbitrary positions. Mounting of a patch at desired position is very simple: one only needs to place a SMA connector at selected position on the grounded shell.

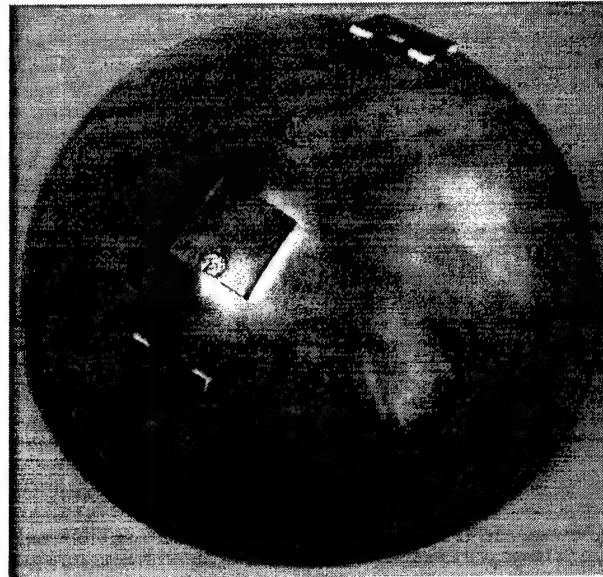
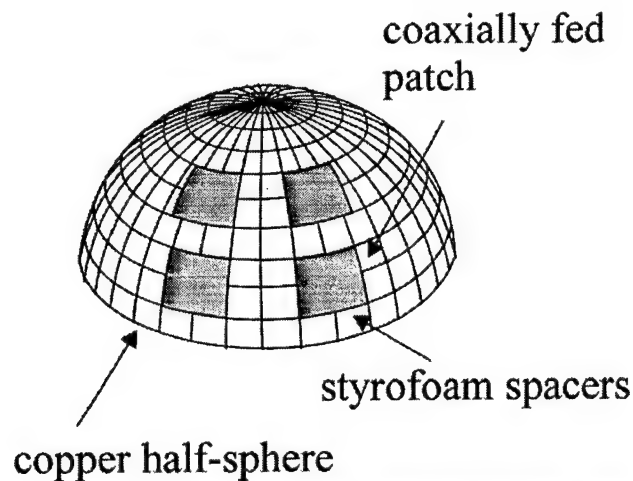


Figure 4.13. Sketch and photo of the developed laboratory model.

The selected dimensions of the patches are $5.1 \text{ cm} \times 5.1 \text{ cm}$, and the appropriate styrofoam cubes are used as spacers between patches and grounded shell (therefore $\epsilon_r = 1.0$; the cube thickness of 0.52 cm is selected). Fig. 4.14 shows the comparison of calculated and measured input impedance. The mutual coupling of two patches in E-plane is studied as a function of the

frequency and spacing between the elements (Figure 4.15). The calculated and measured mutual impedances are in a good agreement.

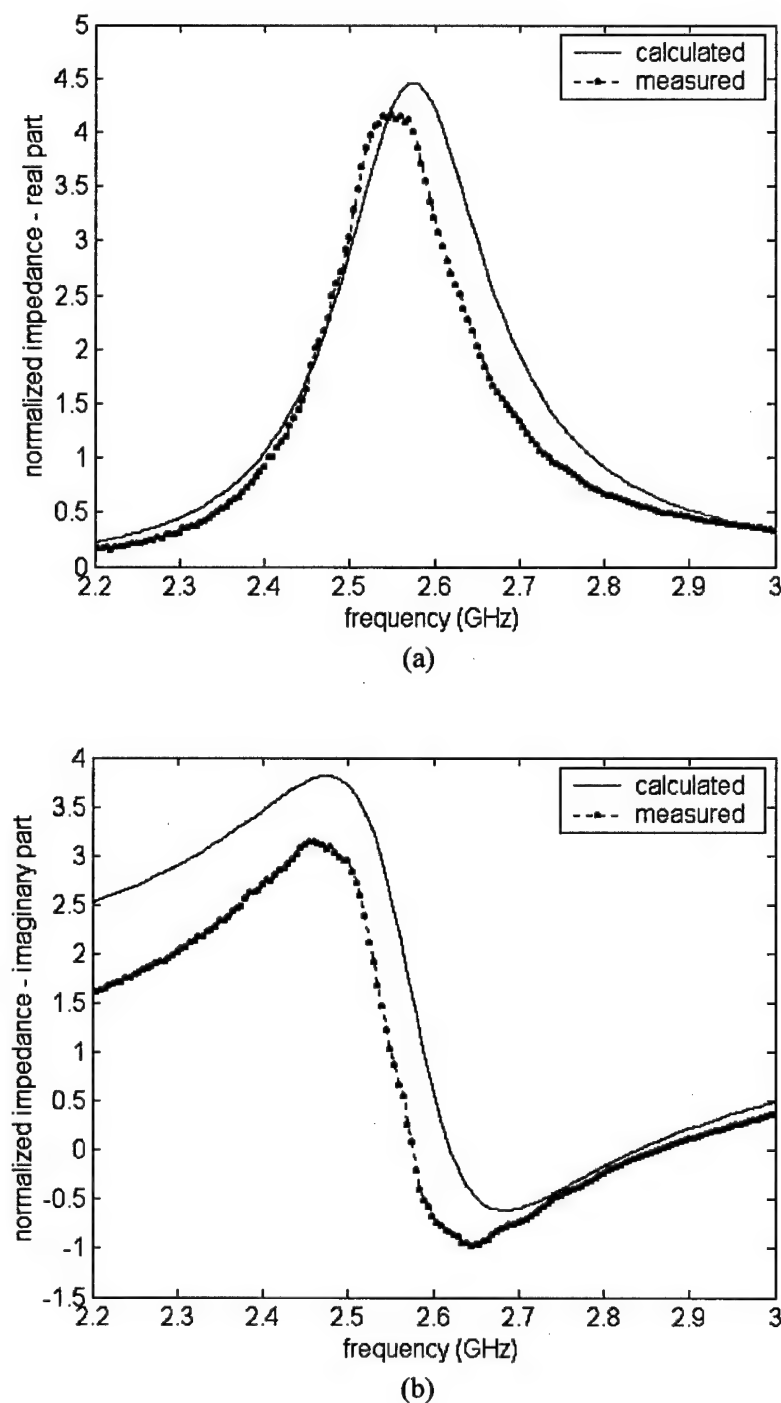
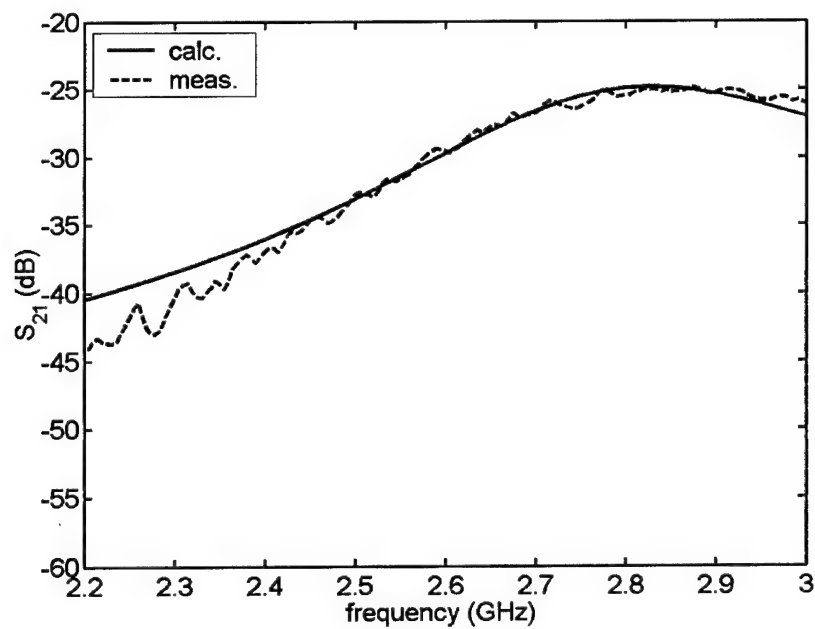
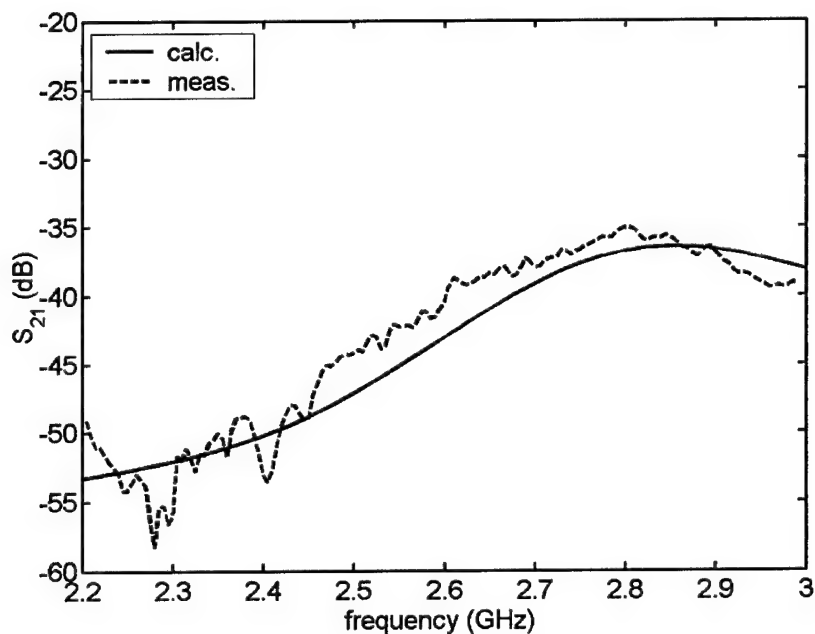


Figure 4.14. The comparison of calculated and measured input impedance; (a) real part, (b) imaginary part.



(a)



(b)

Figure 4.15. The comparison of calculated and measured mutual coupling coefficient of two patches in E-plane as a function of frequency and spacing between elements; (a) 10 cm, (b) 20 cm.

APPENDIX I: Selection of Basis Function

As basis functions we have used entire-domain basis functions, i.e., basis functions that are defined on the whole patch. For rectangular patches basis functions are sinusoidal in the current direction and they are of constant distribution in the perpendicular direction, which is a common approximation since patch antennas are resonant structures. For example, the k th mode of θ -polarized current is

$$J_{\theta}(\theta, \phi) = \frac{1}{2r_{patch}\phi_p} \sin\left(\frac{k\pi}{2\theta_p}\left(\theta + \theta_p - \frac{\pi}{2}\right)\right), \quad (34)$$

and its vector-Legendre transformation is:

$$\tilde{J}_{\theta}(n, m) = \frac{\sin(m\phi_p)}{m\phi_p} \frac{1}{r_{patch}\sqrt{2\pi S(n, m)}} \int_{\frac{\pi}{2}-\theta_p}^{\frac{\pi}{2}+\theta_p} \frac{\partial P_n^{|m|}(\cos\theta)}{\partial\theta} \sin\left(\frac{k\pi}{2\theta_p}\left(\theta + \theta_p - \frac{\pi}{2}\right)\right) \sin\theta d\theta \quad (35a)$$

$$\tilde{J}_{\phi}(n, m) = \frac{j \sin(m\phi_p)}{r_{patch}\phi_p \sqrt{2\pi S(n, m)}} \int_{\frac{\pi}{2}-\theta_p}^{\frac{\pi}{2}+\theta_p} P_n^{|m|}(\cos\theta) \sin\left(\frac{k\pi}{2\theta_p}\left(\theta + \theta_p - \frac{\pi}{2}\right)\right) d\theta \quad (35b)$$

The k th mode of ϕ polarized rectangular patch is:

$$J_{\phi}(\theta, \phi) = \frac{1}{2r_{patch}\theta_p} \sin\left(\frac{k\pi}{2\phi_p}(\phi + \phi_p)\right) \quad (36)$$

and its vector-Legendre transformation is

$$\tilde{J}_{\theta}(n, m) = \frac{j m \phi_p k \pi \left[(-1)^k e^{-j m \phi_p} - e^{j m \phi_p} \right]}{r_{patch} \theta_p (k^2 \pi^2 - 4 m^2 \phi_p^2) \sqrt{2\pi S(n, m)}} \int_{\frac{\pi}{2}-\theta_p}^{\frac{\pi}{2}+\theta_p} P_n^{|m|}(\cos\theta) d\theta \quad (37a)$$

$$\tilde{J}_{\phi}(n, m) = \frac{-\phi_p k \pi \left[(-1)^k e^{-j m \phi_p} - e^{j m \phi_p} \right]}{r_{patch} \theta_p (k^2 \pi^2 - 4 m^2 \phi_p^2) \sqrt{2\pi S(n, m)}} \int_{\frac{\pi}{2}-\theta_p}^{\frac{\pi}{2}+\theta_p} \frac{\partial P_n^{|m|}(\cos\theta)}{\partial\theta} \sin\theta d\theta \quad (37b)$$

If circular patch is analyzed, then the basic current mode is given as:

$$\mathbf{J} = \alpha_{11} J_1(\alpha_{11} r_{patch} \theta) \cos\phi \hat{\theta} - \frac{1}{r_{patch} \theta} J_1(\alpha_{11} r_{patch} \theta) \sin\phi \hat{\phi} \quad (38)$$

where α_{11} denotes constant ($\alpha_{11} r_{patch} \theta_p = 1.84118$), and J_1 is the Bessel function. The vector-Legendre transformation is

$$\tilde{J}_\theta(n, m) = \frac{\pi}{\sqrt{2\pi S(n, m)}} \cdot \left[\int_0^{\theta_p} \bar{P}_n^{(m)}(\cos\theta) \frac{J_1(\alpha_{11} r_{patch} \theta)}{r_{patch} \theta} d\theta + \int_0^{\theta_p} \frac{d\bar{P}_n^{(m)}}{d\theta} \alpha_{11} \sin\theta \left(J_0(\alpha_{11} r_{patch} \theta) - \frac{J_1(\alpha_{11} r_{patch} \theta)}{\alpha_{11} r_{patch} \theta} \right) d\theta \right] \quad (39a)$$

$$\tilde{J}_\phi(n, m) = \frac{j m \pi}{\sqrt{2\pi S(n, m)}} \cdot \left[\int_0^{\theta_p} \bar{P}_n^{(m)}(\cos\theta) \alpha_{11} \sin\theta \left(J_0(\alpha_{11} r_{patch} \theta) - \frac{J_1(\alpha_{11} r_{patch} \theta)}{\alpha_{11} r_{patch} \theta} \right) d\theta + \int_0^{\theta_p} \frac{d\bar{P}_n^{(m)}}{d\theta} \frac{J_1(\alpha_{11} r_{patch} \theta)}{r_{patch} \theta} \sin\theta d\theta \right] \quad (39b)$$

APPENDIX II:

Electromagnetic Field Radiated by an Current Shell

The core problem inside the G1DMULT algorithm is to calculate the electromagnetic field in the homogeneous space radiated by an electric current shell of radius r_s

a) from $\tilde{J}_\theta(n, m)$

$$\tilde{E}_\theta(r, n, m) = -\frac{k}{\omega \epsilon} \frac{r_s}{r} \tilde{J}_\theta(n, m) \cdot \begin{cases} \hat{H}_n^{(2)'}(kr_s) \hat{J}_n'(kr) & r \leq r_s \\ \hat{J}_n'(kr_s) \hat{H}_n^{(2)'}(kr) & r \geq r_s \end{cases} \quad (40a)$$

$$\tilde{E}_r(r, n, m) = -\frac{1}{\omega \epsilon} \frac{r_s}{r^2} \sqrt{n(n+1)} \tilde{J}_\theta(n, m) \cdot \begin{cases} \hat{H}_n^{(2)}(kr_s) \hat{J}_n(kr) & r \leq r_s \\ \hat{J}_n(kr_s) \hat{H}_n^{(2)}(kr) & r \geq r_s \end{cases} \quad (40b)$$

$$\tilde{H}_\phi(r, n, m) = \frac{j r_s}{r} \tilde{J}_\theta(n, m) \cdot \begin{cases} \hat{H}_n^{(2)}(kr_s) \hat{J}_n(kr) & r \leq r_s \\ \hat{J}_n(kr_s) \hat{H}_n^{(2)}(kr) & r \geq r_s \end{cases} \quad (40c)$$

b) from $\tilde{J}_\phi(n, m)$

$$\tilde{E}_\phi(r, n, m) = -\frac{k}{\omega \epsilon} \frac{r_s}{r} \tilde{J}_\phi(n, m) \cdot \begin{cases} \hat{H}_n^{(2)'}(kr_s) \hat{J}_n'(kr) & r \leq r_s \\ \hat{J}_n'(kr_s) \hat{H}_n^{(2)'}(kr) & r \geq r_s \end{cases} \quad (41a)$$

$$\tilde{H}_\theta(r, n, m) = \frac{j r_s}{r} \tilde{J}_\phi(n, m) \cdot \begin{cases} \hat{H}_n^{(2)'}(kr_s) \hat{J}_n'(kr) & r \leq r_s \\ \hat{J}_n'(kr_s) \hat{H}_n^{(2)'}(kr) & r \geq r_s \end{cases} \quad (41b)$$

$$\tilde{H}_r(r, n, m) = \frac{j r_s}{k r^2} \sqrt{n(n+1)} \tilde{J}_\phi(n, m) \cdot \begin{cases} \hat{H}_n^{(2)}(k r_s) \hat{J}_n(k r) & r \leq r_s \\ \hat{J}_n(k r_s) \hat{H}_n^{(2)}(k r) & r \geq r_s \end{cases} \quad (41c)$$

Here k is the wave number. The fields excited by the magnetic shell can be easily determined by applying the duality concept. The fields caused by the r -directed sources are evaluated by using the transverse replacement currents (see [4] for details).

4.2 Analysis of aperture coupled patch antennas on circular-cylindrical and spherical structures

4.2.1 Introduction

Microstrip antennas can be simply fed by microstrip or coaxial transmission lines. The microstrip line feeding has advantage of easy fabrication, but it may not be desirable due to the radiation of the microstrip line. Coaxial line is not attractive from the fabrication point of view. Both types of feeding structures lead to narrow-band patch designs (typically 1-3%). The aperture-coupled feeding structure has advantage of both fabrication simplicity and broadband patch antenna design possibility. Furthermore, it has potential in millimeter-wave applications and in monolithic microwave integrated circuits applications.

The purpose of this chapter is to present an electromagnetic model that enables the analysis of aperture-coupled patch antennas mounted on a circular-cylindrical or spherical structure. The analysis method is based on the equivalence principle which is used to separate the inner problem (feeding structure inside the grounded tube or grounded shell) and the outer problem (patch antenna itself). The reciprocity theorem is used to find the interaction between the feedline and the aperture. The antenna structure is rigorously taken into account by using proper Green's functions, and the array is fully analyzed by means of element-by-element approach. The integral equation is numerically solved using spectral domain moment method. The developed program calculates radiation pattern of the antenna, input impedance at each port and mutual coupling between the elements of the array.

4.2.2 Method of Analysis

The analysis of microstrip patch arrays on circular cylindrical structures is given in [13]. Here we will give only the analysis model of aperture-coupling, i.e. we will extend the analysis to the new feeding structure. Furthermore, the same model can be applied both to circular-cylindrical and spherical structures. Therefore, we will give the description of cylindrical case only since the extension of formulation to spherical problems is straightforward.

4.2.2.1 Analysis of one aperture-coupled patch

First we will describe the feeding model for single aperture-coupled patch antenna. The geometry of the patch is given in Figs. 4.16 and 4.17 (notice that the Figure 4.17 shows only a small part of a cylindrical or spherical antenna). The analysis of aperture feeding based on

reciprocity theorem was developed for planar patches by D. Pozar [14]. Here we will give the formulation for patches on circular-cylindrical structures.

It is assumed that a quasi-TEM mode is propagating along the microstrip line oriented in z -direction

$$\begin{aligned}\bar{e}(\rho, \phi) &= e_\rho \hat{\rho} + e_\phi \hat{\phi} \\ \bar{h}(\rho, \phi) &= h_\rho \hat{\rho} + h_\phi \hat{\phi}\end{aligned}\quad (42)$$

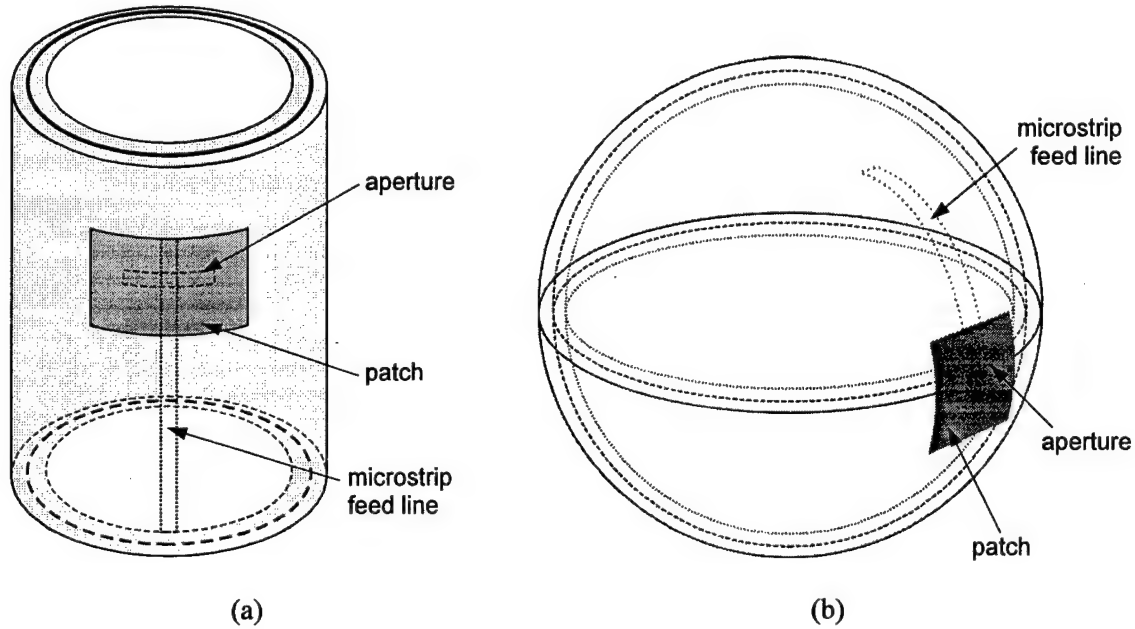


Figure 4.16. Aperture-coupled patch antenna. (a) Circular-cylindrical patch antenna, (b) Spherical patch antenna.

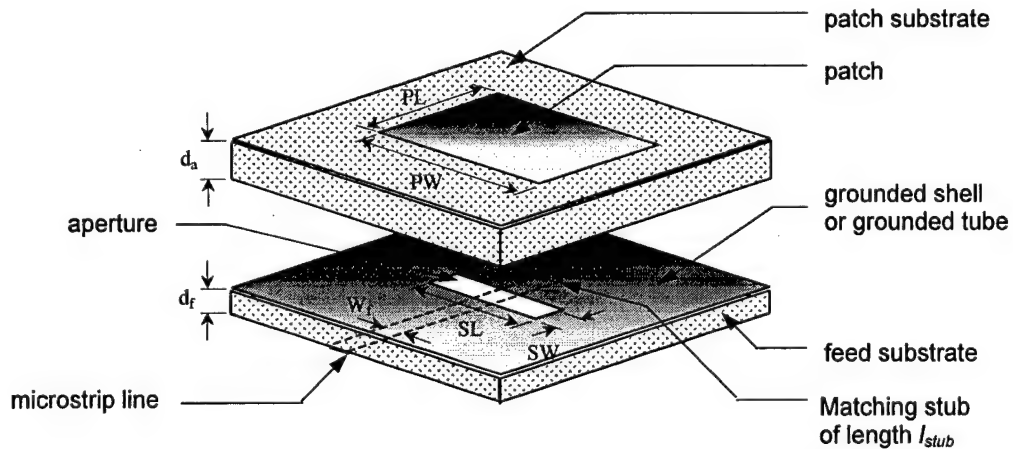


Figure 4.17. Aperture-coupled patch antenna. The antenna is mounted on cylindrical or spherical structure.

The fields of the quasi-TEM mode are:

$$\begin{aligned}\bar{E}^{\pm} &= \bar{e} e^{\pm j\beta z} \\ \bar{H}^{\pm} &= \pm \bar{h} e^{\pm j\beta z}\end{aligned}\quad (43)$$

Here β is a propagation constant, and \bar{e} and \bar{h} are determined from adequate Green's functions. The aperture represents a discontinuity, therefore we can write

$$\bar{E} = \begin{cases} \bar{E}^+ + R\bar{E}^-, & \text{for } z < 0 \\ T\bar{E}^+, & \text{for } z > 0 \end{cases} \quad (44a)$$

$$\bar{H} = \begin{cases} \bar{H}^+ + R\bar{H}^-, & \text{for } z < 0 \\ T\bar{H}^+, & \text{for } z > 0 \end{cases} \quad (44b)$$

where R and T represent reflection and transmission coefficients. By applying the reciprocity theorem [14] on the total fields \bar{E}, \bar{H} and on the forward propagating fields \bar{E}^+, \bar{H}^+ we get:

$$\int_S \bar{E} \times \bar{H}^+ \cdot d\bar{s} = \int_S \bar{E}^+ \times \bar{H} \cdot d\bar{s}, \quad (45)$$

where S represents the closed area consisting of three parts:

- S_0 = effective cross-section of microstrip line ($0 < \rho < \rho_{GND}$, $0 \leq \phi < 2\pi$)
- S_a = aperture area
- S_w = walls of microstrip line at the PEC grounded tube ($\rho = \rho_{GND}$, $0 \leq \phi < 2\pi$)

On S_w we have $\hat{n} \times \bar{E} = \hat{n} \times \bar{E}^+ = 0$, thus there is no contribution when integrating over S_w . On S_a $\hat{n} \times \bar{E}^+ = 0$, but $\hat{n} \times \bar{E} = V_0 \hat{n} \times \hat{\phi} e_{\phi}^a$, where $V_0 e_{\phi}^a$ is the unknown field distribution in the aperture, and we will represent it via piecewise sinusoidal (PWS) basis function:

$$V_0 e_{\phi}^a = V_0 \frac{\sin k_e (L/2 - |\phi - \rho_{GND}|)}{W \sin k_e L/2}, \quad \text{for } |z| < SW/2, \quad |\phi - \rho_{GND}| < SL/2. \quad (46)$$

Here k_e is the effective wave number of PWS basis function, and V_0 is the unknown amplitude to be determined. For k_e it is convenient to use the mean value of wave numbers of two surrounding layers (the layers next to the grounded PEC tube that are inside and outside the tube). Equation (32) can be written in the following form:

$$R = \frac{V_0}{2} \int_{S_a} e_z^a(x, y) h_{\phi}(x, y) ds = \frac{V_0}{2} \Delta v, \quad (47)$$

For narrow slots there is no need to include term $e^{\pm j\beta z}$ in equation (34) since its influence is small. By applying the reciprocity theorem once more

$$\int_S \bar{E} \times \bar{H}^- \cdot d\bar{s} = \int_S \bar{E}^- \times \bar{H} \cdot d\bar{s}, \quad (48)$$

we get expression for transmission coefficient T :

$$T = 1 - \frac{V_0}{2} \int_{S_a} e_z^a(x, y) h_\phi(x, y) ds = 1 - R. \quad (49)$$

Since we have three unknowns R, T and V_0 we need one more equation. We will apply the PEC equivalence theorem [14] and by this we will separate the inner and the outer region. Therefore, we will introduce the equivalent magnetic current at the aperture $\mathbf{M}^{eq} = -\hat{n} \times \mathbf{E}$. The third equation is a consequence of the continuity of the magnetic field across the aperture:

$$H_\phi^e = H_\phi^f + H_\phi^i, \quad (50)$$

where

H_ϕ^e = outside magnetic field ($\rho > \rho_{GND}$) due to the aperture field $V_0 e_x^a$

H_ϕ^i = inside magnetic field ($\rho < \rho_{GND}$) due to the aperture field $V_0 e_x^a$

H_ϕ^f = inside magnetic field ($\rho < \rho_{GND}$) due to microstrip line quasi-TEM mode

At $z = 0^-$ (or $z = 0^+$ since $1 - R = T$), it is valid:

$$H_\phi^f = (1 - R) h_\phi. \quad (51)$$

Therefore,

$$H_\phi^e - H_\phi^i = V_0 \int_{S_a} (G_{\phi\phi}^{e, HM}(\phi, z; \phi_0, z_0) - G_{\phi\phi}^{i, HM}(\phi, z; \phi_0, z_0)) \cdot e_z^a(\phi_0, z_0) ds_0. \quad (52)$$

Here $G_{\phi\phi}^{e, HM}$ and $G_{\phi\phi}^{i, HM}$ are respectively the Green's functions for external and internal regions, and $\hat{\phi} \cdot e_z^a(\phi, z)$ is the equivalent magnetic current. Combining equations (50) – (52) we get

$$V_0 \int_{S_a} (G_{\phi\phi}^{e, HM}(\phi, z; \phi_0, z_0) - G_{\phi\phi}^{i, HM}(\phi, z; \phi_0, z_0)) \cdot e_z^a(\phi_0, z_0) ds_0 = (1 - R) h_\phi(\phi, z), \quad \text{for } \phi, z \in S_a \quad (53)$$

After multiplying (40) with e_z^a and integrating over S_a we get

$$\begin{aligned} V_0 \int_{S_a} \int_{S_a} e_z^a(\phi, z) \cdot (G_{\phi\phi}^{e, HM}(\phi, z; \phi_0, z_0) - G_{\phi\phi}^{i, HM}(\phi, z; \phi_0, z_0)) \cdot e_z^a(\phi_0, z_0) ds ds_0 \\ = (1 - R) \int_{S_a} e_z^a(\phi, z) h_\phi(\phi, z) ds \end{aligned} \quad (54)$$

or

$$V_0(Y^e + Y^i) = \Delta v(1 - R), \quad (55)$$

$$Y^e = \int_{S_a} \int_{S_a} e_z^a(\phi, z) G_{\phi\phi}^{e, HM}(\phi, z; \phi_0, z_0) \cdot e_z^a(\phi_0, z_0) ds ds_0 \quad (56)$$

$$Y^i = \int_{S_a} \int_{S_a} e_z^a(\phi, z) G_{\phi\phi}^{i, HM}(\phi, z; \phi_0, z_0) \cdot e_z^a(\phi_0, z_0) ds ds_0 \quad (57)$$

When the patch is present we need to add contribution of the patch as well (in order to fulfill the continuity of magnetic field). For that first we need to determine the current distribution on the patch, which is done by applying the moment method. The patch current is expanded in entire domain basis functions multiplied by unknown coefficients α_i

$$\mathbf{J}(\phi, z) = \sum_{i=1}^N \alpha_i \mathbf{J}_i(\phi, z). \quad (58)$$

We formulate the electric field integral equation (EFIE) by enforcing the boundary condition that the total tangential electric field must be zero on the surface of the patch. The equation is satisfied in an average sense by weighting the fields with test functions (that are equal to basis functions – Galerkin method). We get the matrix equation to solve

$$[Z][\alpha] = [V], \quad (59)$$

where $[\alpha]$ is vector of unknown coefficients α_i and impedance matrix $[Z]$ and voltage vector $[V]$ are calculated in the following way:

$$Z_{mn} = - \int_{S_p} \int_{S_p} \mathbf{J}_j(\phi, z) \cdot \overline{\mathbf{G}}^{EJ}(\phi, z; \phi_0, z_0) \cdot \mathbf{J}_i(\phi, z) ds ds_0, \quad (60a)$$

$$V_m = \int_{S_p} \int_{S_a} \mathbf{J}_j(\phi, z) \cdot \overline{\mathbf{G}}^{EM}(\phi, z; \phi_0, z_0) \cdot \hat{\phi} e_z^a(\phi_0, z_0) ds ds_0. \quad (60b)$$

The weighted magnetic field at the aperture due to the patch current is given by (notice that we have used the reaction theorem in the derivation):

$$Y^a = [V]^t [Z]^{-1} [V] \quad (61)$$

Therefore, the modified equation (55) with added weighted magnetic field from the patch is

$$V_0(Y^a + Y^e + Y^i) = \Delta v(1 - R). \quad (62)$$

Combining equations (62) and (47) we get

$$R = \frac{\Delta v^2}{\Delta v^2 + 2(Y^a + Y^e + Y^i)} \quad (63)$$

Equation (49), $T = 1 - R$, actually means that the slot represents a series impedance that is connected to the open stub of length l_{stub} (see Fig. 4.18). Finally, we get expression for input impedance of one aperture-coupled patch:

$$Z = Z_0 \frac{2R}{1-R} + Z_{stub} = Z_0 \frac{\Delta v^2}{Y^a + Y^e + Y^i} - jZ_0 \text{ctg}(\beta l_s), \quad (64)$$

where Z_0 is the characteristic impedance of microstrip line.

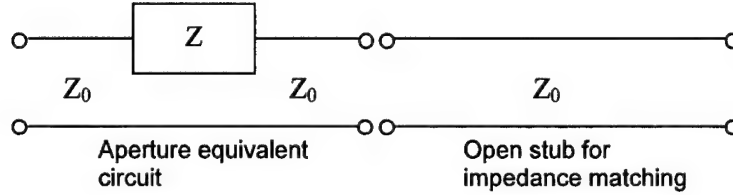


Figure 4.18. Equivalent circuit of aperture in the ground plane

4.2.2.2 Analysis of the array of aperture-coupled patches

The array of aperture-coupled patches is analyzed using the equivalent circuit of an aperture-coupled patch array considered as a multiport device. Notice that each patch is considered as two port device and that one port is connected to the open stub of length l_{stub} (see Figs. 4.17 and 4.18). If we would consider one aperture-coupled patch in this way, then its S-parameters will be $S_{11}=S_{22}=R$, $S_{12}=S_{21}=T=1-R$. Using standard algebra with S-parameters we get the reflection coefficient Γ_{in} of the two port device with a load connected to the second port (the connected load is characterized via reflection coefficient Γ_{stub})

$$\Gamma_{in} = S_{11} + \frac{S_{21}S_{12}\Gamma_{stub}}{1 - S_{22}\Gamma_{stub}}, \quad Z_{in} = Z_0 \frac{1 - \Gamma_{in}}{1 + \Gamma_{in}} \quad (65)$$

which is the same expression as (64).

If we organize the equivalent $2N$ -port device (N is number of patches in the array) in the way that first N ports are ports connected to generators and the second N ports are loaded with open stub of length l_{stub} , then we can divide the S matrix of the $2N$ -port device as

$$[S]_{2N} = \begin{bmatrix} [S_{11}] & [S_{21}] \\ [S_{21}] & [S_{11}] \end{bmatrix}, \quad [S_{21}] = [U] - [S_{11}], \quad (66)$$

where $[U]$ is the unit matrix. Similarly to the one patch case we get $[S]_N$, which is equal to the S-matrix of loaded $2N$ -port device with N open stubs, as

$$[S]_N = [S_{11}] + [S_{12}] \left(\frac{1}{\Gamma_{sub}} [I] - [S_{22}] \right)^{-1} [S_{21}]. \quad (67)$$

The elements of the $[S_{11}]$ matrix are determined in the following way. For each slot we can write (2N-port equivalent of equations (47) and (62))

$$S_{ij} = \frac{V_0^{ij}}{2} \Delta v, \quad \sum_{k=1}^N V_0^{kj} (Y_{ik}^a + Y_{ik}^e + Y_{ik}^l) = \Delta v (\delta_{ij} - S_{ij}), \quad (68)$$

where the index ij means that the j th port is excited and we look at the S-parameter/amplitude of the aperture field at i th patch, and δ_{ij} is the Kronecker symbol. Once we know the S-matrix of the loaded 2N-port device, we determine all needed parameters in the standard way. For example, the impedance port matrix $[Z^{port}]$ is determined as:

$$[Z^{port}] = [Z^0] ([U] - [S]_N) ([U] + [S]_N)^{-1} \quad (69)$$

where $[Z^0]$ is a diagonal matrix with elements Z^0 , the characteristic impedance of the feeding transmission lines.

5 USER'S MANUAL

5.1 Introduction to SMiPA

5.1.1 Introduction

This chapter gives the user's manual for the program SMiPA. The abbreviation SMiPA means the program for analyzing **Spherical Microstrip Patch Arrays**. Since there are different requirements on calculation of radiation pattern and input impedance/mutual coupling, we have actually developed two programs SMiPA and SMiPApat. The main reason for splitting the problem into two parts is that radiation pattern is usually calculated only for one frequency, while input impedance and mutual coupling is usually calculated for frequency band of interest (and thus even hundreds of frequency points can be calculated). Therefore, program SMiPA calculates

- current distribution at each patch in the array
- input impedance at each input port in the array
- mutual coupling between each two patches in the array

and program SMiPApat calculates

- radiation pattern of the array without taking mutual coupling into account
- radiation pattern of the array when all mutual couplings are taken into account.

Program is written in FORTRAN 90, and therefore can be compiled and run at each machine where FORTRAN 90 is installed or which support the executable version of the program. The communication with the program is made via input/output ASCII files. For case of simplicity, both programs SMiPA and SMiPApat are using the same input file (smipa.in). The detailed description of input and output files are given in this chapter.

We have also developed a graphical user interface, called SMiPAwin, for IBM PC compatible computers under Windows operating system (the description of SMiPAwin is given in Appendix). By this it is easier to define the input parameters, and to obtain graphical presentation of the results. Programs SMiPA and SMiPApat are working independently of graphical user interface, i.e., graphical user interface is used only for writing the input file, running the SMiPA and SMiPApat programs, reading the output files, and displaying the results.

5.1.2 Problem Domain Description

The SMiPA and SMiPapat programs analyze microstrip patch antennas or antenna arrays placed on spherical structures, as illustrated in Fig. 5.1. If an array is analyzed, following assumptions are made:

- all antenna elements are identical, both in terms of dimensions, shape and feed/port types
- the patch elements are of circular or rectangular shape
- the dielectric structure can be multilayered with losses
- the patch array must be placed at the top of one such layer
- three types of feeding structures can be analyzed: coax feeding, microstrip line feeding and aperture-coupled patch elements
- multiple ports can be defined on patch, e.g. when designing circularly polarized arrays.

By means of SMiPA program current distribution at each patch in the array can be calculated, as well as input impedance at each input port and mutual coupling between each two patches. The SMiPapat program calculates then radiation pattern of the array, with or without taking mutual coupling into account.

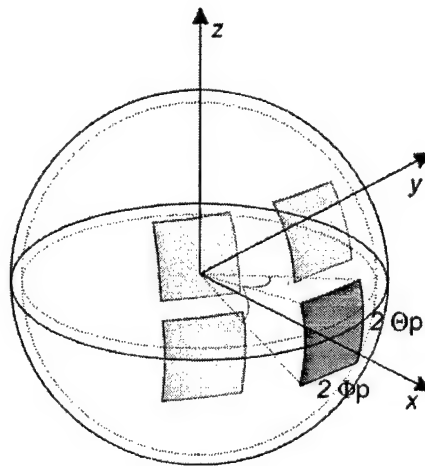


Figure 5.1. The geometry of the spherical patch array

5.1.3 Text File Interface

The programs SMiPA and SMiPapat interact with the user and with each other using ASCII text files. This scheme, with all files in question is presented in Fig. 5.2.

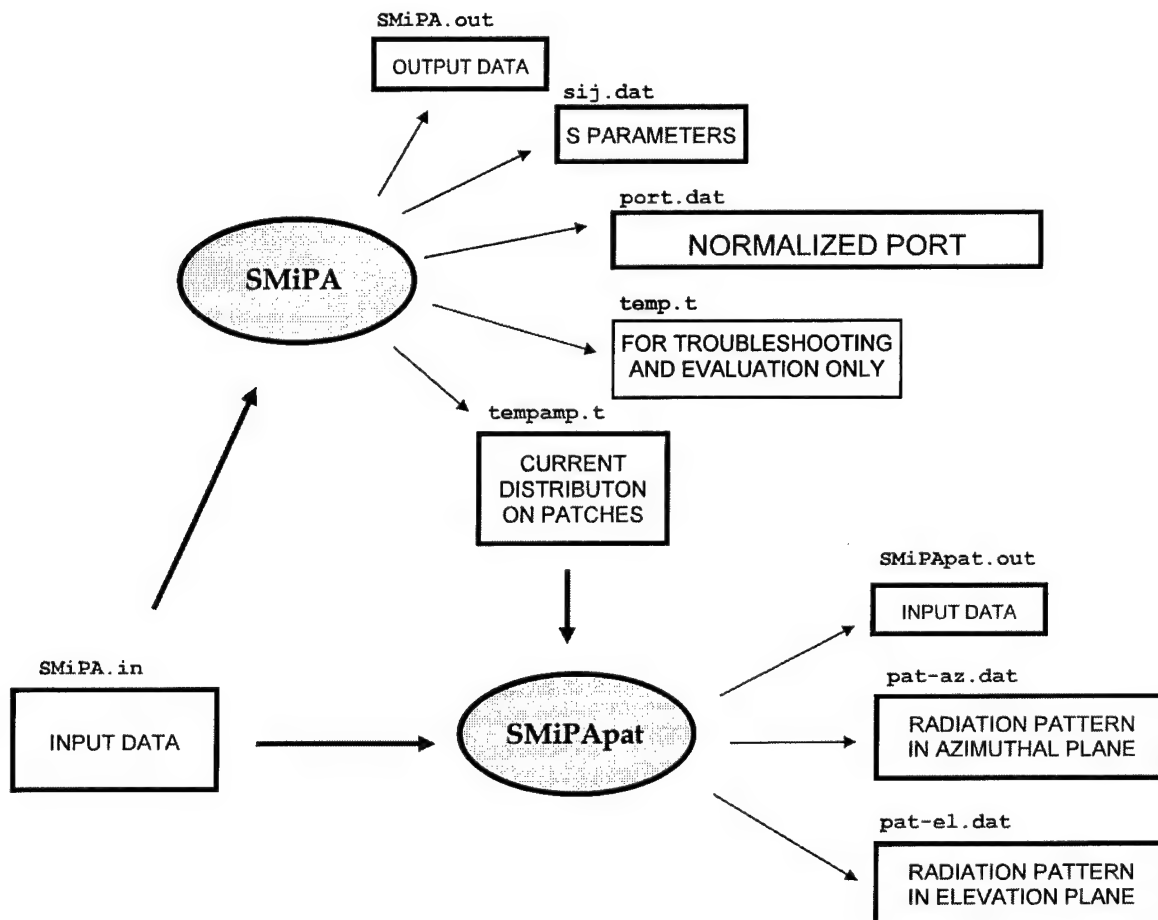


Figure 5.2. Input and output files for the programs SMiPA and SMiPapat.

The program can calculate the following antenna characteristics:

- current distribution at each patch in the array
- input impedance of each patch in the array
- mutual coupling between each two patches in the array
- radiation pattern of the array when all mutual couplings are taken into account
- radiation pattern of the array without taking mutual coupling into account (fast calculations of the radiation pattern needed for making the first design of the array).

5.1.3.1 The SMiPA.in file

The name of the input file for both SMiPA and SMiPapat programs is **SMiPA.in**. Each line possesses the value of several variables and short description of these variables. The input variables, which must have values when the call of the SMiPA and SMiPapat is made, are:

First line:

<u>Fmin, Fmax, Nfrequency, Modecal</u>	<u>REAL, REAL, INTEGER, CHARACTER</u>
--	---------------------------------------

Fmin and *Fmax* are the minimum and maximum frequency (in GHz). *Nfrequency* is the number of frequency points for which the array is analyzed. These values are used only when the call of the SMiPA program is made. SMiPapat program calculates the radiation pattern only for one frequency, and that frequency is *Fmin*. If we first calculate the patch currents at *Nfrequency* frequency points (by calling SMiPA program), then we can choose the frequency point for which we want to calculate the radiation pattern by choosing *Fmin*. The only condition is that the patch currents are calculated for the chosen frequency point. *Modecal* represents the calculation mode – *R* means accurate (rigorous) mode suggested for final design, and *F* means less-accurate (fast-design) mode suggested for first design.

Second line:

<u>R_{GND}</u>	<u>REAL</u>
------------------------	-------------

R_{GND} is the radius of the grounded tube (in cm).

Third line:

<u>Nlayer</u>	<u>INTEGER</u>
---------------	----------------

Nlayer is the number of dielectric layers.

Next *Nlayer* lines:

<u>h, EpsilonR, Tdelta</u>	<u>REAL</u>
----------------------------	-------------

Each line contains three parameters: *h*, *EpsilonR* and *Tdelta* which describe the thickness, the relative permittivity and loss tangent of each dielectric layer, respectively.

Next line:

<u>Npat1, Npat2, Lattice</u>	<u>INTEGER, CHARACTER</u>
------------------------------	---------------------------

Lattice represents the type of the grid lattice – *R* means rectangular lattice, *I* means icosahedron lattice, and *F* means that the position of each patch is read at the end of the input file. For rectangular lattice *Npat1* and *Npat2* are the number of patches in the θ - and ϕ -directions, respectively. For icosahedron lattice *Npat1* is the number of rings in the array, and *Npat2* denotes the ratio between the sides of equilateral triangles of the icosahedron structure and of the considered array (for example, in Fig. 4.6 *Npat1*=3 and *Npat2*=4). If the patch position is read from the file, then *Npat1*

and N_{pat2} have no meaning and therefore they can have arbitrary values.

Next line:

$N_{patlayer}$

INTEGER

$N_{patlayer}$ is the number of the dielectric layer at top of which the patches are placed. In other words, patches are placed between dielectric layers $N_{patlayer}$ and $N_{patlayer}+1$. If the patches are placed in the middle of some dielectric layer, an additional dielectric layer should be introduced, i.e. the considered dielectric layer should be split into two parts and the patches should be placed at the interface between these two dielectric layers.

Next line:

W_{patth} , W_{patphi} , $Patshape$

REAL, CHARACTER

For rectangular patches W_{patth} and W_{patphi} denote the patch width (in cm) in the θ - and ϕ - directions, respectively. For circular patches W_{patth} denotes the patch diameter (in cm). $Patshape$ represents the type of the patch shape: R means rectangular shape and C means circular shape.

Next line:

$Modefeed$

CHARACTER

$Modefeed$ denotes the type of the patch feeding. M or m means microstrip line feeding, C or c means coax feeding, and A or a means aperture coupled patch elements.

Next line:

N_{port}

INTEGER

N_{port} denotes the number of ports per patch (i.e. how many ports has each patch).

Next N_{port} lines:

$Feedth$, $Feedphi$

REAL

$Feedth$ and $Feedphi$ determine the position of the feeding line (in cm) in the θ - and ϕ -direction, respectively. For aperture coupled patch elements $Feedth$ and $Feedphi$ denote position of the center of the feeding aperture. Each line describes one port of the patch. This position is relative to the patch center, i.e., the feeding line placed at patch center has coordinates $Feedth = 0$ and $Feedphi = 0$. If the patch is fed by the microstrip line, one value should be $\pm W_{patth}/2$ or $\pm W_{patphi}/2$, depending at which edge the patches are excited. $Feedth$ and $Feedphi$ also determine the polarization of the patch elements when SMiPApat is used in the simple mode. In more details, when $Feedth = 0$ current on patches is ϕ -directed, and when $Feedphi = 0$ current on patches is θ -directed. For aperture-coupled patches the dimensions of the slot are also used in determining the polarization of patch elements. Otherwise, the

current on patches is a linear combination of θ - and ϕ -directed basic basis functions.

Next line:

Modeexci

CHARACTER

Modeexci determines if the ports have equal excitations, both in amplitude and phase. *Y* or *y* means that the ports are equally excited, *N* or *n* means that the excitations are read at the end of the input file SMiPA.in.

Next line:

Dpatth, Dpatphi

REAL

In the case of rectangular array grid (i.e. if the variable *Lattice* is equal *R*) *Dpatth* and *Dpatphi* are the distances between centers of the patches (in cm) in the θ - and ϕ -directions, respectively. If the variable *Lattice* is equal *I* or *F*, *Dpatth* and *Dpatphi* can be arbitrary numbers

Next line for coax feeding or microstrip line feeding:

Z0

REAL

Z0 is the characteristic impedance of the input transmission line (either microstrip or coax line).

Next several lines for aperture-coupled patch elements:

Next line:

Slotth, Slotphi

REAL

Slotphi and *Slotz* are the widths of the slots (in cm) in the ϕ - and z -directions, respectively.

Next line:

Nlayerin

INTEGER

Nlayerin is the number of dielectric layers inside the sphere.

Next *Nlayer* lines:

h, EpsilonR, Tdelta

REAL

Each line contains three parameters: *h*, *EpsilonR* and *Tdelta* which describe the thickness, the relative permittivity and loss tangent of each dielectric layer inside the sphere, respectively. First considered layer is the layer next to the grounded shell that contains the aperture.

Next line:

Nfeedlayer

INTEGER

Nfeedlayer is the number of the dielectric layer (starting from grounded shell) at top of which a microstrip feed line is placed. In other words, the microstrip feed line is placed between dielectric layers *Nfeedlayer* and *Nfeedlayer*+1.

Next line:

Wfeed, Lstub

REAL

Wfeed is the width of the input microstrip line (in cm).

Lstub is the length of the open stub (in cm).

The next six lines are needed only when the call of the SMiPapat program is made. They are:

Phimin, Phimax, Nphi

REAL, REAL, INTEGER

The minimum and maximum angles of ϕ (in deg) in the azimuthal plane, and the number of points which are calculated in the azimuthal pattern, respectively. The azimuthal plane is defined by $\theta = 90^\circ$ (the coordinate system is in Fig. 1).

Thetamin, Thetamax, Ntheta

REAL, REAL, INTEGER

The minimum and maximum angles of θ (in deg) in the elevation plane, and the number of points which are calculated in the elevation pattern, respectively.

Phiel

REAL

The ϕ angle of the elevation plane (in deg). In other words, the elevation plane is defined by $\phi = \text{Phiel}$.

Theta0, Phi0

REAL

The values of the θ and ϕ coordinates (in deg) of the main beam, respectively. The E-field values of the radiation pattern are normalized by the amplitude of the E-field with *Theta0* and *Phi0* coordinates. Furthermore, *Theta0* and *Phi0* values are needed when *Nmode* = 4 (see definition of the *Nmode*), and they are used for determining the phase correction of the current on each patch. By using this phase correction the fields from each patch are in phase in the (*Theta0*, *Phi0*) direction.

Typepolar

CHARACTER

Typepolar denotes the type of polarization of radiation pattern. *L* or *l* means linear polarization, *C* or *c* means circular polarization.

Nmode

INTEGER

Nmode is the mode of calculating the radiation pattern. *Nmode*=0, 1 and 5 means that the radiation pattern is calculated rigorously, i.e. the results from the SMiPA program are used (the calculated current distribution is used for chosen frequency point, see explanation of *Fmin*). *Nmode*=0 means calculation of the gain pattern, *Nmode*=1 means that the radiation pattern is normalized to the reference direction, and *Nmode*=5 means calculation of the element pattern. *Nmode* 2, 3 and 4 means that the radiation pattern

is calculated in a simple way, i.e., mutual coupling is not taken into account in calculations of the radiation pattern. When $Nmode = 2$ it is supposed that patch currents have equal amplitudes and phases on each patch. When $Nmode = 3$ amplitudes and phases of each patch current are read from the input file 'SMiPApat.in'. When $Nmode = 4$ all patches have the same amplitude of the current. The phase is corrected in the way that contributions from all patches are in phase in the direction of the main beam, i.e., in the (θ_0, ϕ_0) direction. If $Nmode=5$, then the number of the patch in the ϕ - and z -directions, as well as the port number should be also given in the same line. In that case we need to write additional three integer numbers-coordinates).

The last part of the input file is used in three cases: if the array grid is neither icosahedron nor rectangular, if the ports do not have equal excitations and we want to run SMiPA program, and if we want to calculate the radiation pattern (SMiPApat program) by using the simple method and by selecting the amplitudes and phases of currents on each patch ($Nmode = 3$). In all cases the amplitudes and phases of the excitation currents, as well as patch positions, are read from the end of the input file SMiPA.in. The number of lines in the file is the same as the number of patches times number of ports. Each line has 5 numbers: first two numbers are the patch number-coordinates, the third one is the number of the port of the considered patch, and the fourth and the fifth number in each line are the amplitude and the phase of the excitation connected to the considered port of the patch.

For rectangular grid the patch number-coordinates are the number of the patch in θ - and ϕ direction (the patch number of the lowest most left patch is (1,1)). For icosahedron grid the patch number-coordinates are the number of the circle and the number of the patch along the circle. For non-rectangular grid first two numbers represent the patch position (θ and ϕ coordinate in degrees). We can check if these last lines are correctly given by checking the description of the array given in the output files SMiPA.out and SMiPApat.out. If we consider some other case (e.g. if the ports have equal excitations) there is no need for these input data. Therefore:

If needed, next $Npat \times Nport$ lines after one blank line are:

Ipat1, Ipat2, Iport, Amp, Phase INTEGER, REAL

$Ipat_{\phi}$, $Ipat_z$, $Iport$ are integers which represents the coordinates of each port (coordinate $Iport$) connected to each patch (coordinates $Ipat1$, $Ipat2$). For that port real numbers Amp and $Phase$ denote the amplitude and the phase of the excitation current.

or

Thetapat, Phipat, Iport, Amp, Phase REAL, INTEGER, REAL

$Thetapat$ and $Phipat$ represent the θ and ϕ coordinate (in degrees) of the center of each patch, $Iport$ is the number of the patch port, and Amp and $Phase$ denote the amplitude and the phase of the excitation current.

5.1.3.2 Description of the output files

There are six output files: 'SMiPA.out', 'SMiPApat.out', 'Sij.dat', 'port.dat', 'pat-az.dat' and 'pat-el.dat', and in them we can find data about the geometry as well as the calculated values of the input impedance, S-parameters and radiation pattern in the elevation and azimuthal planes.

SMiPA.out The file contains data about the input impedance of a single patch (S parameters for array case are given in Sij.dat). When constructing the array we need first to determine the parameters of a single patch, e.g. input impedance, return loss, and impedance bandwidth. The structure of the SMiPA program (and output file 'SMiPA.out') enables these calculations. First part of the file contains the values of the input file. Therefore the first part looks similar to the input file 'SMiPA.in'. The second part contains the input impedance and return loss for all calculated frequencies. Each line is for one frequency point, and it has four values: frequency (in GHz), normalized input impedance (real and imaginary part) and return loss (in dB). The calculated input impedance is normalized by the characteristic impedance of the feeding transmission line Z_0 (the value of Z_0 is given in the file 'SMiPA.in'; for aperture-coupled patch antennas it is calculated from the geometry of feeding structure).

SMiPApat.out The file contains data about the array geometry. The first part of the file contains the values of the input file. Therefore the first part looks similar to the input file 'SMiPA.in'. The second part describes the array that is analyzed. It is a list of the all patch elements in the array with their coordinates and amplitude and phase of the patch current. First two columns are the patch number-coordinates, the third column is the number of the basis function on the considered patch, and the forth and fifth columns are the θ - and ϕ -coordinate of the patch. The sixth and seventh columns are the amplitude and phase (in deg) of the considered basis function, respectively.

Sij.dat The file contains the calculated S-parameters. The file is in the Touchstone format, i.e., using this file it is possible to connect SMiPA and Touchstone programs. The first line is a specification line: '# GHz S DB R' and at the end of the line there is a value of the normalization impedance. GHz means that the frequency values are in GHz, DB means that S-parameters are written in the dB-angle format. Other lines in the file are the S-parameters for different frequencies. If we have one port (one patch) then each line contains frequency, $|S_{11}|$ in dB, and angle of S_{11} , respectively. In the case of two ports (two patches) each line contains frequency, $|S_{11}|$ in dB, angle of S_{11} , $|S_{21}|$ in dB, angle of S_{21} , $|S_{12}|$ in dB, angle of S_{12} , $|S_{22}|$ in dB, and angle of S_{22} , respectively. In the case of N ports each frequency is described with N lines, each containing $|S_{i1}|$ in dB, angle of S_{i1} , $|S_{i2}|$ in dB, angle of S_{i2} , etc. Frequency is written at the beginning of the first of N lines.

port.dat The file contains the calculated port impedances for each port. For each frequency point port impedances are given in the form of real and imaginary part. The values of port impedances are normalized, i.e. port impedances are divided by Z_0 .

pat-az.dat The file contains the field values in the azimuthal plane (the azimuthal plane is defined by $\theta=90^\circ$). The input values of variables $Phimin$, $Phimax$ and $Nphi$ determine the ϕ values in the azimuthal plane for which the radiation pattern is calculated. The field values are normalized with the field value with $Theta0$ and $Phi0$ coordinates that are defined in the input

file (the exception is for $Nmode = 0$ and $Nmode = 5$). The first and second columns are the θ and ϕ coordinates (in deg) for which the radiation pattern is calculated. If the chosen type of polarization is linear (parameter *Typepolar* in the input file), then the third and the fourth columns are the normalized θ - and ϕ -components of the electric field, respectively. If the chosen type of polarization is circular, then the third and the fourth columns are the normalized right-hand circular polarization (RHCP) and left-hand circular polarization (LHCP) components of the electric field, respectively.

pat-el.dat The file contains the field values in the elevation plane which is defined by $\phi = \phi_{hiel}$ (the value of ϕ_{hiel} is defined in the input file). The input values of variables *Thetamin*, *Thetamax* and *Ntheta* determine the θ values in the elevation plane for which the radiation pattern is calculated. The field values are normalized with the field value with coordinates *Theta0* and *Phi0* that are defined in the input file (the exception is for $Nmode = 0$ and $Nmode = 5$). The first and second columns are the θ and ϕ coordinates (in deg) for which the radiation pattern is calculated. If the chosen type of polarization is linear (parameter *Typepolar* in the input file), then the third and the fourth columns are the normalized θ - and ϕ -components of the electric field, respectively. If the chosen type of polarization is circular, then the third and the fourth columns are the normalized right-hand circular polarization (RHCP) and left-hand circular polarization (LHCP) components of the electric field, respectively.

5.2 Upgrade of the Program CyMPA

5.2.1 Introduction

This chapter gives the short description and the realized improvements for of the program CyMPA. The abbreviation CyMPA means the program for analyzing **Cylindrical Microstrip Patch Arrays**, and previous version of the program was designed to analyze two types of feeding structures: coax feeding and microstrip line feeding [13]. The upgraded version of the program can also analyze aperture-coupled cylindrical patch antennas. Since there are different requirements on calculation of radiation pattern and input impedance/mutual coupling, we have actually developed two programs CyMPA and CyMPApat. The main reason for splitting the problem into two parts is that radiation pattern is usually calculated only for one frequency, while input impedance and mutual coupling is usually calculated for frequency band of interest (and thus even hundreds of frequency points can be calculated). Therefore, program CyMPA calculates:

- current distribution at each patch in the array and field distribution in each aperture
- input impedance at each input port in the array
- mutual coupling between each two patches in the array,

and program CyMPApat calculates

- radiation pattern of the array when all mutual couplings are taken into account
- radiation pattern of the array without taking mutual coupling into account (fast mode).

In order to determine the radiation pattern, program CyMPApat is using the results of program CyMPA, i.e. current distribution on patches and field distribution in apertures calculated at selected frequency point is used.

Program is written in FORTRAN 90, and therefore can be compiled and run at each machine where FORTRAN 90 is installed or which support the executable version of the program. The communication with the program is made via input/output ASCII files. For case of simplicity, both programs CyMPA and CyMPApat are using the same input file (CyMPA.in). Furthermore, there is a big similarity between input/output files for program CyMPA and for program SMiPA. Therefore, only the differences between cylindrical and spherical case will be explained in this chapter.

5.2.2 Differences between Cylindrical and Spherical Program

The CyMPA and CyMPApat programs analyze rectangular patch antennas or antenna arrays placed on circular cylinders, as illustrated in Fig. 5.3. If an array is analyzed, following assumptions are made:

- all antenna elements are identical
- the patch elements are of rectangular shape
- constant spacing between neighboring patches in circumferential (ϕ) direction
- constant spacing between neighboring patches in axial (z) direction
- the dielectric structure can be multilayered with losses
- the patch array must be placed at the top of one such layer
- in the case of aperture-coupled patch antennas the apertures are of rectangular shape (with unequal sides)
- there must be a constant spacing between the patch center and the aperture center

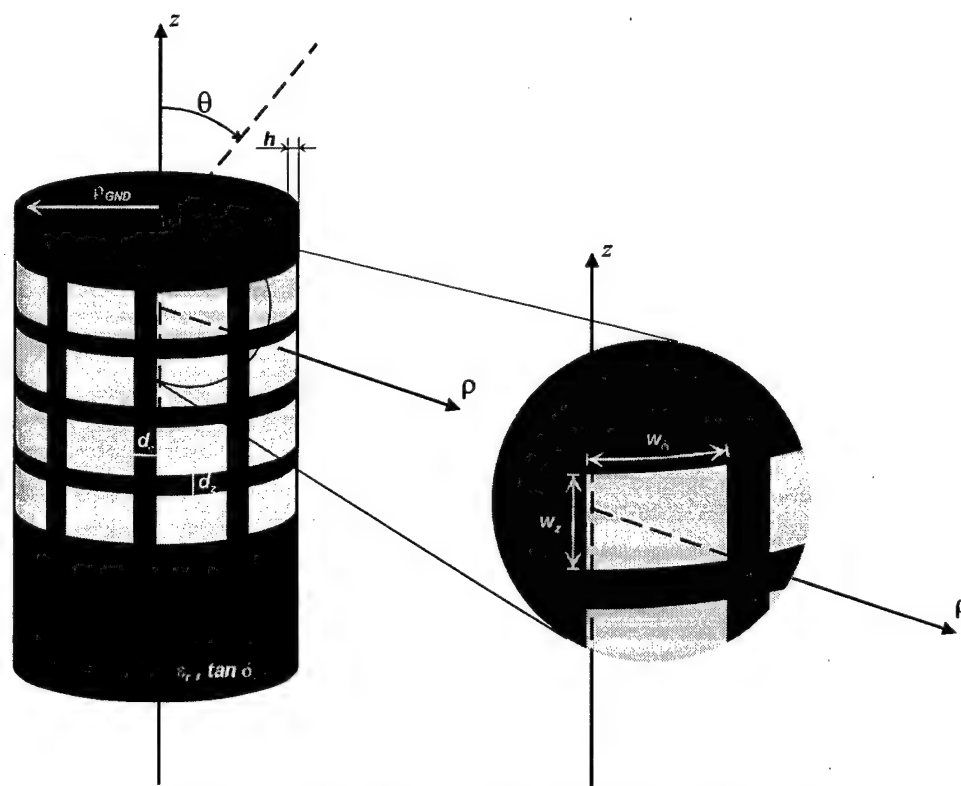


Figure 5.3. The geometry of the cylindrical patch array

The differences between SMiPA and CyMPA and their input/output files are:

- In the cylindrical case the patch elements are of rectangular shape, while in the spherical case patch elements can be both rectangular and circular.
- In the cylindrical case only the rectangular grid of patch elements can be considered. In the spherical case icosahedron grid can be also considered, as well as arbitrary grid.
- The input files for programs CyMPA and SMiPA are called cympa.in and smipa.in, respectively. However, their structure and meaning of variables is very similar.
- In the cylindrical case the patch width / feed point / slot width / grid dimensions are given first in ϕ -direction and then in z -direction. In the spherical case dimensions are given first in θ -direction and then in ϕ -direction.
- Two different output files (but with almost identical meaning) are cympa.out / cypapat.out, and smipa.out / smipapat.out. All other output files have the same meaning and structure.

More details about program CyMPA can be found in [13].

6 BENCHMARKS

6.1 Spherical 16 element Array Following the Icosahedron Grid –Radiation by Simple Model

6.1.1 Introduction

Icosahedron grid is a very suitable concept for spherical arrays that steer the beam throughout the whole hemisphere. This benchmark presents the radiation properties of 16 element microstrip array on the spherical structure following icosahedric grid, as depicted in figure 6.1. This number of elements corresponds to hemisphere coverage of 30 degrees. The step of 15° for each next circle comes from dividing by 4 the side of triangle of basic icosahedron structure.

The calculations are performed using the grounded shell of radius 20 cm, dimensions of patches are 2.5 cm \times 2.5 cm. The patch excitation for each patch is phase corrected in order to compensate the propagation path difference. In this benchmark input file and calculations for simple and fast equiamplitude model are presented. This model gives only radiation pattern and does not include mutual coupling. Radiation pattern calculation procedure when using this **simple approach** will follow the diagram in Fig. 6.2. Notice that only SMiPApat program must be applied. The next benchmark deals with the same configuration calculated rigorously, so that a comparison can be performed.

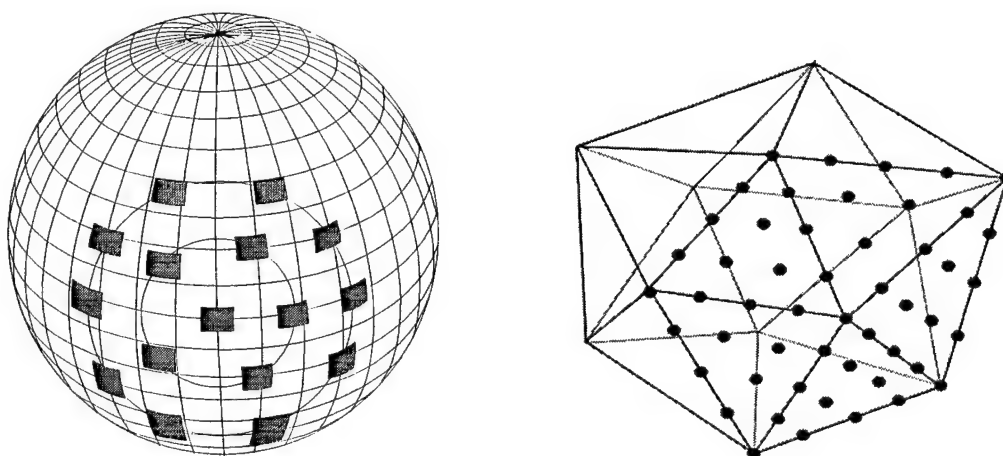


Figure 6.1. Spherical array with 16 elements following the icosahedron grid

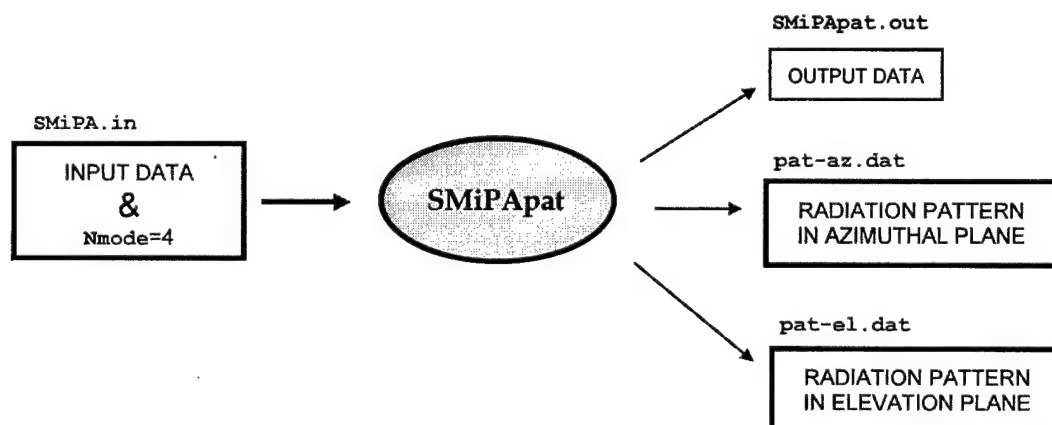


Figure 6.2. Procedure for calculating radiation pattern using simple approach

6.1.2 Summary technical description

Antenna / Antenna Array description

Type: 16 element spherical array following icosahedron grid

Frequency: 3.64 GHz

The mechanical and dielectric data of the structure:

no. of layer	layer description	relative permittivity	loss tangent	inner radius	outer radius	thickness
-	ground sphere	-	-	20 cm	20 cm	-
1	PTFE sphere	2.52	0.0019	20 cm	20.1576 cm	0.1576 cm

Rectangular patch element data:

Element is printed on	azimuthal dimension	elevation dimension
outer shell of layer no. 1	2.5 cm	2.5 cm

Coaxial excitation position, relative to patch center:

elevational position	azimuthal position
0.3 cm	0 cm

Array configuration: 16 element icosahedron grid

number of rings	icosahedron side subdivision factor
3	4

6.1.3 Numerical results

The radiation pattern in E and H plane were calculated using assumption of equiamplitude identical patch currents that does not take mutual coupling into account. The calculation is performed at frequency of 3.64 GHz. Figure 6.3 shows the input file for this case. Light printed are the values and rows that are irrelevant for this case.

The SMiPapat routine was run to calculate the radiation pattern. The calculated radiation pattern in E and H plane is given in Figure 6.4. and Figure 6.5.

3.64	3.64	1	R	! Frequency (GHz)
20.0				! Ground shell and patch radius (cm)
1				! Number of dielectric layers
0.1576	2.52	0.0019		! Relative permittivity and loss tanges
1				! Die. layer at which patches are placed
3	4	I		! Array grid parameters and grid type
2.5	2.5	R		! Patch width in theta and phi dir(cm),rectang.sh
C				! Feeding type: 'c'=coax, 'm'=microstrip, 'a'=apertu
1				! Number of ports per patch
0.3	0.0			! Port position
Y				! Equal port excitations? (Y - yes, N - no)
0.0	0.0			! Distance between patch centers
50.0				! Characteristic impedance of the feed line
-180.0	180.0	361		! Azimuthal pattern
-89.0	269.0	359		! Elevation pattern
0.0				! Phi angle of the evelation pattern
90.0	0.0			! Theta and phi angle of the main beam
L				! Polarization (L - linear, C - circular)
4				! Phase corrected excitation

Figure 6.3. Input file smipa.in

A few lines from the radiation pattern output file 'pat-az.dat' around $\phi = 0$ are:

:	:	:	:
90.0000	-5.0000	-0.7020	-200.0000
90.0000	-4.0000	-0.4477	-200.0000
90.0000	-3.0000	-0.2512	-200.0000
90.0000	-2.0000	-0.1114	-200.0000
90.0000	-1.0000	-0.0278	-200.0000
90.0000	0.0000	0.0000	-200.0000
90.0000	1.0000	-0.0278	-200.0000
90.0000	2.0000	-0.1114	-200.0000
90.0000	3.0000	-0.2512	-200.0000
90.0000	4.0000	-0.4478	-200.0000
90.0000	5.0000	-0.7021	-200.0000
:	:	:	:

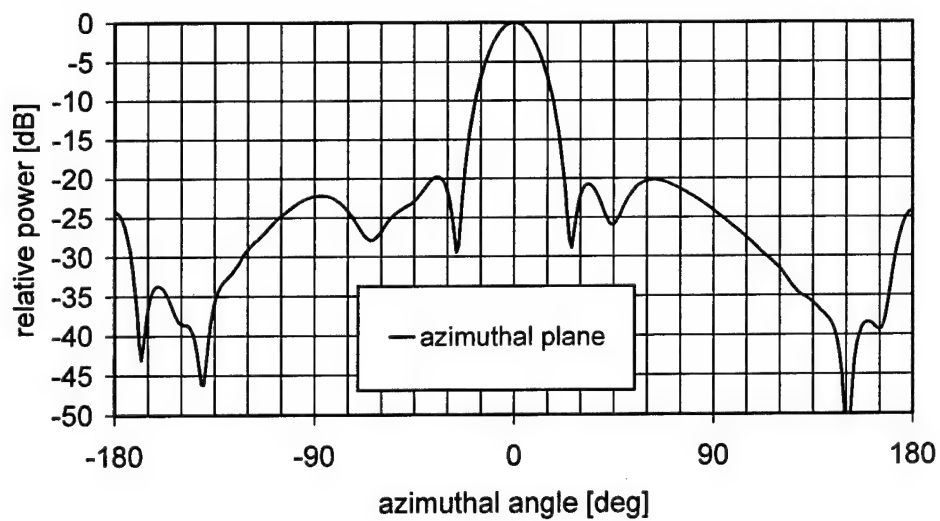


Figure 6.4. Calculated radiation pattern in azimuthal plane

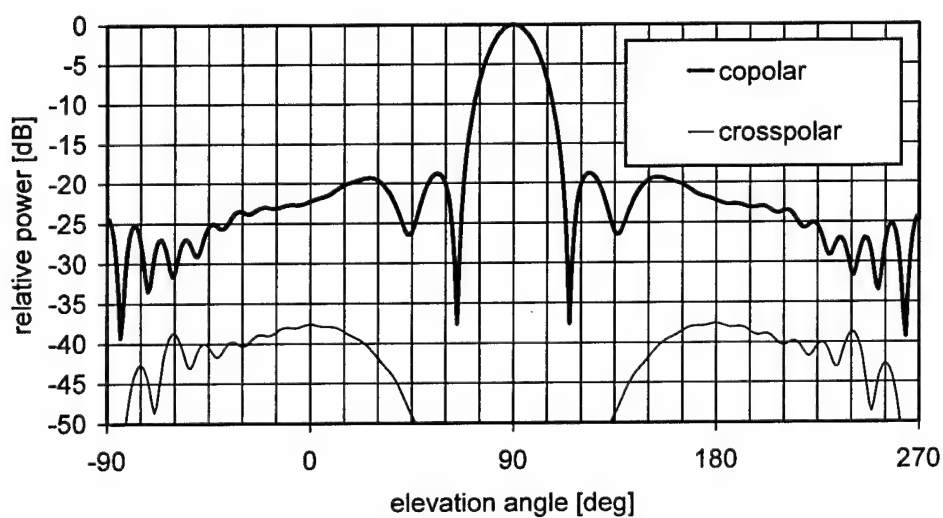


Figure 6.5. Calculated radiation pattern in elevation plane

6.2 Spherical 16 element Array Following the Icosahedron Grid –Radiation by Rigorous Model

6.2.1 Introduction

In the previous benchmark we considered the radiation properties of 16 element microstrip array on the spherical structure following icosahedric grid (Fig. 6.6). The radiation pattern was calculated without taking mutual coupling into account. In this benchmark the radiation pattern calculated in a rigorous way will be considered. Therefore, after running SMiPA program and obtaining currents on each patch, SMiApat program must be run in order to obtain radiation pattern. The comparison of radiation pattern with the simple calculation model that is used in previous benchmark is performed.

The calculations are performed using the grounded shell of radius 20 cm, dimensions of patches are $2.5 \text{ cm} \times 2.5 \text{ cm}$. The patch excitation for each patch is phase corrected in order to compensate the propagation path difference. 16 elements correspond to hemisphere coverage of 30 degrees. The step of 15° for each next circle comes from dividing by 4 the side of triangle of basic icosahedron structure.

Radiation pattern calculation procedure, when using **rigorous approach**, will follow the diagram in Fig. 6.7. SMiPA program must be applied to determine rigorous current distributions on the patch before calculating radiation pattern. In order to obtain radiation pattern SMiApat program must be run.

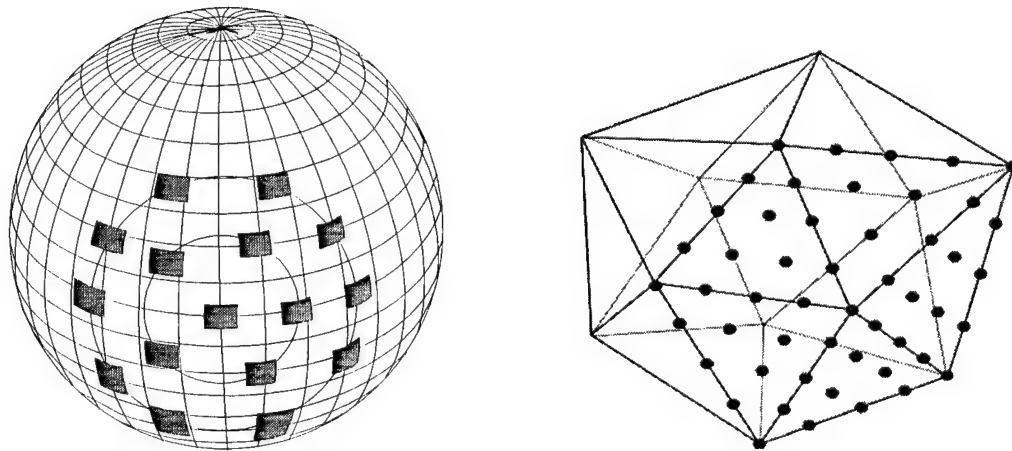


Figure 6.6. Spherical array with 16 elements following the icosahedron grid

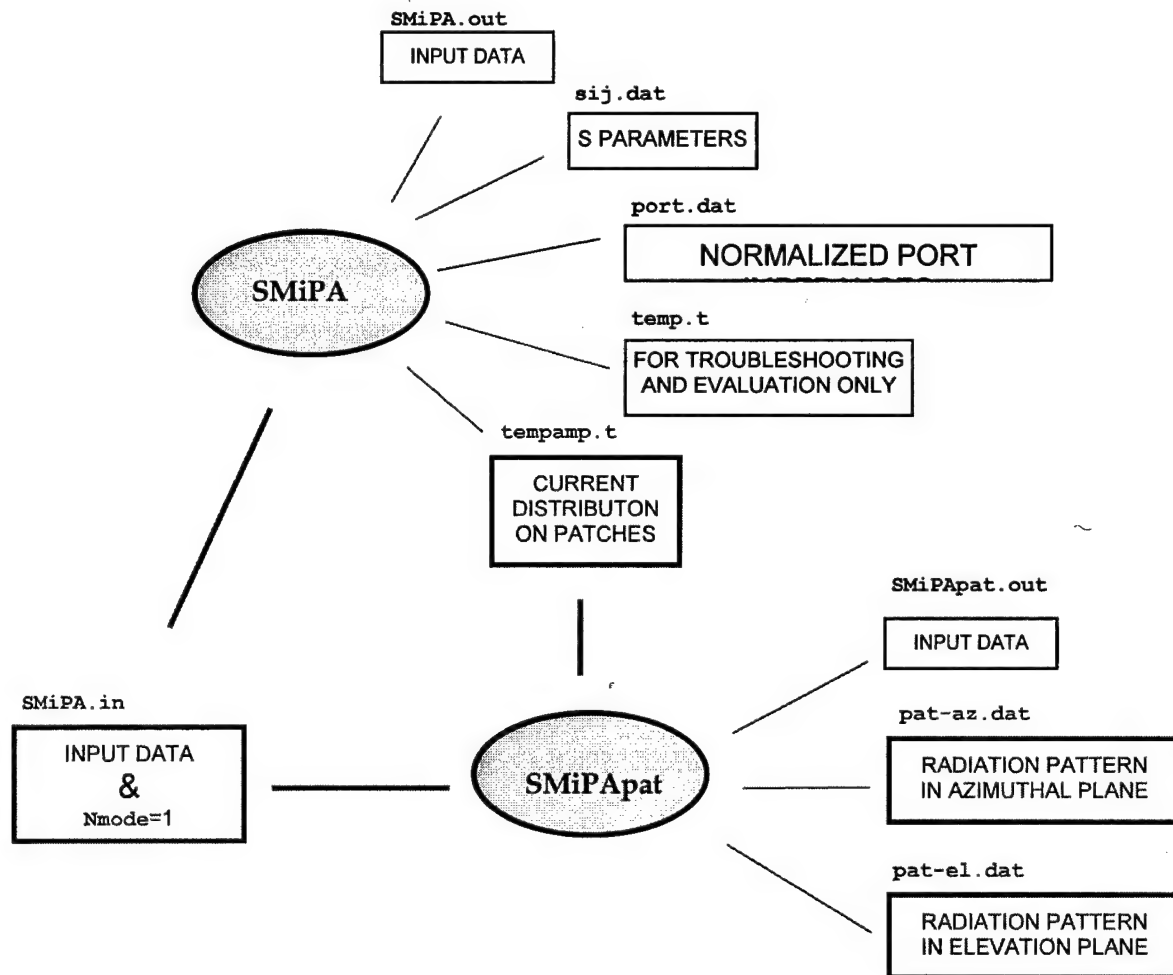


Figure 6.7. Procedure for calculating radiation pattern using rigorous approach

6.2.2 Summary technical description

Antenna / Antenna Array description

Type: 16 element spherical array following icosahedron grid

Frequency: 3.64 GHz

The mechanical and dielectric data of the structure:

no. of layer	layer description	relative permittivity	loss tangent	inner radius	outer radius	thickness
-	ground sphere	-	-	20 cm	20 cm	-
1	PTFE sphere	2.52	0.0019	20 cm	20.1576 cm	0.1576 cm

Rectangular patch element data:

Element is printed on	azimuthal dimension	elevation dimension
outer shell of layer no. 1	2.5 cm	2.5 cm

Coaxial excitation position, relative to patch center:

elevational position	azimuthal position
0.3 cm	0 cm

Array configuration: 16 element icosahedron grid

number of rings	icosahedron side subdivision factor
3	4

6.2.3 Numerical results

The radiation pattern in E and H plane were calculated using assumption of equiamplitude identical patch currents that does not take mutual coupling into account. The calculation is performed at frequency of 3.64 GHz. Figure 6.8 shows the input file for this case. Light printed are the values and rows that are irrelevant for this case.

The SMiPapat routine was run to calculate the radiation pattern. The calculated radiation pattern in E and H plane is given in Figure 6.9.

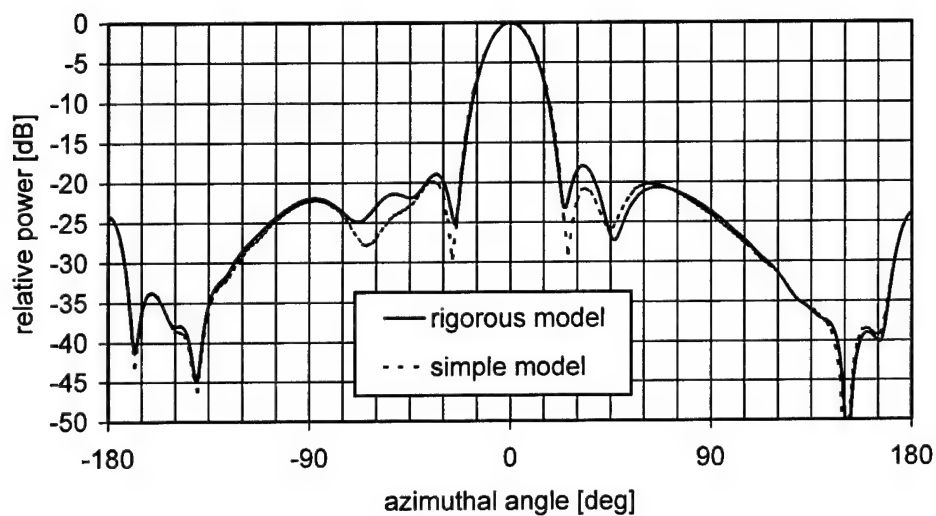
3.64	3.64	1	R	! Frequency (GHz)
20.0				! Ground shell and patch radius (cm)
1				! Number of dielectric layers
0.1576	2.52	0.0019		! Relative permittivity and loss tangents
1				! Die. layer at which patches are placed
3	4	I		! Array grid parameters and grid type
2.5	2.5	R		! Patch width in theta and phi dir(cm),rectang.sh
C				! Feeding type:'c'=coax,'m'=microstrip,'a'=aperture
1				! Number of ports per patch
0.3	0.0			! Port position
N				! Equal port excitations? (Y - yes, N - no)
0.0	0.0			! Distance between patch centers
50.0				! Characteristic impedance of the feed line
-180.0	180.0	361		! Azimuthal pattern
-89.0	269.0	359		! Elevation pattern
0.0				! Phi angle of the elevation pattern
90.0	0.0			! Theta and phi angle of the main beam
L				! Polarization (L - linear, C - circular)
1				! Radiation pattern calculated rigorously
1	1	1	1.0	0.0
2	1	1	1.0	30.0
2	2	1	1.0	30.0
2	3	1	1.0	30.0
2	4	1	1.0	30.0
2	5	1	1.0	30.0
3	1	1	1.0	118.0
3	2	1	1.0	118.0
3	3	1	1.0	118.0
3	4	1	1.0	118.0
3	5	1	1.0	118.0
3	6	1	1.0	118.0
3	7	1	1.0	118.0
3	8	1	1.0	118.0
3	9	1	1.0	118.0
3	10	1	1.0	118.0

Figure 6.8. Input file smipa.in

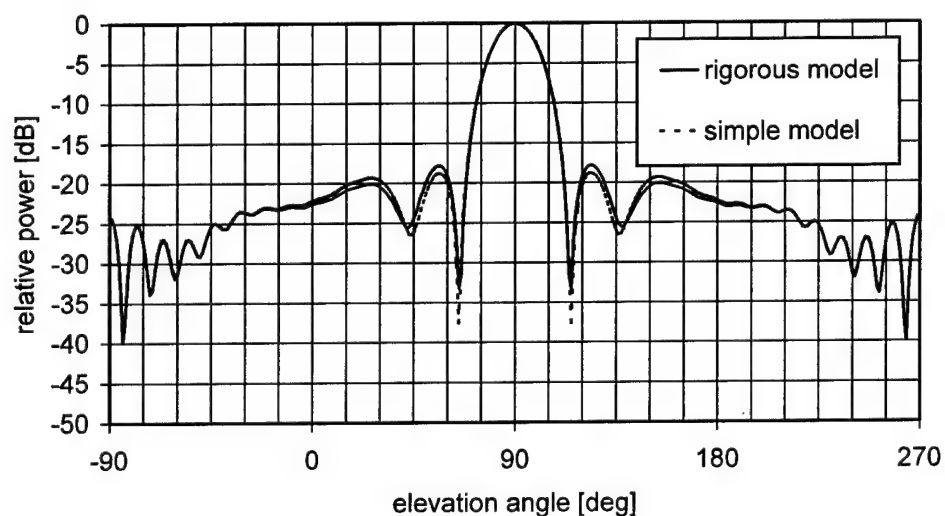
A few lines from the radiation pattern output file 'pat-az.dat' around $\phi = 0$ are:

:	:	:	:
90.0000	-5.0000	-0.7268	-79.3460
90.0000	-4.0000	-0.4627	-81.1226
90.0000	-3.0000	-0.2588	-83.3903
90.0000	-2.0000	-0.1142	-86.4056
90.0000	-1.0000	-0.0281	-90.4843

90.0000	0.0000	0.0000	-93.8173
90.0000	1.0000	-0.0299	-90.8304
90.0000	2.0000	-0.1179	-86.8503
90.0000	3.0000	-0.2645	-83.9390
90.0000	4.0000	-0.4705	-81.7928
90.0000	5.0000	-0.7369	-80.1506
:	:	:	:



(a)



(b)

Figure 6.9. Comparison of calculated radiation pattern in elevation plane using simple and rigorous models. (a) azimuthal plane, (b) elevation plane.

6.3 Rectangular patch antenna on spherical structure

6.3.1 Introduction

This example deals with input impedance of rectangular patch printed on spherical structure. The geometry of the problem is given in Fig. 6.10. The square patch of dimension 5.1×5.1 cm is placed above the ground shell using syrofoam spacers. Therefore, substrate relative dielectric constant is $\epsilon_r = 1.0$ and the air gap due to syrofoam spacers is 0.52 cm thick. For the validation of calculation results a laboratory model was built from a copper half-sphere of radius $a = 18.7$ cm at which patches can be mounted at arbitrary positions.

The detailed data sheet about the calculated/measured antenna is given in 6.3.2. In order to calculate this example a run of SMiPA is needed, with an input file that is shown in section 6.3.3. The comparison of calculation and measurement can be found in section 6.3.3 as well. The calculated and measured impedances are in a good agreement.

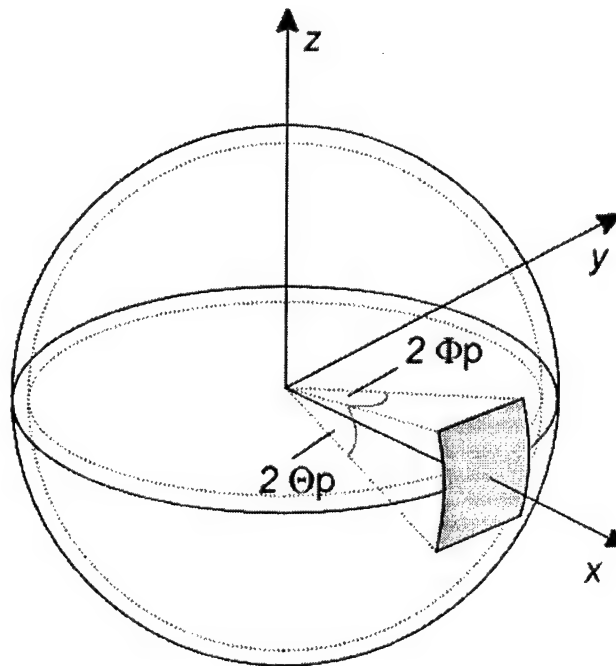


Figure 6.10. Rectangular patch antenna on spherical structure

6.3.2 Summary technical description

Antenna / Antenna Array description

Type: Rectangular patch element printed on spherical grounded substrate

Frequency: 2 GHz – 3 GHz, 21 equidistant points

The mechanical and dielectric data of the structure:

no. of layer	layer description	relative permittivity	loss tangent	inner radius	outer radius	thickness
-	ground sphere	-	-	18.7 cm	18.7 cm	-
1	air gap	1.00	0.0000	18.7 cm	19.22 cm	0.52 cm

Rectangular patch element data:

Element is printed on	azimuthal dimension	elevation dimension
outer shell of layer no. 1	5.1 cm	5.1 cm

Coaxial excitation position, relative to patch center:

elevational position	azimuthal position
1.95 cm	0 cm

Array configuration: **single element**

6.3.3 Numerical and experimental results

The calculation is performed in frequency range of 2.0 to 3.0 GHz at 21 equidistant frequency points. Figure 6.11 shows the input file for the program SMiPA. Light printed are the values and rows that are irrelevant for this case. Here, distance between patches is irrelevant since a single patch configuration is considered. Additionally, all data for radiation pattern is irrelevant, since in this benchmark only the input impedance is of interest.

```

2.0      3.0      21      R  ! Frequency (GHz)
18.7     ! Ground shell and patch radius (cm)
1         ! Number of dielectric layers
0.52     1.0      0.0000 ! Relative permittivity and loss tangen
1         ! Die. layer at which patches are placed
1         1       R      ! Array grid parameters and grid type
5.1      5.1      R      ! Patch width in theta and phi dir(cm),rectang.sh
C         ! Feeding type:'c'=coax,'m'=microstrip,'a'=apertu
1         ! Number of ports per patch
1.95     0.0      ! Port position
Y         ! Equal port excitations? (Y - yes, N - no)
0.0      0.0      ! Distance between patch centers
50.0     ! Characteristic impedance of the feed line
-180.0   180.0    361   ! Azimuthal pattern
-89.0    269.0    359   ! Elevation pattern
0.0      ! Phi angle of the evelation pattern
90.0     0.0      ! Theta and phi angle of the main beam
L         ! Polarization (L - linear, C - circular)
1         ! Phase corrected excitation

```

Figure 6.11. Input file smipa.in

A few lines from the file 'SMiPA.out' are:

```

:           :           :           :
2.35000     0.65205     3.13193     -1.01286
2.40000     1.01869     3.43469     -1.28849
2.45000     1.67610     3.72735     -1.66488
2.50000     2.80854     3.72161     -2.19101
2.55000     4.14682     2.68146     -2.94561
2.60000     4.23653     0.69463     -4.05946
2.65000     3.05476     -0.43903     -5.76081
2.70000     1.98459     -0.58367     -8.48768
2.75000     1.32226     -0.39931     -13.24033
:           :           :           :

```

The comparison of the calculated input impedance is given in Fig. 6.12 for the real part and in Fig. 13 for the imaginary part. The measured results are also given.

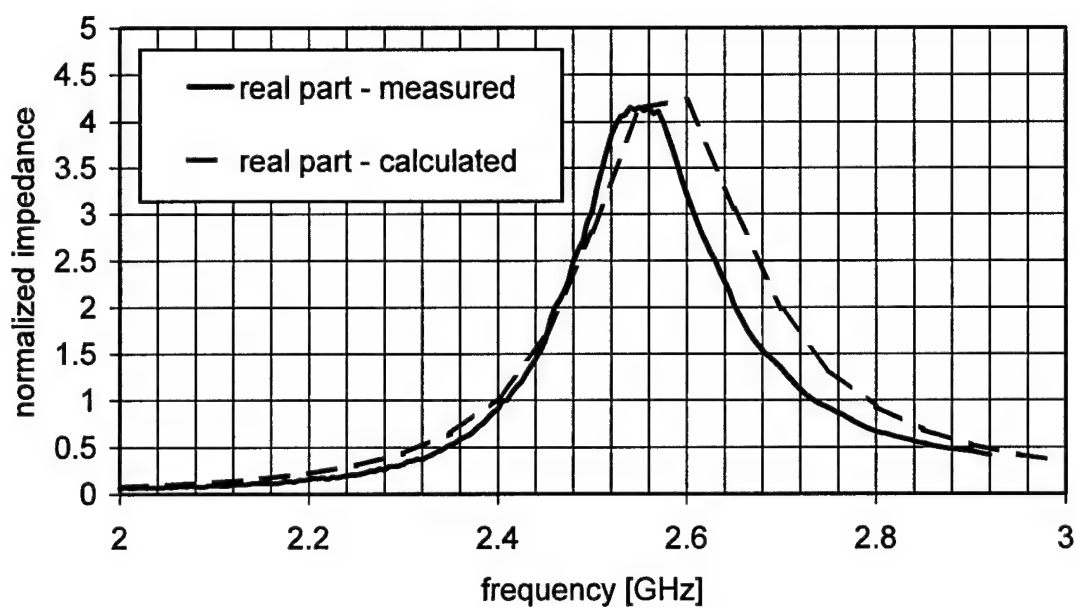


Figure 6.12. Comparison of calculated and measured real part of input impedance

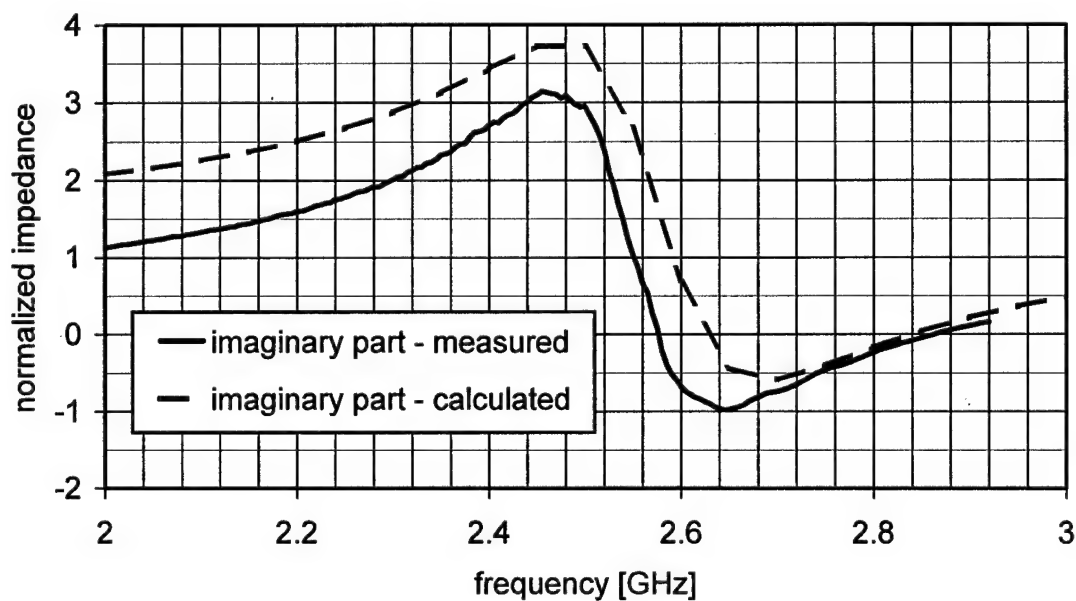


Figure 6.13. Comparison of calculated and measured imaginary part of input impedance

6.4 Circular patch antenna on spherical structure

6.4.1 Introduction

This example deals with input impedance of circular patch printed on the spherical structure. The geometry of the problem is given in figure 6.14. The analyzed circular patch has radius of 1.45 cm, and it is printed on the substrate with dielectric constant $\epsilon_r = 2.52$ and thickness $h = 1.576$ mm.

The detailed data sheet about the calculated/measured antenna is given in 6.4.2. In order to calculate this example a run of SMiPA is needed, with an input file that is shown in section 6.4.3. The influence of the radius of the spherical structure on the input impedance, cases with several different radii (2.5 cm, 4 cm and 10 cm) are calculated and the results compared with measured results of their planar counterpart.

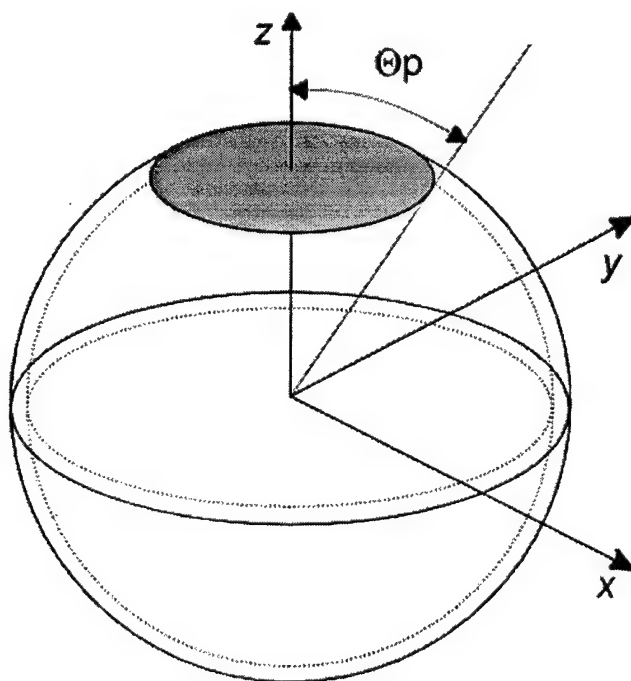


Figure 6.14. Circular patch antennas on spherical structure

6.4.2 Summary technical description

Antenna / Antenna Array description

Type: Circular patch element printed on spherical grounded substrate

Frequency: 3.2 GHz – 4.0 GHz, 81 equidistant points

The mechanical and dielectric data of the structure:

no.of layer	layer description	relative permittivity	loss tangent	inner radius	outer radius	thickness
-	ground sphere	-	-	planar	planar	-
1	PTFE sphere	2.52	0.0019	planar	planar	0.1576 cm

no.of layer	layer description	relative permittivity	loss tangent	inner radius	outer radius	thickness
-	ground sphere	-	-	10 cm	10 cm	-
1	PTFE sphere	2.52	0.0019	10 cm	10.1576 cm	0.1576 cm

no.of layer	layer description	relative permittivity	loss tangent	inner radius	outer radius	thickness
-	ground sphere	-	-	4 cm	4 cm	-
1	PTFE sphere	2.52	0.0019	4 cm	4.1576 cm	0.1576 cm

no.of layer	layer description	relative permittivity	loss tangent	inner radius	outer radius	thickness
-	ground sphere	-	-	2.5 cm	2.5 cm	-
1	PTFE sphere	2.52	0.0019	2.5 cm	2.6576 cm	0.1576 cm

Circular patch element data:

Element is printed on	diameter
outer shell of layer no. 1	2.9 cm

Coaxial excitation position, relative to patch center: 0.3 cm

Array configuration: **single element**

6.4.3 Numerical and experimental results

The calculation is performed in frequency range of 3.2 to 4.0 GHz at 81 equidistant frequency points. Figure 6.15 shows the input file for the program SMiPA in case of 10 cm diameter. Light printed are the values and rows that are irrelevant for this case. Here, distance between patches is irrelevant since a single patch configuration is considered. Additionally, all data for radiation pattern is irrelevant, since in this benchmark only the input impedance is of interest.

3.2	4.0	81	R ! Frequency (GHz)
10.0			! Ground shell and patch radius (cm)
1			! Number of dielectric layers
0.1576	2.52	0.0019	! Relative permittivity and loss tangents
1			! Die. layer at which patches are placed
1	1	R	! Array grid parameters and grid type
2.9	4.0	C	! Patch diameter (cm), circular shape
C			! Feeding type: 'c'=coax, 'm'=microstrip, 'a'=aperture
1			! Number of ports per patch
0.3	0.0		! Port position
Y			! Equal port excitations? (Y - yes, N - no)
0.0	0.0		! Distance between patch centers
50.0			! Characteristic impedance of the feed line
-180.0	180.0	361	! Azimuthal pattern
-89.0	269.0	359	! Elevation pattern
0.0			! Phi angle of the elevation pattern
90.0	0.0		! Theta and phi angle of the main beam
L			! Polarization (L - linear, C - circular)
1			! Phase corrected excitation

Figure 6.15. Input file *smipa.in* for 10 cm ground shell diameter

A few lines from the file 'smipa.out' are:

:	:	:	:
3.62000	0.37823	0.88159	-3.61726
3.63000	0.45047	0.89057	-4.22490
3.64000	0.53641	0.88651	-4.97472
3.65000	0.63469	0.86152	-5.90979
3.66000	0.73924	0.80634	-7.09043
3.67000	0.83714	0.71356	-8.60387
3.68000	0.90922	0.58359	-10.57906
3.69000	0.93675	0.42977	-13.19239
3.70000	0.91200	0.27617	-16.47603
3.71000	0.84339	0.14638	-18.71635
3.72000	0.74956	0.05297	-16.69852
3.73000	0.64904	-0.00401	-13.43902
3.74000	0.55414	-0.03178	-10.82575
3.75000	0.47065	-0.03914	-8.85473
3.76000	0.39997	-0.03357	-7.34775
3.77000	0.34128	-0.02046	-6.17312
:	:	:	:

The comparison of the calculated input impedances is given in Fig. 6.16 for the real part and in Fig. 17 for the imaginary part. The measured results for planar case are also given.

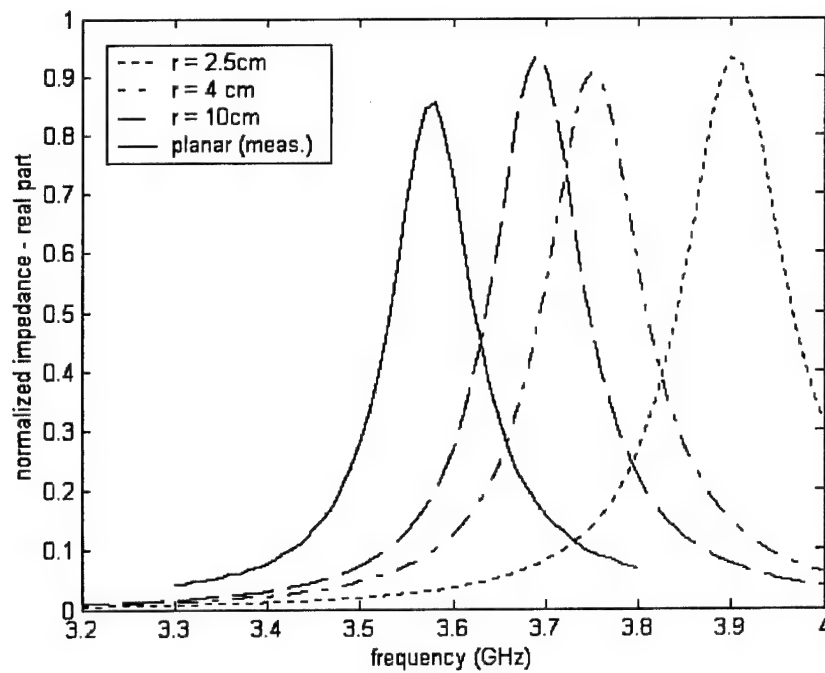


Figure 6.16. Comparison of calculated real part of input impedance for spheres with radii of 2.5, 4 and 10 cm with measurements for the planar case

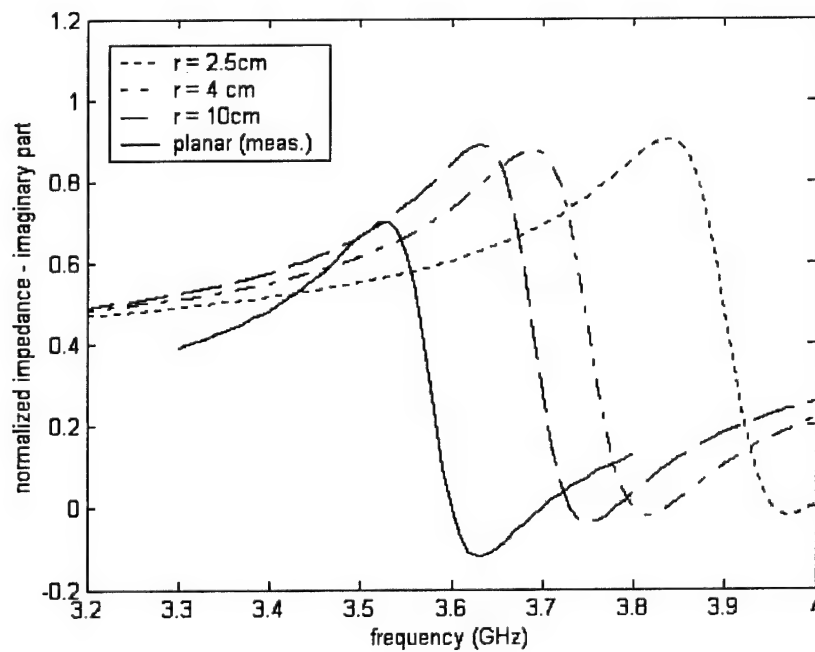


Figure 6.17. Comparison of calculated imaginary part of input impedance for spheres with radii of 2.5, 4 and 10 cm with measurements for the planar case

6.5 Mutual Coupling of Two Rectangular Patches Printed on Spherical Structure

6.5.1 Introduction

This example deals with mutual coupling of two rectangular patches printed on spherical structure. The geometry of the problem is given in Fig. 6.18. The square patches of dimension 5.1×5.1 cm are placed above the ground shell using syrofoam spacers. Therefore substrate relative dielectric constant is $\epsilon_r = 1.0$ and the air gap due to syrofoam spacers is 0.52 cm thick. For the validation of calculation results a laboratory model was built from a copper half-sphere of radius $a = 18.7$ cm at which patches can be mounted at arbitrary positions.

The detailed data sheet about the calculated/measured antenna is given in 6.5.2. In order to calculate this example a run of SMiPA is needed, with an input file that is shown in section 6.5.3. The comparison of calculation and measurement can be found in section 6.3.3 as well. The calculated and measured mutual coupling is in a good agreement.

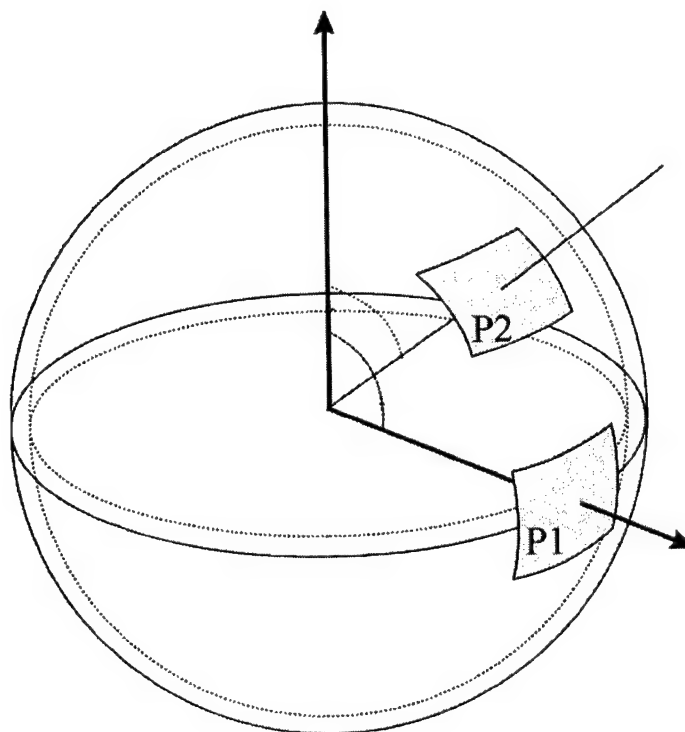


Figure 6.18. Two element array of rectangular patches on spherical structure

6.5.2 Summary technical description

Antenna / Antenna Array description

Type: Rectangular patch element printed on spherical grounded substrate

Frequency: 2 GHz – 3 GHz, 21 equidistant points

The mechanical and dielectric data of the structure:

no. of layer	layer description	relative permittivity	loss tangent	inner radius	outer radius	thickness
-	ground sphere	-	-	18.7 cm	18.7 cm	-
1	air gap	1.00	0.0000	18.7 cm	19.22 cm	0.52 cm

Rectangular patch element data:

Element is printed on	azimuthal dimension	elevation dimension
outer shell of layer no. 1	5.1 cm	5.1 cm

Coaxial excitation position, relative to patch center:

elevational position	azimuthal position
1.95 cm	0 cm

Array configuration:

patch center distances	no. of elements	separation direction
10.25 cm	2	θ (azimuthal)

6.5.3 Numerical results

The calculation is performed in frequency range of 2.0 to 3.0 GHz at 21 equidistant frequency points. Figure 6.19 shows the input file "smipa.in" for the program SMiPA. Light printed are the values and rows that are irrelevant for this case. All data for radiation pattern is irrelevant, since in this benchmark only the input impedances and mutual coupling are of interest.

2.0	3.0	21	R	! Frequency (GHz)
18.7				! Ground shell and patch radius (cm)
1				! Number of dielectric layers
0.52	1.0	0.0000		! Relative permittivity and loss tangen
1				! Die. layer at which patches are placed
2	1	R		! Array grid parameters and grid type
5.1	5.1	R		! Patch width in theta and phi dir(cm),rectang.sh
C				! Feeding type: 'c'=coax, 'm'=microstrip, 'a'=apertu
1				! Number of ports per patch
1.95	0.0			! Port position
Y				! Equal port excitations? (Y - yes, N - no)
10.25	0.0			! Distance between patch centers
50.0				! Characteristic impedance of the feed line
-180.0	180.0	361		! Azimuthal pattern
-89.0	269.0	359		! Elevation pattern
0.0				! Phi angle of the elevation pattern
90.0	0.0			! Theta and phi angle of the main beam
L				! Polarization (L - linear, C - circular)
1				! Phase corrected excitation

Figure 6.19. Input file cimpa.in

A few lines from the file 'Sij.dat' are:

:	:	:	:	:	:	:	:	:
2.2500	-0.65	40.60	-39.53	146.36	-39.53	146.36	-0.65	40.59
2.3000	-0.80	37.61	-38.48	141.07	-38.48	141.07	-0.81	37.60
2.3500	-1.01	34.15	-37.33	135.41	-37.33	135.41	-1.01	34.15
2.4000	-1.28	30.13	-36.05	129.18	-36.05	129.18	-1.29	30.13
2.4500	-1.66	25.39	-34.63	122.07	-34.63	122.07	-1.67	25.39
2.5000	-2.18	19.72	-33.08	113.68	-33.08	113.68	-2.19	19.74
2.5500	-2.94	12.86	-31.42	103.54	-31.42	103.54	-2.95	12.90
2.6000	-4.05	4.46	-29.71	91.13	-29.71	91.13	-4.06	4.52
2.6500	-5.75	-6.05	-28.06	76.04	-28.06	76.04	-5.77	-5.94
2.7000	-8.49	-19.89	-26.61	58.17	-26.61	58.17	-8.50	-19.70
:	:	:	:	:	:	:	:	:

The comparison of the calculated mutual coupling with the measurements is given in Fig. 6.20.

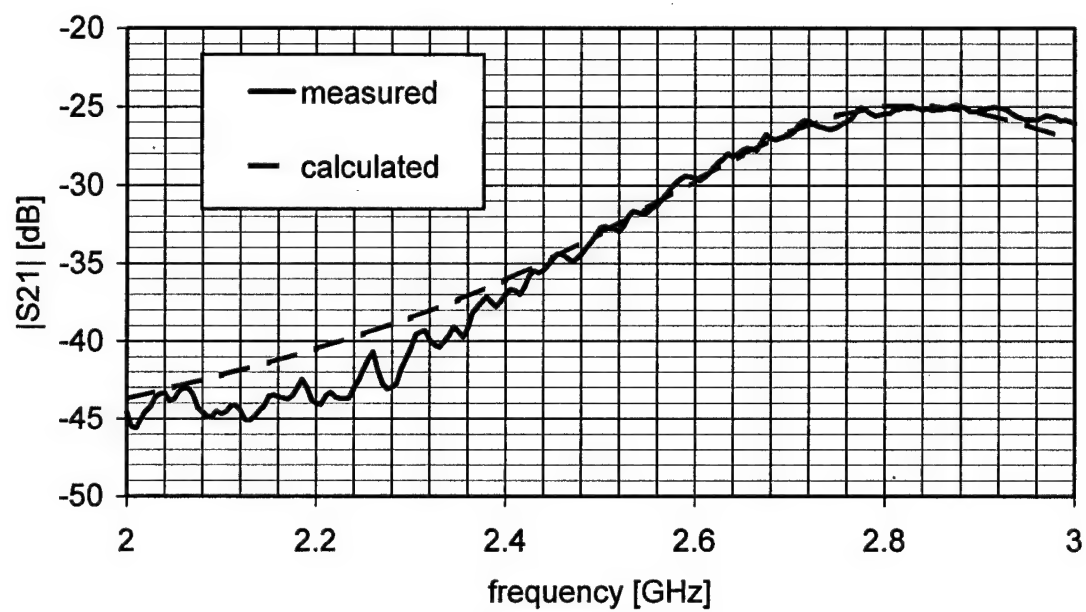


Figure 6.20. Calculated and measured mutual coupling coefficient S_{21} .

6.6 Aperture-Coupled Cylindrical Patch Antenna

6.6.1 Introduction

The developed program for analyzing cylindrical aperture-coupled patches has been verified against measurements made at University of Karlsruhe [16]. The aperture-coupled array was realized in C-band, and it consists of supporting metallic cylinder with radius 2.6 cm, covered with foam spacer of thickness 1.45 mm and with RT/duroid substrate. On RT/duroid substrate both microstrip transmission line (facing supporting metallic cylinder covered with foam) and ground plane with apertures (facing outwards) were printed. The outer region consists of foam spacer (thickness 0.4 cm) and Kapton foil on which patches were printed. Notice that the radius of the ground tube with apertures is calculated as a sum of the radius of the supporting metallic cylinder and of the thicknesses of the foam and RT/duroid substrates. The patch size is 2.5 cm (azimuthal dim.) \times 1.99 cm (axial dim.), the slot size is 1.38 \times 0.09 cm, the length of the open stub is 0.35 cm, and the width of the microstrip line is 0.154 cm. The 2 \times 2 array is considered and as a verification S_{11} parameter, S_{21} parameter and radiation pattern are calculated and compared with measurements. The patches are separated in ϕ -direction with distance between neighboring patch centers of 3.54 cm and in θ -direction with distance between neighboring patch centers of 3.46 cm. The design under analysis is shown in Fig. 6.21.

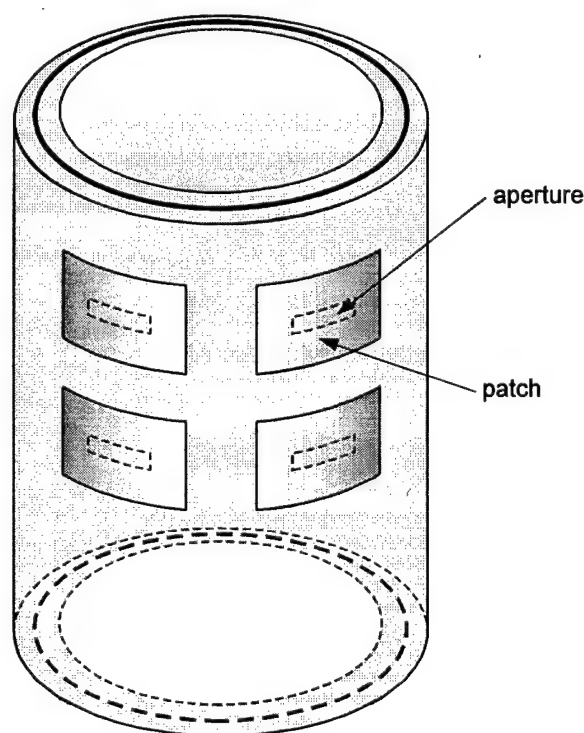


Figure 6.21 – The circular-cylindrical 2x2 aperture-coupled patch array

6.6.2 Summary technical description

Measurements: measurements made at University of Karlsruhe [10]

Antenna / Antenna Array description

Type: 2 x 2 element array

Frequency: C-band, 4.5 GHz - 6.5 GHz, calculation: 11 equally spaced points

The mechanical and dielectric data of the structure:

no. of layer	layer description	relative permittivity	loss tangent	inner radius	outer radius	thickness
inner 2	foam spacers	1.1	0.001	2.6 cm	4.05 cm	1.45 cm
inner 1	RT/duroid substrate	2.2	0.0009	4.05 cm	4.1008 cm	0.0508 cm
-	ground tube	-	-	4.1008 cm	4.1008 cm	-
1	foam spacers	1.1	0.001	4.1008 cm	4.5008 cm	0.4 cm
2	Kapton foil	3.7	0.001	4.5008 cm	4.5083 cm	0.0075 cm

Rectangular patch element data:

Element is printed on	azimuthal dimension	axial dimension
outer shell of layer no. 2	2.5 cm	1.99 cm

Aperture coupled excitation data:

aperture (slot) length	aperture (slot) width	microstrip line width	open stub length	substrate thickness	ϵ_r	substrate loss tangent
1.38 cm	0.09 cm	0.154 cm	0.35 cm	0.0508 cm	2.2	0.0009

Array configuration:

patch center distance	no. of elements	separation direction
3.54 cm	2	ϕ (azimuthal)
3.46 cm	2	z (axial)

6.6.3 Numerical results

As a verification case we wanted to calculate S_{11} parameter, S_{21} parameter and radiation pattern of a 2 x 2 patch array. The input file "cimpa.in" for this case is shown in figure 6.22.

```

4.5  6.5  11  R  ! Frequency (GHz)
4.1008      ! Ground tube radius (cm)
2          ! Number of dielectric layer
0.4  1.100  0.001 ! h, epsilon_r, tan(delta)
0.0075  3.700  0.001 ! h, epsilon_r, tan(delta)
2          ! Die. layer at which patches are placed
2  2  R      ! Number of patches in phi/z direction
2.5  1.99    ! Patch width in phi and z direction (cm)
A      ! Feeding type: 'c'=coax, 'm'=microstrip, 'a'=aperture
0.0  0.0      ! Aperture position in phi/z direction (cm)
Y      ! Equal port excitations? (Y - yes, N - no)
3.54081  3.46154 ! Distance between patch centers
1.38  0.09    ! Slot dimensions
2          ! Number of dielectric layers inside
0.0508  2.2  0.0009 ! h, epsilon_r, tan(delta)
4.05  1.1  0.001 ! h, epsilon_r, tan(delta)
1          ! Die. layer at which feed line is placed
0.154  0.35    ! Feed line width and stub length
-180.0  180.0  361 ! Azimuthal pattern
1.0  179.0  179 ! Elevation pattern
0.0      ! Phi angle of the elevation pattern
90.0  0.0      ! Theta and phi angle of the main beam
L      ! Polarization (L - linear, C - circular)
1      ! Mode of calculating the radiation pattern

```

Figure 6.22 - Input file cimpa.in

First the CyMPA routine was run to calculate the current distribution at each patch and the field distribution in each aperture in the array, as well as mutual coupling and input impedance, in the frequency band of interest 4.5-6.5 GHz. In the output file "Sij.dat" the S-parameters are written as a function of frequency:

```

# GHz S DB R 50
4.5000 -2.85 -144.19 -24.33 -6.86 -21.89 -63.58 -32.05 -123.28
      -24.33 -6.86 -2.85 -144.19 -32.05 -123.28 -21.89 -63.58
      -21.89 -63.58 -32.05 -123.28 -2.85 -144.19 -24.33 -6.86
      -32.05 -123.28 -21.89 -63.58 -24.33 -6.86 -2.85 -144.19
4.6000 -3.99 -159.57 -23.29 -31.30 -22.63 -76.29 -30.13 -147.50
      -23.29 -31.30 -3.99 -159.57 -30.13 -147.50 -22.63 -76.29
      -22.63 -76.29 -30.13 -147.50 -3.99 -159.57 -23.29 -31.30
      -30.13 -147.50 -22.63 -76.29 -23.29 -31.30 -3.99 -159.57
4.7000 -5.62 -176.97 -22.65 -57.39 -23.29 -84.31 -28.48 -172.52
      -22.65 -57.39 -5.62 -176.97 -28.48 -172.52 -23.29 -84.31
      -23.29 -84.31 -28.48 -172.52 -5.62 -176.97 -22.65 -57.39
      -28.48 -172.52 -23.29 -84.31 -22.65 -57.39 -5.62 -176.97
      : : : : : : : :

```

The comparison of calculated and measured S_{11} and the S_{21} parameters is shown in Figs. 6.23 and 6.24. Notice that the peaks and drops in measured S_{11} and S_{21} curves for frequencies larger than 6 GHz are due to the resonances in the feeding structure, i.e. they are due to the finite length of the antenna in the axial direction.

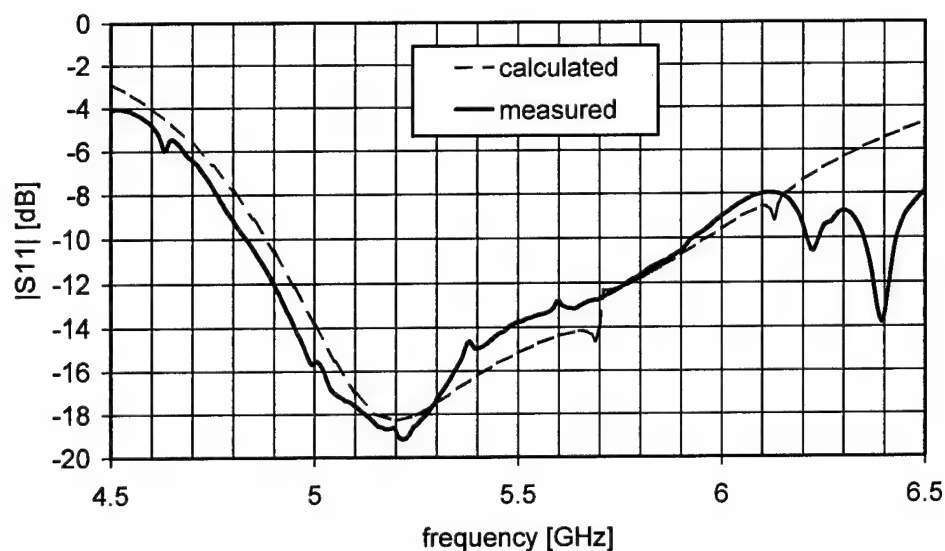


Figure 6.23. Calculated and measured magnitude of S_{11} .

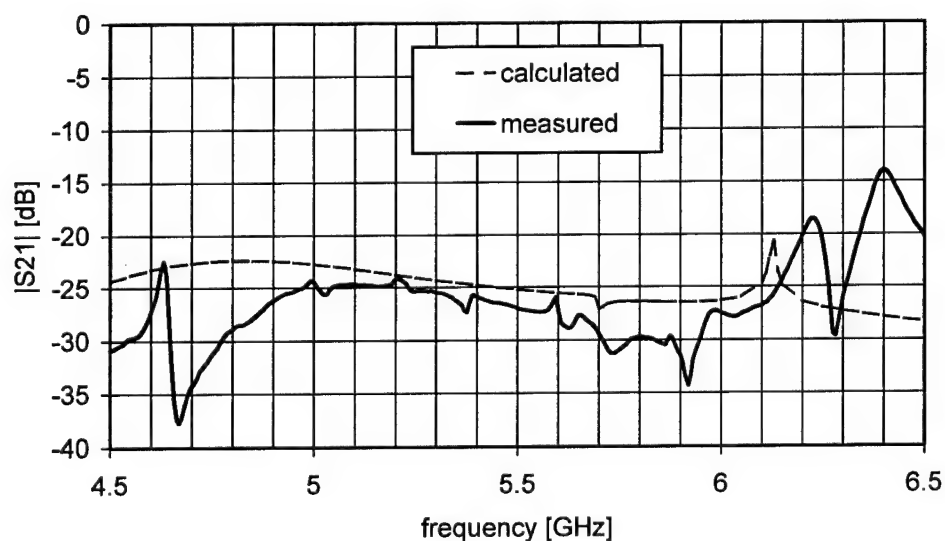


Figure 6.24. Calculated and measured magnitude of S_{21} for patches in azimuthal direction.

The CyMPApat routine was run to calculate the radiation pattern. Since we wanted radiation pattern (with mutual coupling taken into account) at 5.2 GHz, we changed the first line of the input file "cimpa.in" to run this case:

5.2 6.5 11 R ! Frequency (GHz)

The comparison between calculated and measured radiation pattern is given in Fig. 6.25.

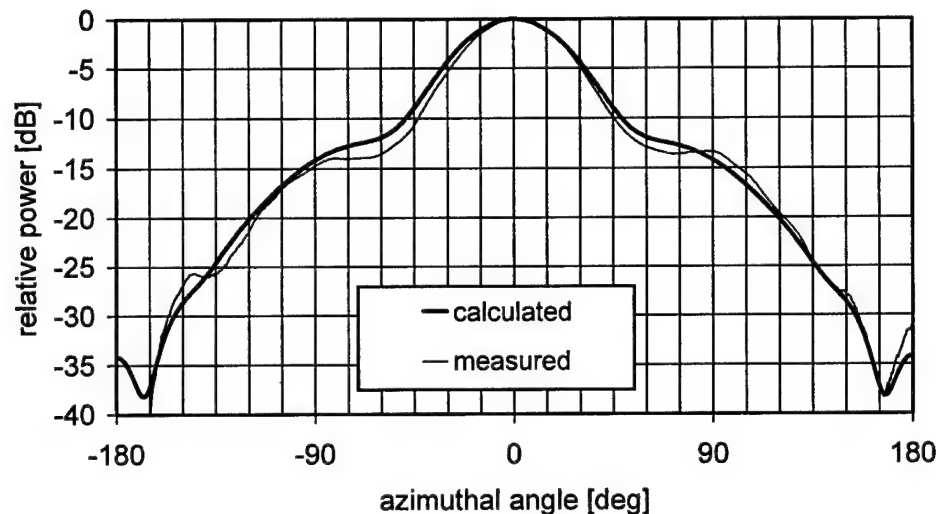


Figure 6.25. Radiation pattern of 2x2 array of aperture-coupled patches in azimuthal plane

7 SMiPAWin and CympaWin

USER'S MANUAL

graphical user interface for

**SMiPA
SMiPApat**

**CyMPA
CyMPApat**

SMiPAWin and CympaWin

USER'S MANUAL

graphical user interface for

**SMiPA
SMiPApat**

**CyMPA
CyMPApat**

Introduction

The SMiPA, CyMPA, SMiPApat and CyMPApat programs have a user interface through text input and output files, for both input and output. For the convenience of their users working on PCs using Microsoft Windows® the SMiPAWin and CympaWin software packages are developed. SMiPAWin package includes the SMiPA, SMiPApat and SMiPAWin – a Windows based graphical user interface. Similarly, CympaWin software package includes CyMPA, CyMPApat and CympaWin - Windows based graphical user interface. SMiPAWin and CympaWin run on IBM compatible PC with at least 386 processor, 16 Mb RAM and Windows 95/98 or later operation system installed. SMiPAWin and CympaWin are very similar from the users point of view, enabling identical features for spherical (SMiPAWin) and cylindrical (CympaWin) curved microstrip structures. Therefore, features of these two software packages are presented in parallel, mentioning both of them at each described feature. For the convenience the SMiPAWin is and the corresponding CympaWin equivalent is mentioned in brackets.

SMiPAWin (CympaWin) enables the following:

- easy, spreadsheet-like creating and editing of the input file **smipa.in (cympa.in)**
- launching of the simulation directly: SMiPAWin (CympaWin) executes SMiPA (CyMPA) and SmiPApat (CyMPApat) from MS - DOS prompt automatically
- display of calculated S-parameters, input impedance or radiation pattern using data from output files

These features enable the user to create input files for SMiPA (CyMPA) and SmiPApat (CyMPApat) with a click of a mouse, without need for careful text editing within **smipa.in** (**cympa.in**) file.

The Installation of the Software

Execute **setup.exe** from SMiPA (CyMPA) installation disk or CD ROM. During installation you can decide in which folder you want to have your SMiPAWin (CympaWin), SMiPA (CyMPA) and SmiPApat (CyMPApat) installed (e.g. in folder **c:\Program Files\Smipa** or **c:\Program Files\Cympa**).

Now you can start the SMiPAWin (CympaWin), entering your first antenna configuration and running calculations.

Using SMiPAWin (CympaWin)

The flow chart for SMiPAWin and CympaWin shows interactions between all identities involved: user, SMiPAWin (CympaWin), SMiPA (CyMPA) and SmiPApat (CyMPApat) programs. SMiPAWin (CympaWin) enables saving the configuration in arbitrary folder we call **design folder**, under the project name (here **project_name** will be used) selected through the standard dialog box. All output files will be named **project_name** plus corresponding extension. The configuration file extension is 'sin' ('cin' for CympaWin), so complete name of the configuration file is **project_name.sin** (**project_name.cin**).

Here are listed some hints that give more in depth information about using and operation of SMiPAWin (CympaWin):

- The SMiPA (CyMPA) and SMiPApat (CyMPApat) use input file **smipa.in** (**cympa.in**) where all configuration information is stored. **smipa.in** (**cympa.in**) file is created by SMiPAWin (CympaWin) as a copy of the **project_name.sin** (**project_name.cin**) file. After calculation, output files with calculation results calculated by SMiPA/SMiPApat (CyMPA/CyMPApat) occur in design folder.
- Rigorous calculation is performed by execution of SMiPA (CyMPA). Thus, input impedance and S parameters are obtained.
- SMiPApat (CyMPApat) can calculate radiation pattern using rigorous models (*Gain pattern, Pattern normalized to reference direction, Element pattern*) or simple models (*Simple model – uniform excitation, Simple model – file for patch excitation, Simple model – maximum predefined → phases corrected*). CAUTION: For rigorous models SMiPA (CyMPA) must be run first!
- It is not possible to run calculations if the configuration was changed without saving it first. The application title bar indicates the file name, and '*' is appended if file was changed but not saved.

- It is possible to view the previous results without running the calculations again. When the configuration name is selected, SMiPAWin (CympaWin) will enable View submenu items if previous output results of the configuration calculation were found in the selected design folder.
- If new results are needed, configuration should be edited, saved, and SMiPA (CyMPA) and/or SMiPApat (CyMPApat) programs should be executed according to the SMiPAWin (CympaWin) flow chart. Then, new results can be viewed under the View menu. Graphs of calculation results will be shown after calculation execution when selected in View menu.

Input and output files

SMiPA (CyMPA) and SMiPApat (CyMPApat) both use fixed file names and will be saved after calculation into the folder we call **design folder** as follows:

temp2.t output of SMiPA (CyMPA) containing the patch mutual coupling and input impedance information, SMiPAWin (CympaWin) copies it automatically as **project_name.sij**

pat-az.dat output of SMiPApat (CyMPApat) containing field values in the azimuthal plane, SMiPAWin (CympaWin) copies it automatically as **project_name.paz**

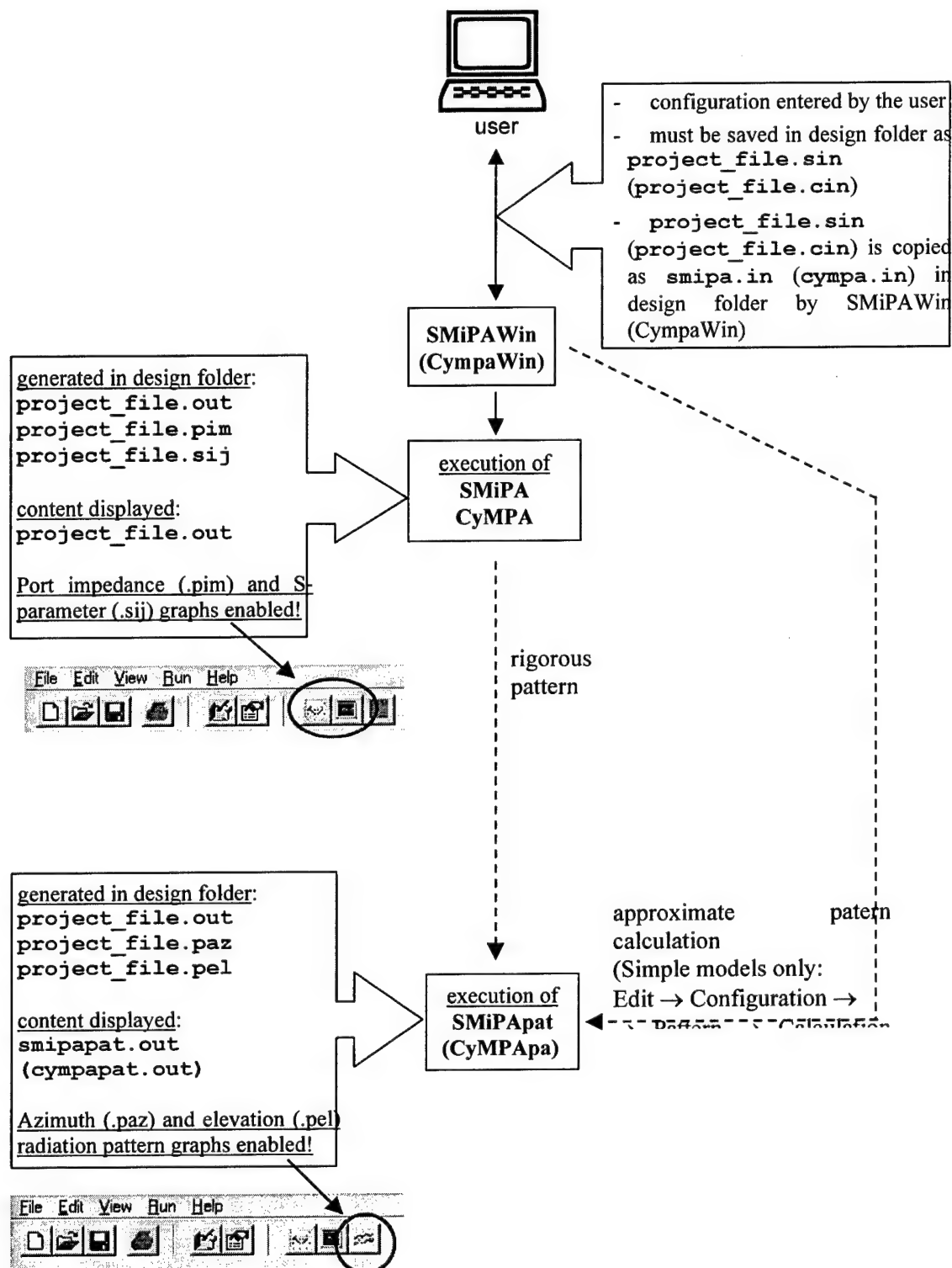
pat-el.dat output of SMiPApat (CyMPApat) containing field values in the elevation plane, SMiPAWin (CympaWin) copies it automatically as **project_name.pel**

These three files contain sufficient information about the simulation run.

Also the various temporary files will be generated during the program run within the design folder. Some of them are used for status information and synchronization between the Windows® and DOS application and are deleted before or after the program execution.

The user interface properties

- SMiPAWin (CympaWin) is designed as the standard Windows SDI (Single Document Interface). It maintains the look and feel of standard Windows applications to minimize the learning curve.
- In order to minimize typing errors SMiPAWin (CympaWin) forces user to enter correct type of parameters, and forbids saving configuration with empty values in forms.
- The SMiPAWin (CympaWin) is menu oriented with submenu items logically grouped, and disabled ('grayed') if operation is not possible within the current context. Standard dialog boxes are used for the file operations.
- The Toolbars exist which duplicate some more frequent operations.



SMiPAWin (CympaWin) Flow Chart: interactions between entities involved

Some SMiPAWin (CympaWin) windows

In this section some typical windows that occur during the use of SMiPAWin (CympWin) are shown and explained. Also, 'Run' and 'View' menus are described.

Window 1

File → New or File → Open

- This should be the first user action, since most of the other operations are not possible until the configuration name is known.
- Window 1 shows, that the configuration file 'Test.cin' is already loaded and some of the toolbars are enabled.

Window 2

Configuration creating, editing, and viewing

- Realized with the Page Control Dialog Box (Style Sheets) as shown in Window 2
- Configuration parameters are grouped logically and placed at the same card

Window 3

Error message box

- Any parameter not entered will cause the error message box to pop up when user tries to leave Configuration dialog box using 'Apply' button
- It is possible to leave the control without filling it completely, by using 'Cancel' button

Window 4

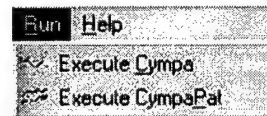
- Confirmation will be requested if user tries to leave the program without saving configuration which was edited/changed.
- The application does not ask for confirmation when 'Cancel' button is used, since it is always possible to go back to editing.

Window 5

- Tables resize automatically when parameters that determine the number of rows change.
- Scroll bars are shown when table does not fit the page control size.

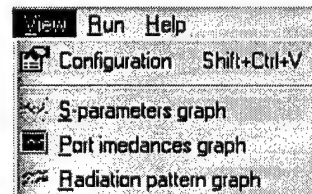
Run Menue

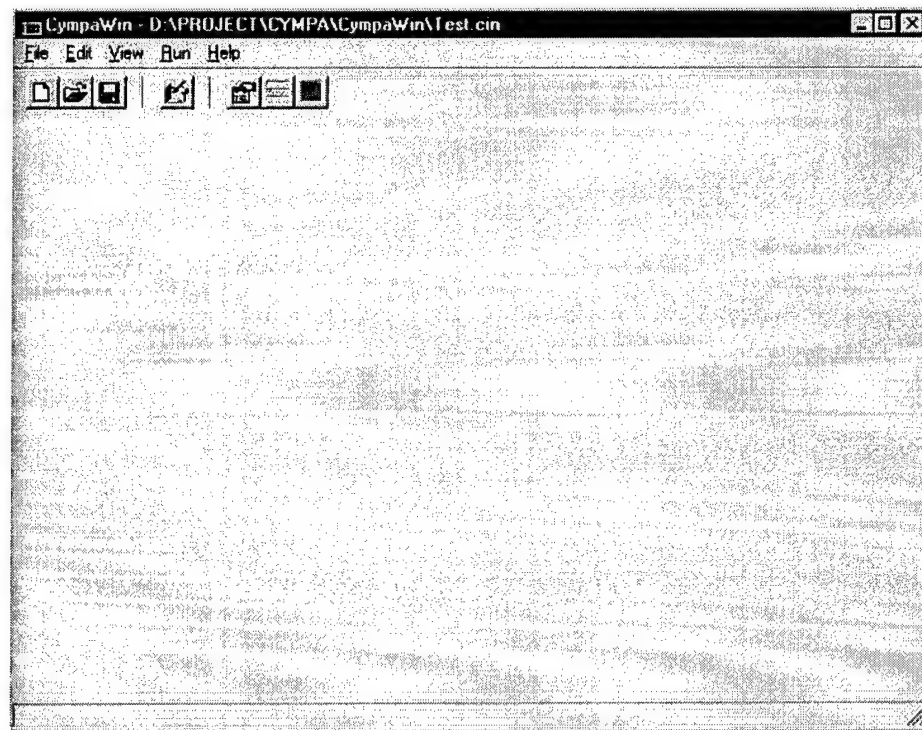
- Run menu contains two submenu items: *Execute SMiPA (Execute Cympa)* and *Execute SMiPApat (Execute CympaPat)*.
- SMiPA (Cympa) and SMiPApat (CympaPat) applications are executed as minimized DOS boxes.
- User can maximize them and watch the program output as within the command line environment.



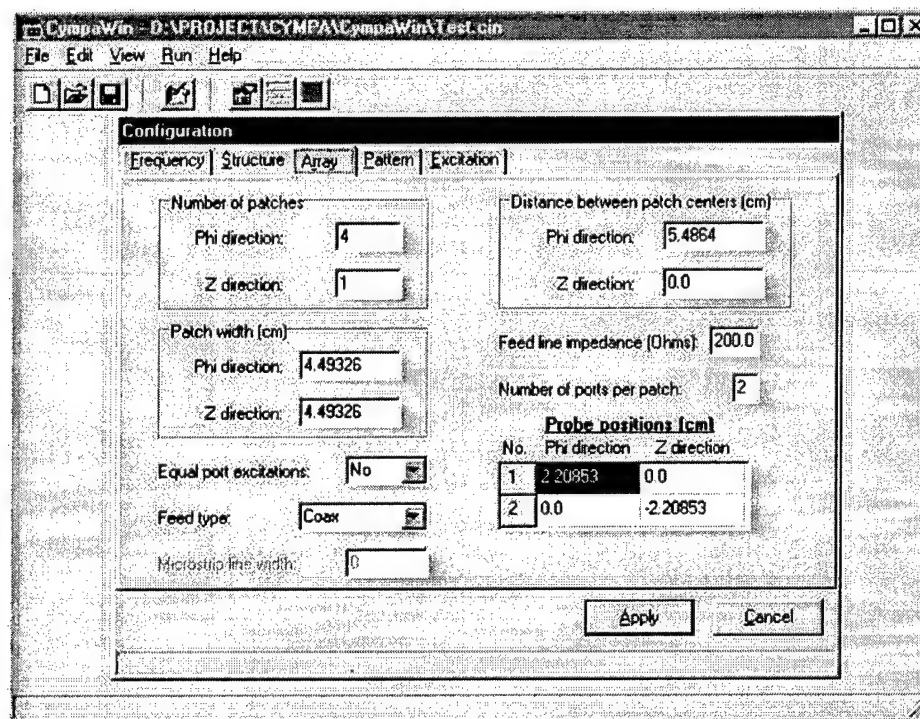
View Menue

- Configuration submenu is enabled first when configuration is created by File → New or reload using File → Open.
- S-parameters graph and Port impedances graph are enabled after execution of SMiPA (CyMPA)
- Radiation pattern graph is enabled after execution of SMiPApat (CyMPApat)

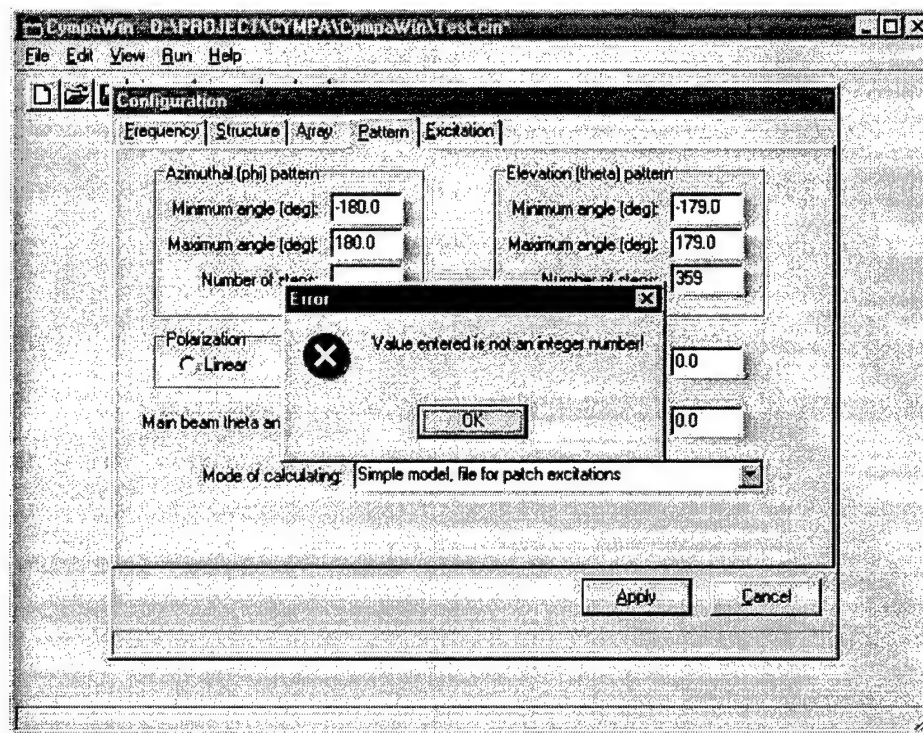




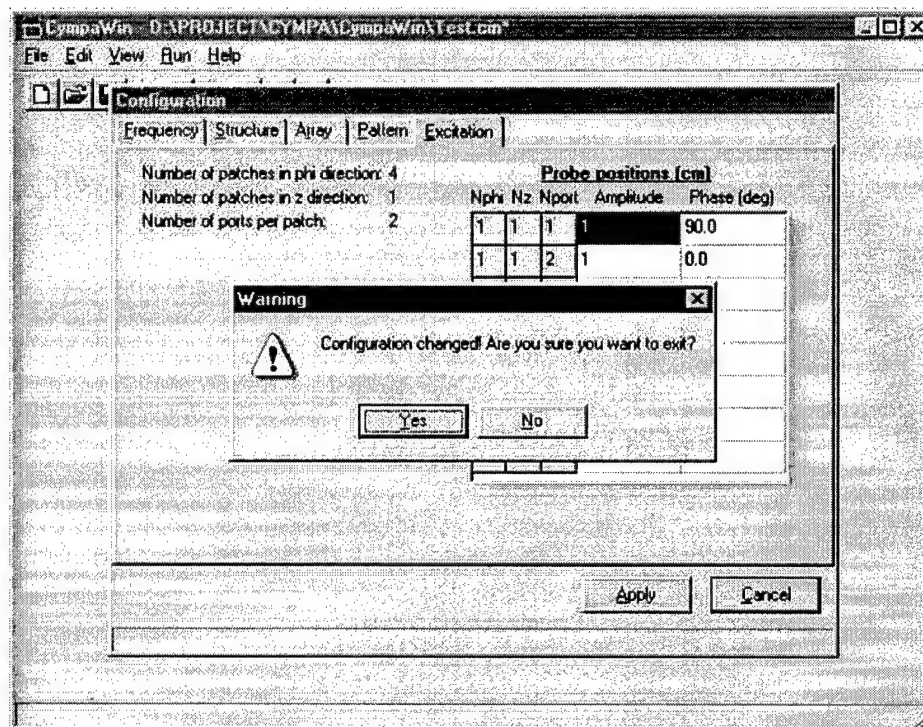
Window 1



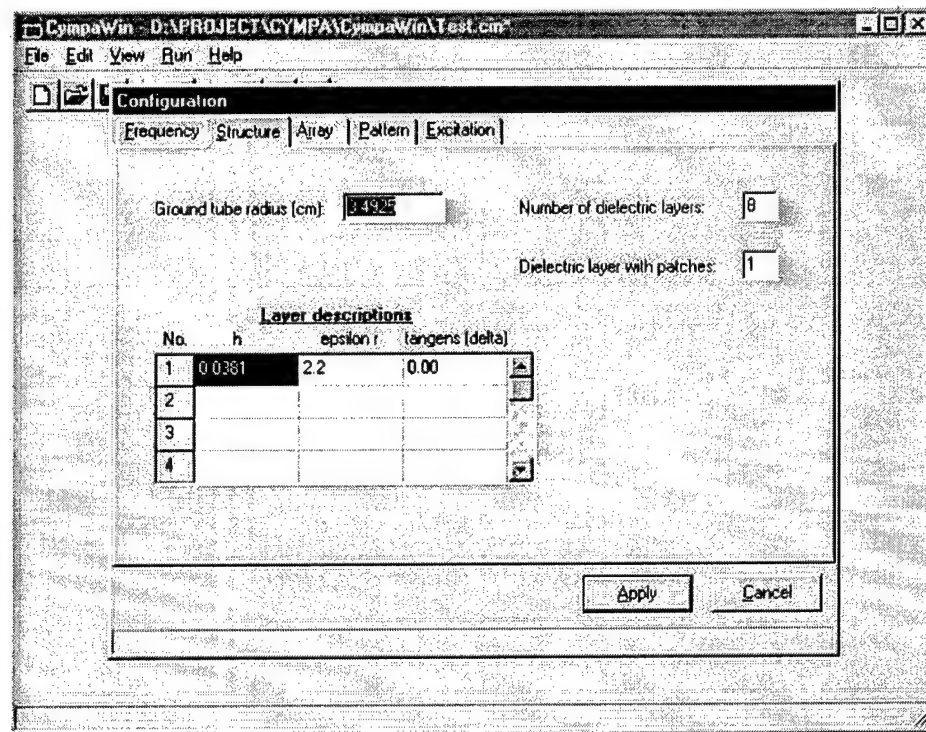
Window 2



Window 3



Window 4



Window 5

Troubleshooting

If SMiPA (CyMPA) or SMiPapat (CyMPApat) would not start, try running them directly from the command line within the folder where they are installed (e.g. in folder **c:\Program Files\Smipa** or **c:\Program Files\Cympa**). This folder must contain the **smipa.in** (**cympa.in**) file that was generated by SMiPAWin (CympaWin). Therefore you must copy it from design folder before running desired program. The output files will in this case appear in the same folder and will be named corresponding to names in section 'input and output files'.

8 CONCLUSIONS

Conclusions

The outcome of the proposed two-phase, 24-month effort was developing a model for analyzing single-curved and double-curved conformal microstrip antennas. Furthermore, it was planned to develop two computer programs: (a) for analyzing patch arrays printed on spherical structures, and (b) for analyzing cylindrical aperture-coupled patch arrays.

We have developed the program SMiPA for analyzing microstrip patch arrays printed on spherical structures. It is assumed that the patches have either rectangular or circular shape. Three types of feeding structures are considered: coaxial and microstrip transmission lines and aperture coupling. The program solves the electric field integral equation, and the moment method is used for solving the integral equation. The analysis of patch antennas printed on (or embedded in) multilayer spherical structures is obtained by implementing a routine for calculating Green's functions of multilayer spherical structures. The numerical evaluation of matrix elements used in moment method is made with special care. In particular, we defined the normalized Legendre polynomials and vector-Legendre transformation by which evaluation of ratios of very large numbers was avoided, and numerical treatment of spherical Bessel and Hankel functions was carefully made.

The program SMiPA calculates the following parameters of the cylindrical patch arrays:

- input impedance at each input port in the array
- mutual coupling between each two patches in the array
- radiation pattern of the array when all mutual couplings are taken into account
- radiation pattern of the array without taking mutual coupling into account (fast calculations of the radiation pattern are needed for making first design of the array).

Furthermore, we have developed the upgrade of the program CyMPA that calculates aperture-coupled patch antennas on cylindrical structures. Program CyMPA is the outcome of the project F61775-99-WE040, "CyMPA - Program for Analyzing Microstrip Patch Arrays on Circular-Cylindrical Structures," sponsored by EOARD. Old version of the program enables the analysis of cylindrical patch arrays fed by a coaxial or microstrip transmission line. With the upgraded program it is possible to fully analyze cylindrical patch arrays with aperture feeding, which is

important since aperture type of feeding enables one to separate radiating and feeding part of the antenna, thus enabling independent design both of antenna parts. The upgraded program fully analyzes the array, i.e. radiation pattern, input impedance at each input port, and mutual coupling between each two elements is calculated.

The programs are tested by comparing the calculated results with measurements and with calculated results obtained by other methods. We have additionally developed an experimental model for testing the program for analyzing spherical arrays since there are only a few experimental results in literature in connection with spherical patch antennas. In all tested cases there is a good agreement between calculated results and test data.

9 Bibliography

- [1] R.F. Harrington, *Field computation by moment method*, MacMillan, New York, 1968.
- [2] E.H. Newman, and J.H. Tehan, "Analysis of microstrip array and feed network," *IEEE Trans. Antennas and Propagat.*, Vol. 33, pp. 397-403, Apr. 1985.
- [3] Z. Sipus, J. Bartolic, and B. Stipetic, "An approach to microstrip patch elements and array design", *Proceedings of COST 223-ESA Workshop on Active Antennas*, ESA-ESTEC, Noordwijk, The Netherlands, 1992, pp. 3.5.1-3.5.8.
- [4] Z. Sipus, J. Bartolic, and B. Stipetic, "Input impedance of rectangular patch antenna fed by microstrip line, *Electronics Letters*, Vol. 28, No. 20, pp. 1886-1888, Sep. 1992. Errata, *Electronics Letters*, Vol. 28, No. 23, pp. 2199, Nov. 1992.
- [5] W. Y. Tam and K. M. Luk, "Resonances in spherical-circular microstrip structures of cylindrical-rectangular and wraparound microstrip antennas," *IEEE Trans. Microwave Theory Tech.*, Vol. 39, pp. 700-704, Apr. 1991.
- [6] R. Leijon, "Radiation from mobile phone antennas close to human body," Technical; Report No.270L, Department of Microwave Technology, Chalmers University of Technology, Gothenburg, Aug. 1997.
- [7] Z. Sipus, "Analysis of planar and circular cylindrical multilayer structures with application to soft and hard surfaces," Ph.D. Thesis, Department of Microwave Technology, Chalmers University of Technology, Gothenburg, Oct. 1997.
- [8] Z. Sipus, P.-S. Kildal, R. Leijon, and M. Johansson, "An algorithm for calculating Green's functions for planar, circular cylindrical and spherical multilayer substrates," *Applied Computational Electromagnetics Society Journal*, Vol. 13, pp. 243-254, Nov. 1998.
- [9] M. Abramowitz and I. Stegun, *Handbook of mathematical functions*, Dover, New York, 1965.

- [10] K. Naishadham and L.B. Felsen, "Dispersion of waves guided along a cylindrical substrate-superstrate layered medium," *IEEE Trans. Antennas and Propagat.*, vol. 41, pp. 304-313, March 1993.
- [11] D. L. Sengupta, T. M. Smith, and R. W. Larson, "Radiation Characteristics of Spherical Array of Circularly Polarized Elements", *IEEE Trans. on Antennas and Propagat.*, Vol. 16, pp. 2-7, Jan. 1968.
- [12] R. P. Jedlicka, M. T. Poe, K. R. Carver, "Measured mutual coupling between microstrip antennas", *IEEE Trans. on Antennas and Propagat.*, Vol. 29, pp. 147-149, Jan. 1981.
- [13] Z. Sipus, "CyMPA – Program for Analyzing Microstrip Patch Arrays on Circular-Cylindrical Structures," Final report for contract F61775-99-WE040, Faculty of Electrical engineering and Computing, University of Zagreb, April 2000.
- [14] D.M. Pozar, "A Reciprocity Method of Analysis for Printed Slot and Slot-Coupled Microstrip Antennas, *IEEE Trans. on Antennas and Propagat.*, Vol. 34, pp. 1439-1446, Dec. 1986.
- [15] R.F. Harrington, *Time-harmonic electromagnetic fields*, McGraw-Hill, New York, 1961,
- [16] D. Loeffler, W. Wiesbeck, and B. Johannisson, "Conformal Aperture Coupled Microstrip Phased Array on a Cylindrical Structure," *Proc. of IEEE Antennas Propagat. Symposium*, Orlando, USA, 1999, pp. 882-885.